An Imaging Mass Spectrometer with Ultrashort Laser Pulses as its Ionization Source

Martin Chiasson

A thesis submitted to the

Faculty of Graduate and Postdoctoral Studies

In partial fulfillment of the requirements for the

M.Sc degree in Physics

Department of Physics

Faculty of Science

University of Ottawa

Table of Contents

Common Acronymys

ICP: Inductively Coupled Plasma

EI: Electron Ionization

TOF: Time-of-Flight

SIMS: Secondary Ion Mass Spectrometry

MALDI: Matrix-Assisted Laser Desorption and Ionization

NRC: National Research Council

ARC: Advanced Research Complex

CPA: Chirped Pulsed Amplification (Amplifier)

CW: Continuous Wave

PC: Pockels Cell

QWP: Quarter Wave Plate

BW: Brewster Window

TOF-MS: Time-of-Flight Mass Spectrometer (Spectrometry)

MCP: Micro Channel Plate

TDC: Time to Digital Converter

CCD: Charge-Coupled Device

DC: Direct Current

AC: Alternating Current

DDG: Digital Delay Generator

ITO: Indium Tin Oxide

List of Figures

Abstract

We have built an imaging mass spectrometer adapted for ultrashort laser pulses as its ionization technique, as an alternative to other imaging techniques. Before my arrival, the mass spectrometer has only been subject to preliminary tests on noble gases. Since then, we've made some modifications to the system in order to properly analyze solids. This thesis shows how we obtain our ultrashort laser pulses, the inner workings of our homemade imaging mass spectrometer, and the results that we've obtained with it so far. We tested two modes of operation concerning the extraction of the ions from the system into the mass analyzer: continuous and pulsed. We discuss the advantages and disadvantages of each configuration. We also display preliminary imaging results with our imaging technique of a simple WO_3 and ITO structure. We conclude by comparing the resolution of this image to the different techniques in imaging mass spectrometry, how we can further improve our mass spectrometer, and the future use of this machine.

Nous avons construit un spectromètre de masse adapté pour les pulses de laser très courts comme technique d'ionisation, pour acquisition des images d'un échantillon. Avant je suis arrivé, le spectromètre de masse avait seulement été utilisé pour des tests préliminaires de gaz nobles. Depuis ce moment, nous avons modifié le système pour analyser les solides. Cette thèse démontre comment on obtient nos pulses de laser très courts, comment notre spectromètre fait maison fonctionne et les résultats nous avons obtenus jusqu'à présent. Nous avons testé deux configurations différentes au sujet de l'extraction des ions du système : constant et pulsé. Nous discutons aussi les avantages et désavantages de chaque mode d'opération. Nous démontrons aussi des images préliminaires d'un substrat mixte de WO_3 et ITO. Nous concluons par comparer la résolution des images aux autres techniques de collection d'images, comment nous pouvons améliorer notre spectromètre de masse et les plans pour la machine dans le futur.

1 Introduction

In order to discuss the subject of mass spectrometry, we need to understand its concept. To start off, let's begin with a typical car. If I were to ask the components of the car and where they are located, one could point out the location of the tires, doors, hood, bumpers, engine, etc. Now, if I were to take the door and ask what are its components and location, one could point out the window, the steel frame, etc. If we continue to break the car into smaller and smaller components, we can determine the molecules and elements that make up the vehicle.

However, unlike a car where we can point our finger to its different components, we can't do this for molecules. We need to be able to distinguish one element from the other. Simply by observing a periodic table can we see that each element has its own mass. Thus, if we can find the masses of the elements (and the molecules that are formed from these elements), we can determine the elements themselves. This is the basis of a mass spectrometer; to break down samples into its elements and molecules and detect their mass. With this information, we can determine what are the elements and molecules that make up the car.

While this is all well and good, if we were to completely break down the car into its atoms and molecules, we would be able to find its components, but not where they are located. If we were to break down the car door, we would not be able to identify the location of the window from the frame. However, if we were to ablate (or break down) a single small area in that door, we can keep the spatial information of the door, now knowing where the window ends and the frame begins. This is the basis of imaging mass spectrometer; breaking down a single area of a sample and determine the masses of the elements in only that single location, and then moving the ablation area, and repeating the process. With this, we can reconstruct the car completely with not only its components, but their location as well.

Since the inception of its concept in the late 19th century, mass spectrometers have had multiple different designs and techniques to analyse the mass spectrum of samples. Each of these techniques include three common components; the detector, the ionization source, and the mass analyser. The mass analyser separates the ions with different mass to charge ratios with the help of electromagnetic fields. The detector measures these different masses, which allows the creation of the mass spectrum. The detector needs to be compatible with the mass analyser component used in the design of the mass spectrometer. The ionization source creates the ions from the sample and sends them into the mass analyser. This component of the mass spectrometer is the most important and the most studied, as there are multiple techniques that

exist. One such method consists of the interaction between an electron source and gaseous atoms (Electron ionization or EI), while another inserts the sample into an inductively coupled plasma (ICP).

In fact, this is the method used at DVS Science (now acquired by Fluidigm) in their product Cy-TOF 2, the only commercially available mass cytometer. They have developed a technique consisting of attaching particular rare-earth metals to antibodies, which can pass through the cell membrane and attach themselves to vital components of biological cells. This allows them to scan for the rare earth element in their mass spectrum that represents a specific component inside the cell, and not the component itself. Utilizing an ICP as its ionization source pulls the cell apart and ionizes it before it enters the mass analyzer; it doesn't matter if the components remain in their molecular form or not. As long as the mass analyzer can detect the rare earth element that corresponds to a specific molecule in the cell, the measurement will be the same if the molecule remains intact or completely blows up.

However, the ICP does have a drawback, as it has no spatial resolution outside of a specific cell. Results can show what was in the cell, but not where it was located. In order to improve on this, we need an ionization method that keeps spatial resolution. Two respected designs of this is secondary ion mass spectrometry (SIMS), and matrix-assisted laser desorption/ionization (MALDI). Both of these have their disadvantages, such as SIMS being expensive and limited in terms of quantitative data, and MALDI needing a specific matrix for any given sample tested. Although both of these techniques are still used quite regularly for ionization and ablation in mass spectrometry and keeping spatial resolution, the main disadvantage is that they were developed over 30 years ago. Since then, laser technology has developed further and ultrashort laser pulse physics has advanced by leaps and bounds.

At the National Research Council of Canada (NRC), experiments have shown laser desorption using focussed femtosecond pulses of a sample off a substrate as a valid method of extracting the sample, with less data lost around the edges of the focus point as the pulses are shorter in time. Focused laser pulses have also shown they can ionize gases and solids like in MALDI. For these reasons and as motivation, we've constructed a homemade mass spectrometer that utilises femtosecond laser pulses as its ionization and desorption source, without the need of matrix assistance. The final goal of this mass spectrometer is for it to be adapted for mass cytometry, while maintaining spatial resolution of biological cell tissues, improving the spatial resolution by a couple of orders of magnitude, compared to previous designs in mass cytometers with an ICP.

The problem is that, while this newly constructed mass spectrometer at NRC was preliminarily tested on noble gases, not much else has been done with it. Considering that we want to apply this to solids, we need to analyze the ion's path through the ion optics of the system until detection, and perfect it for later use in imaging. Because of their known mass spectrums, gases are ideal for preliminary tests before moving on to solids, especially since the mass spectrometer itself is designed for sub atmospheric pressure to limit outside sources from interfering with our collection of data. Once this is analyzed, the move to solids can be done. We can find and analyze problems that appear, transitioning from gases to the ablation of solids. Afterwards, we can begin scanning materials to obtain images, starting off with simple structures and moving forward with smaller, more complicated structures all the way to biological cell tissues.

However, this is final vision of this newly constructed system. In order to reach that point, there needs to be some work done to determine if this mass spectrometer, with the use of ultrashort laser pulses, can properly function. There are multiple goals that I try to achieve in my thesis. First, I need to verify that ultrashort laser pulses can be used to ionize noble gases and be applied in mass spectrometry to collect their mass spectrums. Once that is achieved, I can properly calibrate the system. Second, I need to verify that ultrashort laser pulses can be used to not only ionize, but ablate solids. With this, we can see if these pulses can be used as a proper ionization method in mass spectrometry. Only once all of this is done can I move on to the main goal: To see if can apply these ultrashort laser pulses towards imaging mass spectrometry, by trying to collect images of structures of the solids that I ablate and ionize in the system. Once that is done, we can focus our attention towards improving the system to be comparable with the two known methods of imaging mass spectrometry (SIMS and MALDI), and hopefully one day even improve on its spatial precision.

Chapter 2 presents the laser itself. It describes how the laser pulses are made and their characteristics before they enter the mass spectrometer. Chapter 3 presents the mass spectrometer, its design and reasoning behind it, and how the sample and the laser focal spot are manipulated inside the machine. This chapter is presented as a tutorial and learning tool for new students who will work with this mass spectrometer in the future at the Advanced Research Complex (ARC) on the uOttawa campus. Chapter 4 presents the data obtained, such as how we calibrate our mass spectra results and the analysis of our sample from those spectrums. Chapter 5 presents some issues that we encountered and how we fixed them. This thesis concludes with a look ahead at what we can do with this technology and how it can apply to different fields.

2 The Laser

Chirped pulse amplification [1] allows us to generate high power femtosecond laser pulses. This system consists of four components; an oscillator to create short pulses with relatively low energy, a stretcher to create a spatial chirp on our pulses, a regenerative amplifier afterwards to safely increase the energy of the stretched pulses, and a compressor to undo the chirp created by the stretcher. In this way, we create ultrashort pulses in the femtosecond range with an energy in the micro and millijoule range. Each of these components will be discussed in detail in their respective sub chapters.

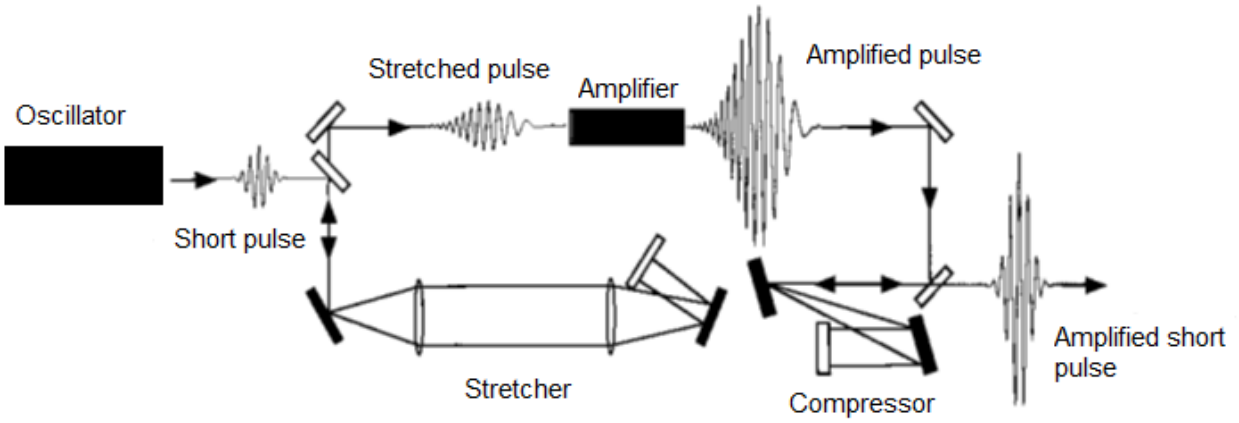

Figure 1: A Chirped Pulse Amplification (CPA) system. Modified from source [2].

2.1 Short Pulse Oscillator

2.1.1 Basics of Operation

We use a Ti:Sapphire laser tuned at 800nm as our primary laser sources to generate our short pulses. The gain medium, a Ti:Sapphire crystal, is pumped by a frequency-doubled Nd:Yag laser (532nm) to start the population inversion of the crystal. We use a pair of prisms inside our cavity to compensate for dispersion in the cavity. One of the mirrors at the end of the cavity doesn't reflect completely. This mirror, the output coupler, transmits a small portion of light to the next stage of the chirped pulse amplification process. This creates our laser light, but it might be in a continuous wave (CW) mode. To create our ultrashort pulses, we use a technique called Kerr lens mode locking.

2.1.2 Kerr Lens Mode Locking

When the intensity is high enough, the laser pulse induces nonlinear effects in the propagation medium, changing the index-of-refraction of the material. This is called the Kerr effect and the index-of-refraction obeys the following relationship:

$$n = n_0 + n_2 I \tag{1}$$

Here, n represents the index-of-refraction of the propagation medium, n_0 is the weak field index-of-refraction, and n_2 represents the constant in which the index changes with intensity, represented by I. Assuming n_2 is positive, the index-of-refraction increases with the intensity. In a typical Gaussian beam, the intensity of the beam increases towards the center. This leads to a spatially varying index-of-refraction of the propagating medium across the beam profile, and focusses the beam much like a lens. A visual representation of this can be seen at Figure 2. This can be used as a mode locking technique [3].

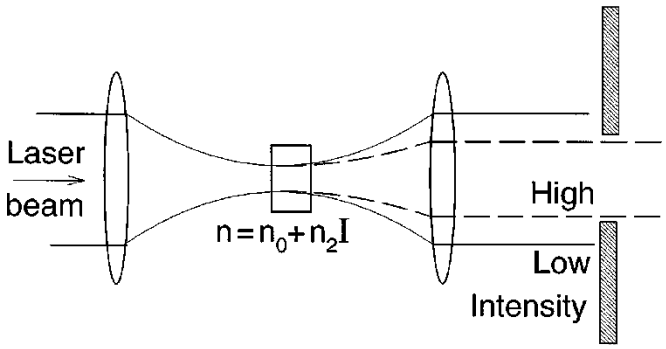

Figure 2: Visual representation of the effect of a hard aperture Kerr lens mode locking apparatus. Since the laser beam is more intense towards the center of the beam, the index-of-refraction is different throughout the material depending on the intensity at that point. This causes the laser beam to focus and pass through the blocking aperture. Source from [3]

There are two different techniques that utilise the Kerr effect in laser cavities. The hard-aperture Kerr lens mode locking technique [4] simply reduces the loss inside of the cavity after each round trip inside the cavity. A soft-aperture Kerr lens mode locking technique [5], which is what we use inside the oscillator, takes advantage of the different spatial states inside the cavity at different intensities of light. Due to the higher peak intensity of mode locked lasers compared to CW lasers, a cavity can have a slightly different transverse mode structure between a CW operation and a mode locked operation. The cavity can be designed to favour the mode locked

state. Since the mode locked state is closer to that of the spatial profile of the pump beam, more energy can be extracted from the crystal, leading to a higher gain and improved efficiency.

However, the process of mode locking is not self-starting, but once it is achieved, it is self-sustained. A source of artificial noise is required to start the mode locking process. For our laser, moving one of the prisms with a screwdriver creates the noise required and creates our short pulses thanks to mode locking process.

2.1.3 Creation of Short Pulses with Mode Locking

Lasers are often thought as perfectly monochromatic, but that isn't the case. There will always be some bandwidth in the light spectrum, caused by the gain medium and the physical design of the laser cavity itself. Because of this, multiple longitudinal modes can exist in the cavity. Of course, destructive interference will lead to the cancellation of much of the intensity. However, if the phases of each of the modes are in sync, they will constructively interfere and create a pulse of light. The time lapse of this pulse depends on how many modes are in phase and the bandwidth of the gain medium. If the bandwidth is large, like that of a Ti:Sapphire crystal (roughly 250 nm, [3]), the amount of interference increases, be it destructive or constructive. Since there are more longitudinal cavity modes in larger bandwidths, the interval of time which these modes can constructively interfere decreases, leading to shorter pulses. The creation of short pulses is shown in Figure 3.

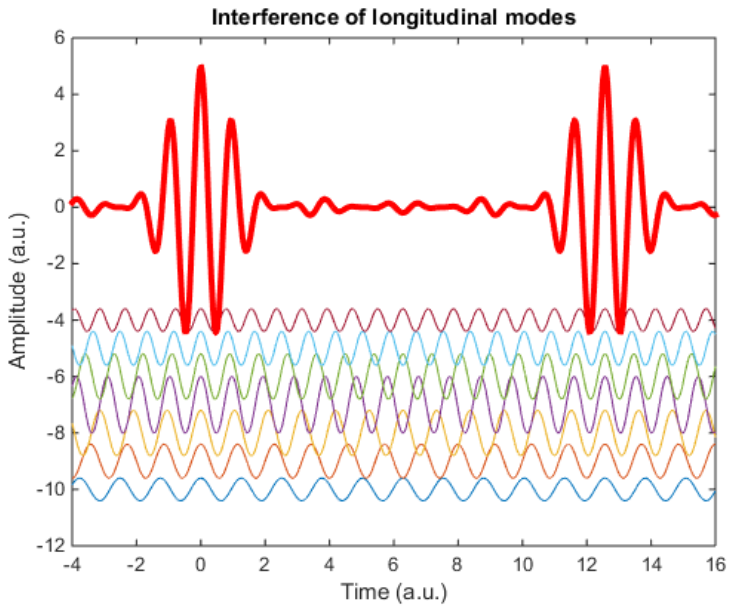

Figure 3: Interference of longitudinal modes and the resulting pulse (red). When the modes aren't in phase, the signal is weak and random. However, when the modes are in phase, they interfere constructively. This forms the short pulse.

2.2 Regenerative Amplifier

The amplifier comes third in our laser system components, after the stretcher but before the compressor. It takes advantage of the polarization state of the pulse, combined with well-timed activation of two Pockels cells and another Ti:Sapphire crystal to increase the pulse energy, and dumps it out of the amplifier and into the compressor. The Ti:Sapphire crystal is pumped by another frequency-doubled Nd:Yag laser.

Pockels cells are useful because not only are they birefringent, but their birefringence can be controlled by an electric voltage. For our setup, when turned on, they act like a quarter wave plate, while they don't modify the polarization if they are turned off. Initially, both Pockels cells in the amplifier are turned off.

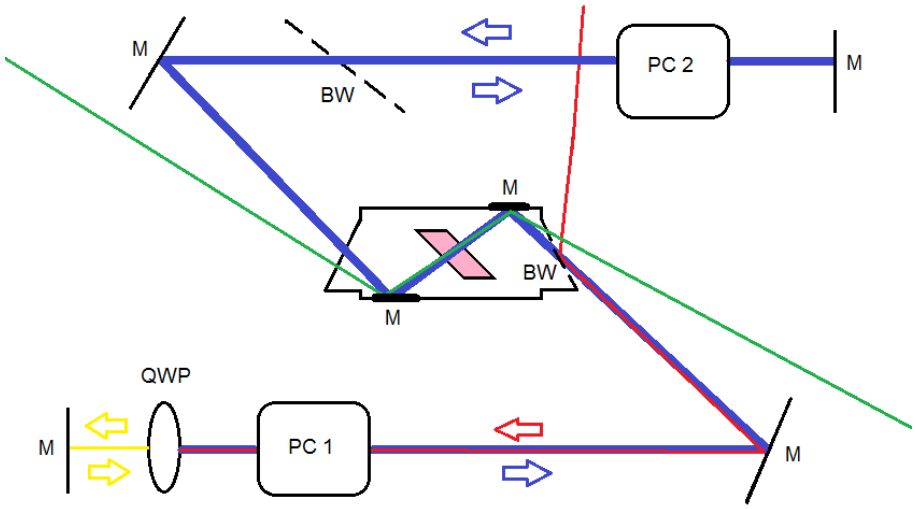

Figure 4: Regenerative amplifier setup during the first pass of the laser pulse, with mirrors (M), both Pockels cells (PC 1 and PC 2), a quarter wave plate (QWP) and Brewster windows (BW). In this figure, S-polarized light is red, P-polarized light is blue, and circularly polarized light is yellow. Both Pockels cells are initially off. There is also continuous pumping of the crystal (pink) by another laser source (green).

The pulses hit a Brewster window, which reflects all s-polarization (Transverse electric, TE, or the electric field of the photon is perpendicular to the surface of the window) and transmits all p-polarization (Transverse magnetic, TM, or the electric field of the photon is parallel to the surface of the window). This polarizes our pulse. The pulse is then directed towards a quarter wave plate, immediately followed by a Pockels cell, initially turned off, and then a mirror, which reflects the pulse back through these two optics. If turned off, the double pass through the quarter wave plate will change the pulse from s-polarization to p-polarization, resulting in a transmission through the Brewster window into the gain medium. Upon a second trip, however, if the Pockels cell stays off, it will turn the pulse back to s-polarization, resulting in a reflection off the Brewster window out of the cavity. If this Pockels cell is turned on while the pulse completes its first round trip in the cavity, it will act as a quarter wave plate. This will result in four passing of a quarter wave plate, which won't change the polarization state, and it will remain in p-polarization during the second round trip and thereafter. Now the pulse can constantly extract energy from the Ti:Sapphire crystal.

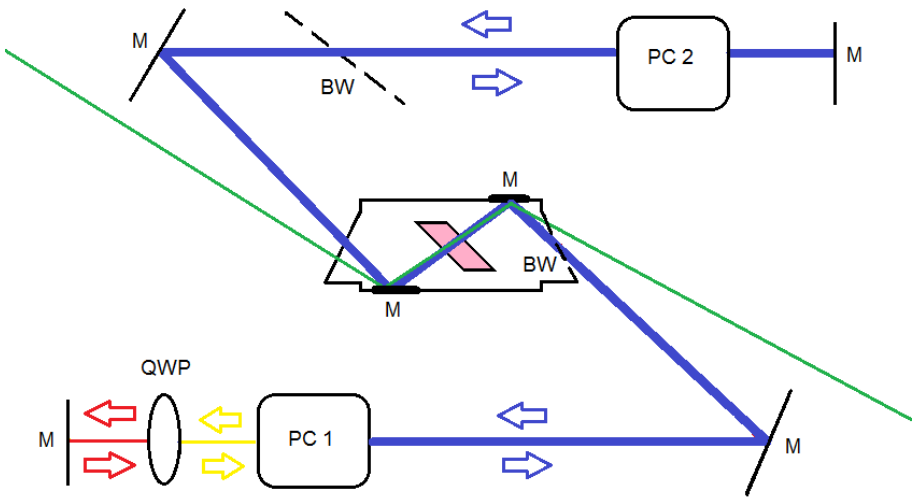

Figure 5: Regenerative amplifier setup during the second pass and onwards, amplifying P-polarized light. The first Pockels cell is activated, behaving like a quarter wave plate. Compared to its first pass, the pulse gets amplified as it maintains its P-polarization throughout the round trip in the amplifier.

In the second half of the cavity, there is a second Brewster window, followed by another Pockels cell, also initially turned off. The p-polarized pulse passes through the window and Pockels cell, reflects off a mirror and passes once again through these two optics. This keeps the polarization state of the pulse the same for its return trip into the gain medium. Once the pulse has extracted enough energy for our satisfaction, we turn this Pockels cell on, turning it into another quarter wave plate, changing the pulse from p-polarization to s-polarization. With this polarization change, the second Brewster window will reflect the high energy pulse out of the cavity into the compressor. Once this pulse has been extracted out of the regenerative amplifier, both Pockels cells are turned off and the process is repeated.

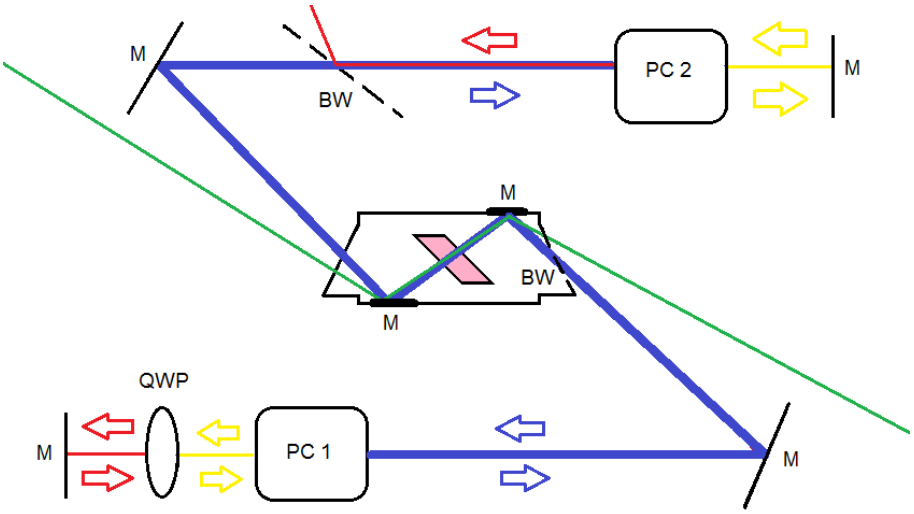

Figure 6: Regenerative amplifier setup and output of the laser pulse. Both Pockels cells are turned on, behaving like quarter wave plates. Thus, the new S-polarized light pulse reflects off the Brewster window and out of the amplification system.

All subsequent pulses from the seed beam coming into the regenerative amplifier during the amplification process remain s-polarized because of the trip through four quarter wave plates (because the first Pockels cell is on at this point), and reflects off the Brewster window, resulting in a loss of energy.

2.2.1 Requirement of a Chirp

As discussed in Chapter 2.1.2, Gaussian beams lends themselves to self-focusing when the beam intensity is high enough. As the intensity is relatively low compared to the critical power (the power where self-focusing begins), the oscillator can be operated efficiently and safely without the risk of damage to the gain medium or the optics. However, as we continuously increase the intensity of our pulses after each round trip inside the amplifier, the likelihood of self-focusing increases up to a point where it can pass the damage threshold of the gain medium and create significant damage to the system. By adding the chirp before the amplifier, the intensity is spread out in time (which leads to a slightly longer pulse in the time domain), leading to a smaller index-of-refraction throughout the materials, which leads to a smaller focussing effect and will not reach the damage threshold to destroy the materials inside the amplifier. After compressing the pulse spatially, we safely reach ultrashort, high energy pulses.

2.3 Stretcher and Compressor

The stretcher and compressor [2] are used to protect the materials and optics in the regenerative amplifier, discussed in chapter 2.2, and to compensate for dispersion through the multiple round trips through it. This is done by spatially stretching and compressing the pulse, hence the name. In our particular setup, we use gratings at specific distances and angles to give the pulse a spatial chirp before being amplified by the regenerative amplifier, then recompressing the pulse while compensating for dispersion after the amplification process.

Similar to the interference pattern of light passing through multiple slits, the reflection of light off gratings has multiple orders. For convention's sake, we'll call the Fresnel reflection, where all wavelengths are reflected in the same direction, the zeroth order. After that, diffraction can happen on both sides of the normal. Those on the opposite side of the zeroth order with respect to the normal shall be referred as negative orders and positive otherwise. Since the first order diffraction, positive or negative, has the highest intensity of the non-zeroth orders and the first positive order can be negated if the gratings are placed at certain angles, we will be working with first negative order, or -1 order for simplicity.

The two relevant angles for gratings reflections are the angle of the incident beam with respect to the normal (γ) and the angle between the reflected beams of the m^{th} order with respect to the normal (θ_m). They are related by:

$$\sin\gamma + \sin\theta_m = m\frac{\lambda}{a} \tag{2}$$

Here, a represents the distance between two grooves on the grating, and λ represents the wavelength of the incident beam. There is a third angle which is important, the blazing angle of the grating. However, this only controls the intensity of the diffraction orders, specifically to maximise the intensity of a particular order. Since we are working with the -1 order, we simply designed gratings with blazing angles that maximise this particular order.

A single grating creates a spatial chirp on our laser pulse, since the incident beam is not monochromatic. A second grating corrects the dispersed angles of the spatially chirped pulse, resulting in a pulse spatially chirped along the beam profile and temporally chirped. This temporal chirp is obtained because of the different beam paths each specific wavelength travels, caused by the dispersion induced by the two gratings. If that same pulse is reflected back towards those two gratings, the spatial chirp is removed, but the temporal chirp increases. This is the general

idea of two grating stretcher and compressor systems; to add a temporal chirp to a laser pulse, without adding a spatial chirp in the beam profile.

Specific setups of gratings and mirrors are required to add a temporal chirp to our pulses, since the beam path is different for every wavelength in the -1 order. This chirp is determined by the distance between the gratings. No matter what the design, the stretchers and compressors never subtracts chirp from our pulse, only adds chirp. However, the pulse can be chirped two different ways. The longer wavelengths could have a shorter path in the setup, resulting in longer wavelengths at the spatial front end of the pulse. This is called a positive dispersion. When shorter wavelengths have a shorter path, resulting in shorter wavelengths at the spatial front end of the pulse, it is called negative dispersion.

We chose to give the pulse a positive dispersion in our stretcher, since the regenerative amplifier presents positive dispersion as well. To achieve this, we need the gratings distance to be negative. Since a negative distance is physically impossible, we used a 4-f grating setup and moved the gratings inwards by a small distance Δx (Figure 4a). If the stretcher would negatively disperse our pulse, it would be compressed in the amplifier, leading to damage to the optics and the crystal in the amplifier. Afterwards, the compressor presents negative dispersion to our pulse, counteracting the positive dispersion presented in the stretcher and the amplifier. This leads once again to an ultrashort laser pulse in the femtosecond range, compared to the picosecond range after the stretcher. Similar designs to those of Figure 4 were used. However, the mirrors after the two gratings for both the compressor and stretcher vertically displaces the beam, so that the output beam doesn't overlap with the input beam.

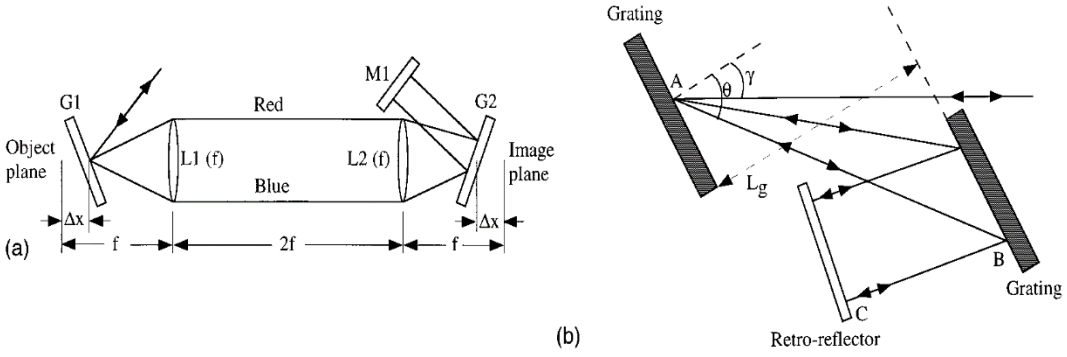

Figure 7: An example of the design of a) a pulse stretcher and b) a pulse compressor. The pulse stretcher has a longer path for the blue wavelengths, thus giving positive dispersion. Source from [2].

Dispersion theory calculates the angles and distances needed in order to properly stretch and compress the pulse in our setup. However, it isn't the main crux of this particular thesis. If one would like to read more about dispersion theory, there are many articles that elaborates the theory thoroughly, such as [2].

2.4 Characteristics of the Laser Pulses

At ARC, we used two different laser systems; the RegA and the Legend. Each of these lasers have their own settings, repetition rate, maximum power, etc. The following table notes the characteristics of these lasers.

	RegA	***Legend***
Maximum pulse energy (μJ)	6	120
Repetition Rate (Hz)	Varies, 500 000 maximum	1000
Pulse Length (fs)	45	35
Diameter of pulse (cm)	1	3.2

Table 1: Parameters of both of our laser systems.

The Legend beam that we use actually has a pulse energy in the order of millijoules and passes through a 90/10 beam splitter. We take the 10% transmission beam. The repetition rate on the RegA system can be altered through the trigger division, and we chose a frequency under 10 kHz (in this case, 8930 Hz), as this frequency is the upper limit our pulsed extraction unit can handle safely (Chapter 3.2). We use an iris to limit the diameter size of the Legend pulses to a centimeter, as it is the proper beam size for our reflective lens in our system. We've placed a half wave plate and polarizer pair to control the intensity and pulse energy of our beam.

3 The Imaging Mass Spectrometry System

Our laser would be useless if there weren't any applications. For this experiment, it is used as a source of ablation and ionization of samples inside a homemade imaging mass spectrometer. Designed at the National Research Council of Canada (NRC) in 2013 and moved to the University of Ottawa in 2015, it has never been tested up to its full potential. Before my arrival, it has only been tested on a few noble gases and not much else. I am the first student to use the system, properly optimizing its function and acquiring mass spectrums from ionized solids with the mass spectrometer. This chapter presents the mass spectrometer, its components for sample manipulation, and the basic understanding of its functions. This chapter will also serve as an information manual for new students who'll work with the mass spectrometer in the future.

3.1 General Overview of the Mass Spectrometry System

The system in its entirety can be seen in figure 8 below:

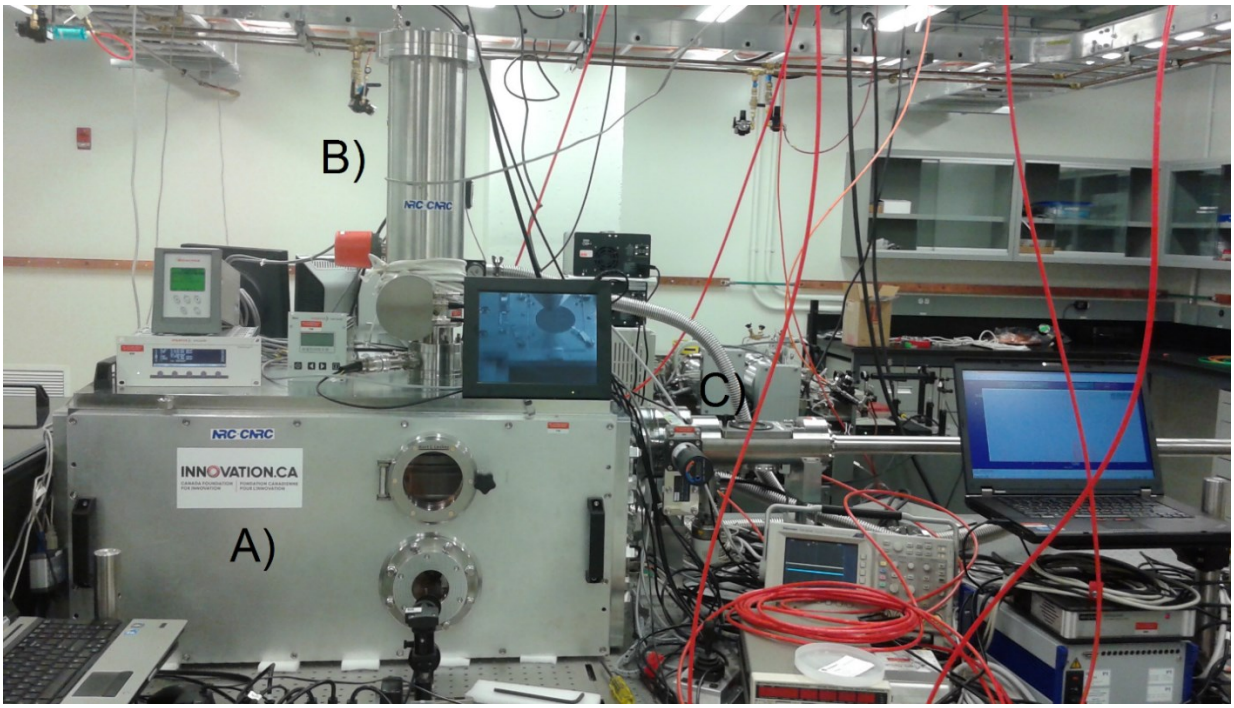

Figure 8: The Mass Spectrometry system, with a) the chamber containing the sample and manipulation system, b) the Time-of-Flight Mass Spectrometer (TOF-MS) and c) the load lock system

The system has four main components.

- The vacuum chamber contains the sample in which we analyse. The laser pulse enters the chamber through an open port and is focussed close to the sample. The focal spot can be changed along the z-axis, so that we can either analyse the gas above the sample, or onto the sample itself. The sample is placed onto a series of position stages to control the position of desorption. Once ions are created, a high voltage electric pulse sends the ions up through the lens of the TOF-MS, where we measure the mass of the molecules.
- The load-lock system is separated from the main vacuum chamber by a removable gate. Its main purpose is to easily remove a sample or place it into the main chamber without breaking vacuum, limiting the exposure of the system to water particles.
- The TOF-MS serves as our mass analyzer in our mass spectrometry system, determining the amount of time that the ions travel inside. Depending on the time delay, the mass of each individual ion can be calculated. It contains many high voltage plates to manipulate the path of the ions, collecting the different kinetic energies of ions with the same mass, and to direct them onto a microchannel plate (MCP) to be detected.
- The MCP, integrated inside the TOF-MS, detects the electrical signal caused by the ions after their flight inside the mass separator. It sends this information to a Time to Digital Converter (TDC), which processes the amount of time each signal was received, and calculates its respective mass. After the mass for each ion has been calculated, this information creates our mass spectrum which we can then analyse.

Each of the following subchapters explains in greater detail how each of these different components of the system function, how they can be manipulated and controlled, and explains possible problems one can have while operating each part of the system. Since the maintenance and operation of the vacuum is a common element throughout the system and can't be operated by an isolated part of the system, it shall need its own subchapter.

3.2 Chamber and Sample Manipulation

Every mass spectrometer needs an ionization source to create ions that are to be measured in the system. As already mentioned earlier in this thesis, both Matrix Assisted Laser Desorption and Ionization, or MALDI [6], and Secondary Ion Mass Spectrometry, or SIMS [7] are accepted and well known ionization and ablation sources for imaging mass spectrometry. However, ultrashort laser pulses have shown that they are efficient at creating ions resulting from ablating a given sample as well. In fact, while being focussed onto a sample, when the pulse length is shorter, less information is lost when ablating the sample, maintaining high spatial

resolution [8, 9]. This happens because the pulse energy has less time to spread out on the sample outside of the laser focal spot. Considering that laser pulses can be tightly focussed, they in theory should be able to be used as a valid alternative to other ionization and ablation techniques used in imaging mass spectrometry.

Our homemade imaging mass spectrometry system has been adapted to use femtosecond laser pulses as the ionization and ablation source. The main chamber of the system contains both the optics to focus the laser and the sample in which we wish to analyse. It also contains the means to manipulate the position of both the laser focal spot and the sample, in order to obtain the spatial imaging of the sample.

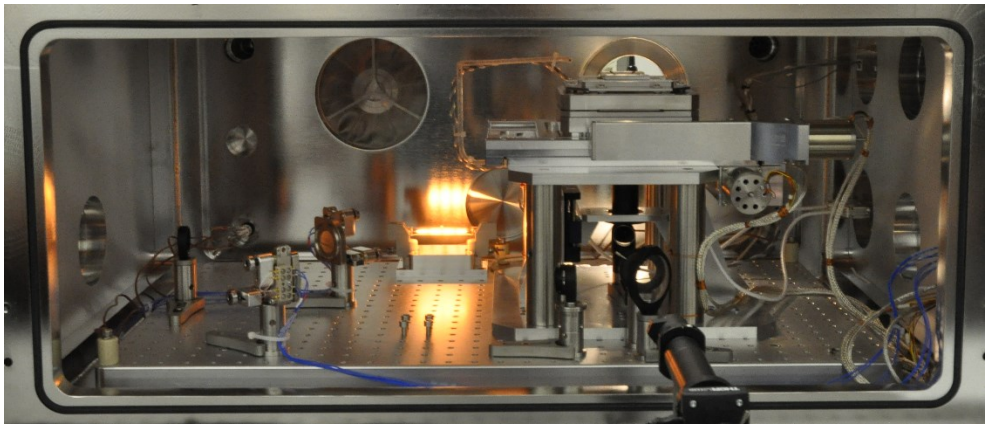

Figure 9: View inside the main chamber, with motorized mirrors, lit lightbulb and the sample manipulation stage.

The chamber itself is constantly pumped with a roughing pump followed by a turbo pump to a high vacuum pressure (1E-6 Torr), to prevent any uncontrolled outside substance and water particles from interfering with our tests. The chamber can also be heated with a lightbulb that can be turned on and off from outside the chamber. This bakes the chamber, reducing the amount of water particles inside the chamber, and consequently the pressure when the chamber is cooled.

The laser pulses enter the chamber through a port hole on the side of the chamber and reflect off two motorized mirrors. These mirrors can be controlled from outside the chamber with a manual controlled joystick, for alignment inside the chamber while it is under vacuum. The pulse then goes through a set of irises and a beam splitter. The beam splitter reflects the pulse towards the manipulation stage, while the transmitted beam is dumped. We use a beam splitter instead of a conventional mirror to allow a CCD camera to see through the optic and focus onto the sample on the manipulation stage.

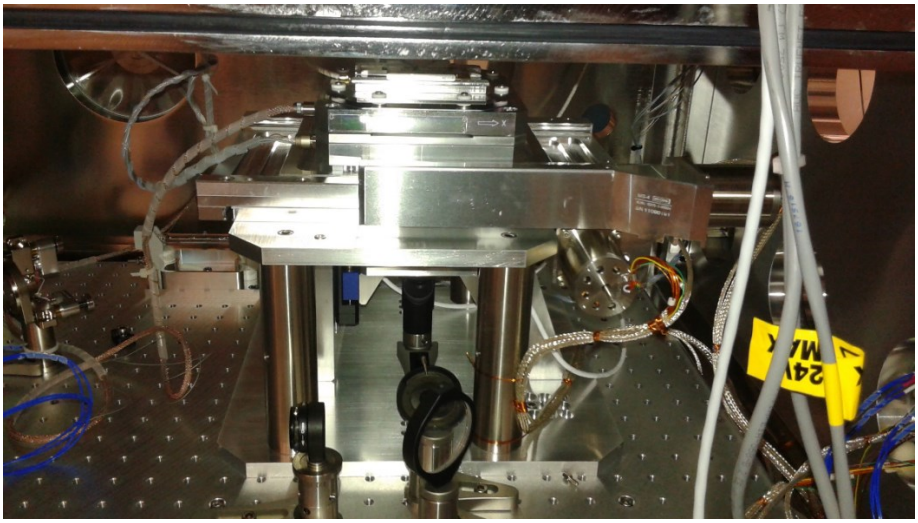

Figure 10: Sample manipulation stage inside the main chamber of the system.

The sample and its holder are placed onto a homemade stage, which contains a series of translation stages and optics. To be clear, the sample is placed onto a nano-precision translation stage, which is situated on top of a micro-precision translation stage, for precise and rough movement respectively of the sample. The microstage has a range of -5 to 5 millimeters in the X and Y axes. The nanostage has a range of 0 to 100 micrometers in the X, Y and Z axes, and can tip and tilt the sample with respect to the X and Y axis up to 500 microradians. This serves the purpose of controlling the location of the laser focal spot on the sample without moving the beam's direction inside the chamber.

The homemade stage also contains our focussing objective to create the laser focal spot needed for ionization and ablation. The focussing objective itself is a Newport 15x Magnification Reflective Mirror system. These are reverse Cassegrain reflectors, which follows the design of a Schwarzschild objective. Light that enters the objective is reflected off a secondary convex mirror that expands the beam onto a primary concave mirror, which focusses the beam past the secondary mirror and the objective altogether. This type of lens design limits any aberrations in the focal spot, compared to transmittance lenses. The design of the focussing objective requires a collimated laser beam, and will only transmit light that is within 9.72 millimeters of the center of the beam. Because of its design, it also obscures 27% of light, since it is a reflective lens and to prevent any backwards reflection off the secondary mirror of the objective, as the center of the beam (and most of the beam's intensity) is reflected back through the hole in the primary concave mirror and doesn't get focussed (Figure 11). It is placed onto a translation stage, which has a

range between 0 and 25 millimeters in the Z axis, which means we can focus the laser pulse either above, onto, or below the sample we wish to analyze.

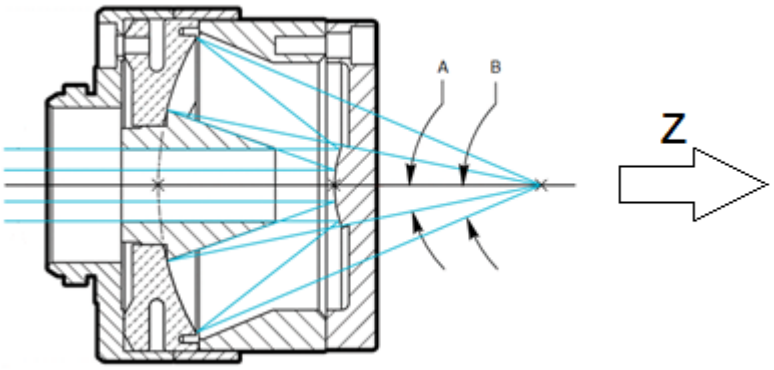

Figure 11: Sketch of the Newport 15x Reflective Objective Lens, taken and modified from Newport. Only the outside of the beam passes through the objective and is focussed. The center of the beam, where most of the intensity of the pulse is situated, is reflected backwards, which corresponds to 27% of the intensity. Since the reflected light is expanding, this light is absorbed by the length of a black tube attached to the entrance of the objective lens. The angles represented by A and B are 12° and 23.6° respectively.

In order for the ions to enter the mass analyzer, they are exposed to an electric field directed upwards towards the grounded funnel entrance of the TOF. This field is made by applying a certain voltage to our substrate. This creates a potential difference between it and the grounded funnel of the lens system, sending the ions upwards into the mass spectrometry system. This substrate requires to be both transparent and conductive, such as ITO or a metallic mesh. This isn't much of a limitation, as a sample desired for analysis can be deposited or placed onto the substrate. There are two modes of operation: constant DC extraction and a pulsed electric field.

A constant DC voltage can be applied to the stage directly by connecting it to the high voltage controller, powered by the high voltage supplier. This supplies a voltage between 1687 and 1891 volts. As soon as the ions are created, they would be exposed to this extraction field and propelled into the TOF cylinder to be analyzed. Because of this, we don't need to worry about the resulting ion cloud, as the ions won't have time to spread away from the ionization point.

We can also pulse the substrate with an electric field. This pulse is created by a high voltage supplier and connected to a pulsed extraction unit. The strength of this electric field can be adjusted between 2065 and 2493 volts on the high voltage supplier, has a rise time of 22 nanoseconds, and a fall time of 24 nanoseconds. Note that this is indeed higher than the voltages

that reflect the ions towards the detector. However, the ions will not receive all of the energy from the stage. Since the sample is ablated off the substrate, the ions will have created some distance between themselves and the pulsed stage. Depending on their position between the pulsed stage and the grounded funnel, they will only acquire a fraction of the energy of the electric field created by the stage as they rise through the lens system of the TOF-MS.

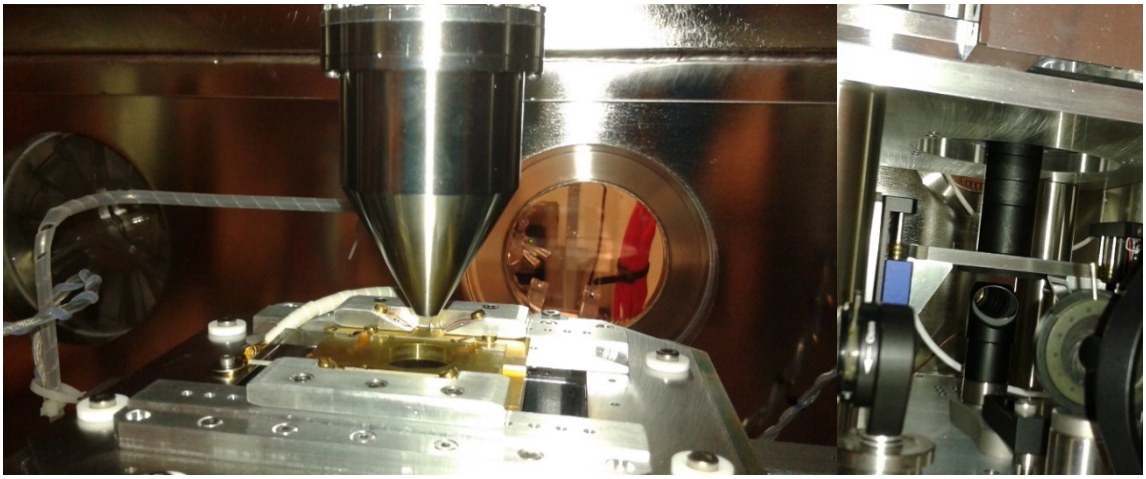

Figure 12: (Left) View of the top of the manipulation stage and the grounded funnel leading to the TOF. The pulsed extraction is connected by the white strand to the left of the manipulation stage, which is conductively connected to the substrate. (Right): View of the translation stage holding the reflective lens, above the mirror directing the beam upwards.

After the ions are created by the laser pulses in our pulsed extraction configuration, they can spread into all directions, not necessarily up into the TOF-MS. To control how much the ion cloud can expand before we apply the extraction field, we apply an adjustable delay between the signal from the master clock of the laser system, and the extraction field. The delay can be controlled with a delay function generator. This delay is needed in order to electrically pulse the substrate after the ions are created, not before. The delay is set to have the highest ion yield, to the precision of a nanosecond. The delay between the signal input of the master clock and the output pulse can further be modified with a ten-pot gauge on the extraction unit, but is left constant. The extraction unit can only fully operate at frequencies under 10 kHz, however. This limits the repetition rate of the lasers that is being used. For the RegA system, which has a repetition rate of 500 kHz, the trigger division was changed so that its new repetition rate is under the threshold frequency of the pulsed extraction unit.

The chamber also contains a leak valve, in which we can allow a limited flow of gas inside the chamber. With this, we can control the pressure inside the chamber, and also choose which

gas to fill the chamber. Typically, we fill the chamber with a noble gas, such as Argon, Krypton and Xenon, and ionize them with the laser pulse. Since noble gases don't react with other substances in the chamber and their isotopes and masses are well known; they are very suitable for calibration of the TOF system.

3.3 Load-Lock System

The load-lock system was designed and implemented into the imaging mass spectrometer to reduce the exposure of air and water particles to the main chamber and TOF-MS of the system. It serves to insert and remove samples from the main manipulation chamber without breaking the vacuum. Thus, replacing and/or manipulating the sample can be done easily outside the chamber without taking time away by frequently breaking vacuum and pumping it back down to a suitable pressure.

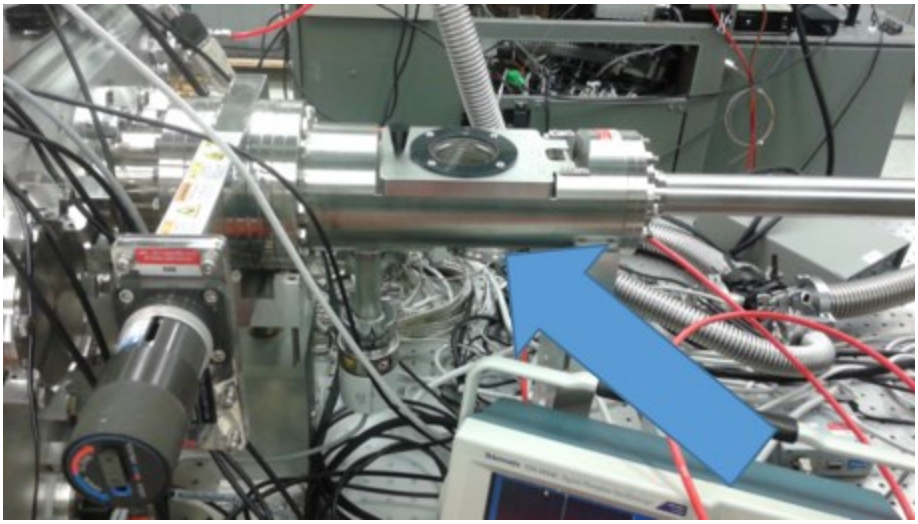

Figure 13: Load-lock chamber, with the main chamber to its left.

This part of the system contains a small vacuum chamber, a gate valve and a long metallic rod. The vacuum chamber is the sample's entry/exit point into the main chamber, as it is easier and quicker to alter the pressure inside this relatively small space, compared to the main chamber of the system. The sample is placed onto a conductive sample holder, which is then screwed onto a metallic rod which can be magnetically rotated and displaced along the rod's axis. The gate valve separates the load lock from the main chamber, so that we can change the pressure of the load lock without affecting the vacuum inside the chamber. Once pressure for both the chamber and the load-lock are equal, the gate valve is opened and the sample holder is placed onto the sample manipulation stage in the main chamber, with the help of a camera and monitor.

The sample holder is held in place on the manipulation stage while the metallic rod is being unscrewed. Once the rod is removed from the chamber, the gate valve is closed, and manipulation of the sample and operation can begin.

3.4 Time-of-Flight Mass Spectrometer

Every mass spectrometer needs a mass analyzer, an apparatus to separate the ions with different mass per charge ratio. There are many analyzers compatible for mass spectrometry, each with their own advantages and limitations. Some utilise magnetic sectors [10], exposing the ions to a magnetic field to take advantage of the ions circular motion to gain resolution of the mass-per charge ratio value. However, they can require a vast amount of space and the magnetic field by itself cannot take into account similar ions with different kinetic energies. Others use quadrupoles [10], a set of four electric rods that filter the ions to allow a certain range of masses to pass through. Some mass spectrometers use a combination of multiple mass analyzers together as one [11]. For our mass spectrometer, we need a mass analyzer that is relatively small to conserve lab space, and can obtain a large range of mass per charge ratios while maintaining some precision. For these reasons and its simplicity, a Time-of-Flight apparatus was chosen as our mass analyzer.

The Time-of-Flight Mass Spectrometer (TOF-MS) separates the ions that were created in the main chamber (3.2) by their respective mass through the various ion optics inside the cylinder. Depending on the amount of time between the ions being sent up into the TOF-MS by the electric pulse on the manipulation stage (3.2) to being detected on the microchannel plate (MCP) detector inside the cylinder, the mass can be calculated. Since it only requires the time between extraction and detection of each ion, it is potentially unlimited in its range of ion mass detection, whether they be heavy or light. The details of the detection and measurement of these signals will be elaborated in the next section. This subchapter explains how the ions are separated and focussed onto the detector with the aid of the various ion optics inside the system, their use and how one can change these settings at a later time.

Generally, after the ions are created and sent up to the TOF-MS, they are focused by a lens system. Afterwards, their path is shifted in a particular direction so that the ions will hit the detector after their trajectory is complete and not fall back down into the main chamber of the system. After that, they are reflected onto the detector by a reflectron (3.5.3), which cancels out any kinetic energy differences between ions of the same mass.

3.4.1 How is the Mass per Charge Ratio Related to Time?

In order for a Time-of-Flight mass analyzer to determine the mass per charge ratio of each ion that passes through, we need to know how one is related to the other. For this example, we will assume that the detector is at the end of the TOF cylinder. In any given electromagnetic system, energy is conserved. The ions in our system are given potential energy based on the voltage that we supply them from the pulsed extraction unit. Since there is no loss of energy in the system, all the potential energy of the ion gets transformed into kinetic energy. Thus,

$$E_P = E_K \tag{1}$$

To be more specific, for the ion,

$$qU = \frac{1}{2}mv^2 \tag{2}$$

Where *q* is the charge of the ion, *U* is the extraction field voltage of our system, *m* is the mass of the ion, and *v* is its velocity. We isolate our mass per charge ratio in (2), because we want to know more about its relationship to the other variables in our system.

$$m/q = 2\,U/v^2 \tag{3}$$

The ions path can be separated into two parts; one where the ion is accelerated and its energy converted from potential to kinetic, and one where its velocity remains constant through the TOF cylinder as it drifts. Considering that the distance travelled during the former is negligible compared to the latter, we can approximate the velocity of the ion as a function of the drift distance over time.

$$v = D/t \tag{4}$$

Substituting (4) into (3):

$$m/q = 2U\left(t/D\right)^2 \tag{5}$$

Considering the voltage we provide, the distance of the ion's path through the TOF tube, and the number 2 are constant, we can replace this by a constant *C*, so that the relation between the time of flight of the ion and its mass per charge ratio is evident.

$$m/q = Ct^2 \tag{6}$$

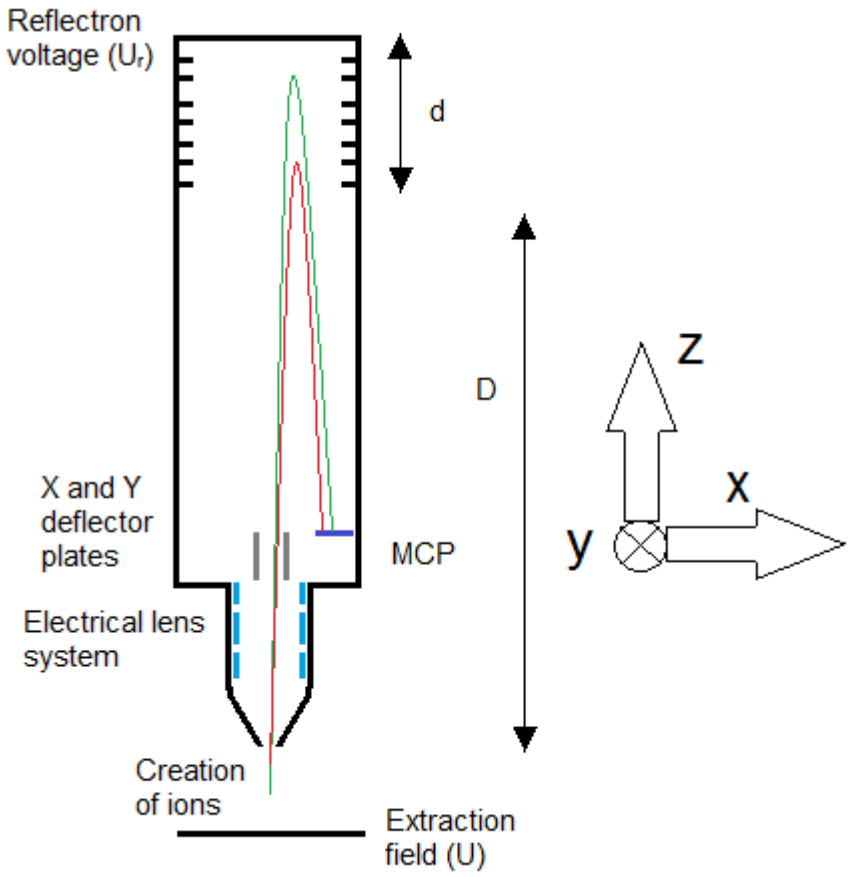

Figure 14: Sketch of the path of the ions, from creation to detection.

The path of the ion might slightly vary, depending on its kinetic energy, location of the ion creation, etc. These are corrected through various electrical optics in our system, such as the electrical lens system, the X and Y deflector plates, and the reflectron. The latter is especially important, as it corrects the kinetic energy spread of the ions, by adding to their time of flight to those of similar mass, but higher energy. For a single voltage reflectron system, it adds time to their path following this equation [12]:

$$t_{reflectron} = 2d\left(\sqrt{2U}/U_r\right)\left(\sqrt{m/q}\right) \quad (7)$$

Where *Ur* is the highest voltage on the reflectron. What is crucial is that the mass per charge ratio is directly proportional to the time of flight, squared. This general relation between the two is needed when calibrating the TOF-MS. For those students who are learning how to use this system, the calibration process and how this general equation comes into play is discussed further in both Chapter 4 and appendix B.

3.4.2 Lens System

When the ions are created, they will naturally repel each other. This happens because of their similar positive charges. In addition, the transfer of heat of the plasma to kinetic energy of the ion also makes the ions separate. Approximating the temperature of the plasma is a couple of electronvolts (or 30 000 K) and a Maxwell-Boltzmann distribution, the most probable velocity of these ions can range between 1.5 mm/μs (Radon) and 22 mm/μs (Hydrogen). This is quite large, considering the distance between the substrate and the entrance to the TOF-MS is millimeters, and we're working in the timescale of a microsecond between ionization and the electrical pulse that sends the ions into the TOF-MS. In addition, the electric pulse will only send the ions in one direction, which doesn't change the velocity and spread of the ion cloud in the two other dimensions. The lens system counteracts the lateral movement of the ions and pulls them into the TOF-MS through a series of electric plates.

Figure 15: The lens system outside of vacuum, with the grounded funnel not attached. The funnel would normally be over the insulator (in white on the right). Repairs were done on the wire near the insulator. This is discussed more at figure 17. The wire connects the active element underneath the insulator to the voltage controller. The length of the tube after the insulator is grounded as well.

The lens system that we use for our mass spectrometer is an einzel lens. It has three sets of cylindrical electric apertures, with only the middle aperture being set at a certain voltage. Both of the apertures at either end of the lens system are grounded. An einzel lens has a symmetrical electrostatic potential so that the ion's energy isn't altered, but focuses the ion beam at a certain point after the lens system. The focus point can be tuned, depending on the voltage we place on the active element. At the end of these elements is an aperture that limits the size of the ion beam, preventing unwanted particles from entering the mass analyzer (Chapter 3.4.4). The outer particles are blocked by this aperture. This is ideal because they arrive at the focus point later compared to the ions at the center of the beam because of their longer distance travelled, and

will prevent further ion beam dispersion inside the mass analyzer. The active element is tuned in a way that the focus point arrives at this aperture. However, the einzel lens needs a somewhat collimated ion beam, where our cloud of ions is spreading in all directions. This is why we need a second lens to create this initial partially collimated beam. This is done by the grounded funnel situated at the entrance to the TOF cylinder (as seen in Figure 12 on the left). It is the first aperture in the lens system.

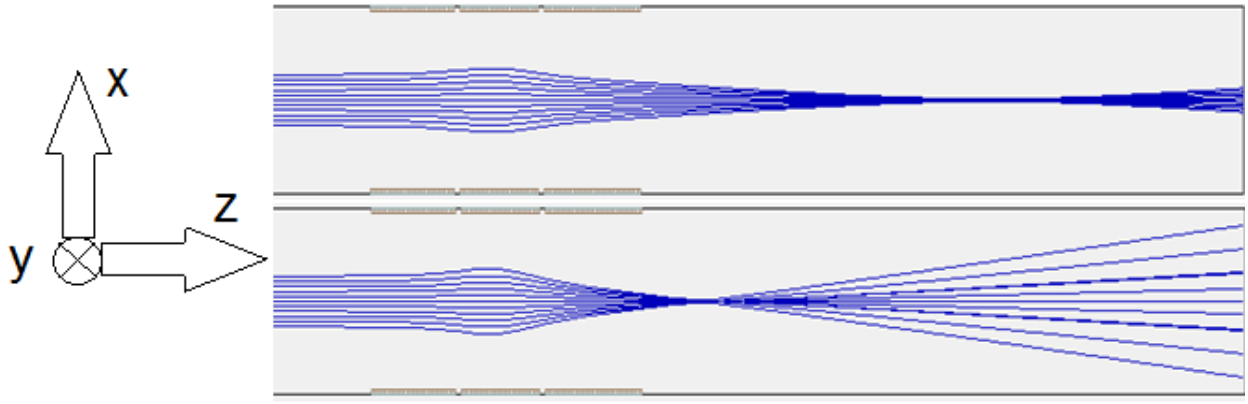

Figure 16: Two slightly collimated ion beams going through an einzel lens system run on SIMION 7.0, one with the active element set at 150 Volts (top) and the other set at 180 Volts (bottom). Changing the active element's voltage changes the focal spot of the ions after the lens system. The ion beam is slightly diffracted by adding a 1.00E-7 charge repulsion on the program.

The aperture is curved as a funnel to compensate the lateral movement of the ions away from the lens. The funnel also serves to block ions that move too far laterally from its entrance. The compensation of the ions with small lateral movement and the rejection of the ions with large lateral movement creates our partially collimated ion beam needed for the einzel lens system after the funnel (figure 15).

There was a problem with this lens, however. As one can see from the figure below, while the system was at the National Research Council (NRC), one of the lens' wires, the one supplying the high voltage to its active element, burned through the insulation and caused electrical damage. As it was necessary to remove the TOF system from the main chamber and take it apart to reach this wire on the lens, we decided that it would be an ideal time to move the system from NRC to the Advanced Research Complex (ARC) on the University of Ottawa's campus. This delayed in the research project. During the move, the insulator was fixed and the lens now functions properly.

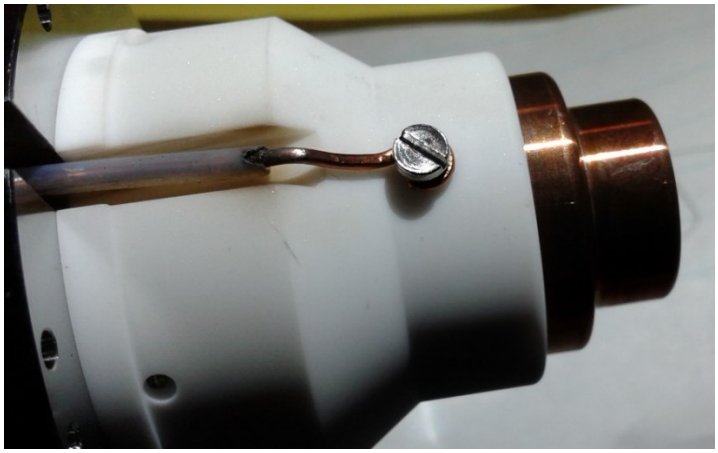

Figure 17: Close up of the active element of the lens system of the TOF-MS and the damage to the wire connected to it. The wire burned through the insulation and caused an electrical short to the system.

3.4.3 X and Y Deflector Plates

After being focussed through the lens system, the ions need to be detected. However, they are sent along a straight line along the lens' axis. If there isn't any ion optic to shift the ions laterally in the X and Y axes (Figure 14), the ions would enter the system and after being reflected by the reflectron, they would follow the same trajectory downward, back into the system, never being detected by the MCP. The X and Y deflector plates gives the ions a slight push in these axes so that their parabolic trajectory arrives onto the detector and not back into the main chamber.

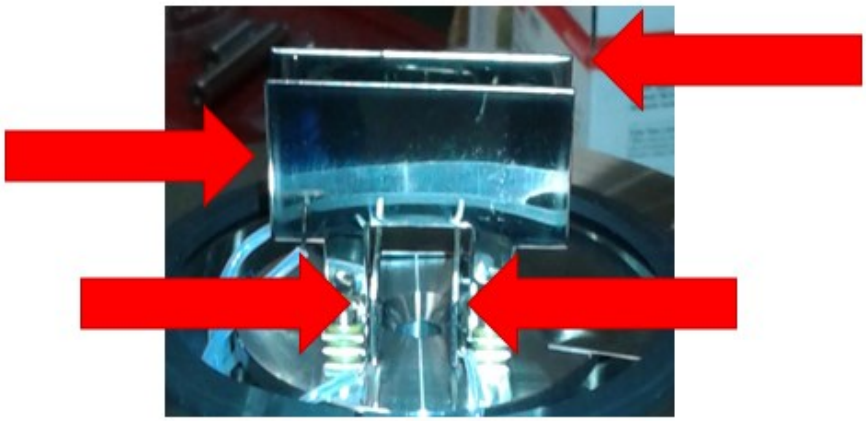

Figure 18: The X and Y deflector plates, attached above the lens system. In the picture, it is situated outside the chamber.

The X and Y deflector plates are two pairs of electronic plates. Each pair can be set at a certain voltage independent of the other. For each pair, one of the plates can be set at a voltage between -50 and 50 volts. The other plate of the pair will be set at the same voltage, but with the inverse sign. For example, if one plate is set at 34 volts, the other will automatically be set at -34 volts. These voltages are supplied and controlled by the high voltage controller (Kore TOF-MS Voltage Controller, see Appendix A-v). Depending on the voltage we set on one pair of plates, the ions are shifted in that axis (the X axis for the X pair, and the Y axis for the Y pair). This way, we can set it so the ions will be shifted from the lens system onto the detector inside the mass spectrometer system.

3.4.4 Reflectron

Since the ions are spread out before being sent into the TOF-MS, they will each acquire a different amount of kinetic energy, depending on their position relative to the substrate and its electrical pulse, and the grounded entrance to the mass spectrometer. Two ions of the same mass with different kinetic energies will have different flight paths, similar to two bowling balls of equivalent mass being thrown straight up into the air at different speeds. The thrown bowling ball with the higher velocity will have a longer trajectory in the air compared to the one with a smaller velocity. Since the principle of TOF-MS requires that ions of the same mass have the same time-of-flight (thus the term Time-of-Flight Mass Spectrometer), we need to cancel out the difference of kinetic energies of these ions with similar mass. This can be achieved with a reflectron.

Figure 19: A view of the reflectron inside the mass spectrometer. Each individual electrode can be seen as lines and gaps between the grounded electrode at the end of the chamber.

A reflectron is a series of electrodes, reflecting the ions back onto the detector. Each of these electrodes can be set at a different voltage to create a gradient. This is how we cancel the kinetic energy of the ions. The first plate is grounded, and two other plates can be set at a precise voltage that we control. The middle electrode can be set between 937 and 1139 volts, and the electrode at the other end of the reflectron can be set between 1891 and 2092 volts, both supplied by the high voltage supplier. Each electrode between these are linearly charged to create two distinct electric gradients, allowing for second-order corrections. Let's take two ions of the same mass (say, Argon) but with different kinetic energies as they enter the reflectron. The argon ion with the higher velocity penetrates further into the reflectron before it is reflected back onto the detector, resulting in a longer flight path. The argon ion with the smaller velocity doesn't penetrate as far, but it takes a smaller flight path. If the voltages are properly set, all the ions with the same mass will arrive at the same time onto the detector, and thus have the same time of flight inside the mass spectrometer.

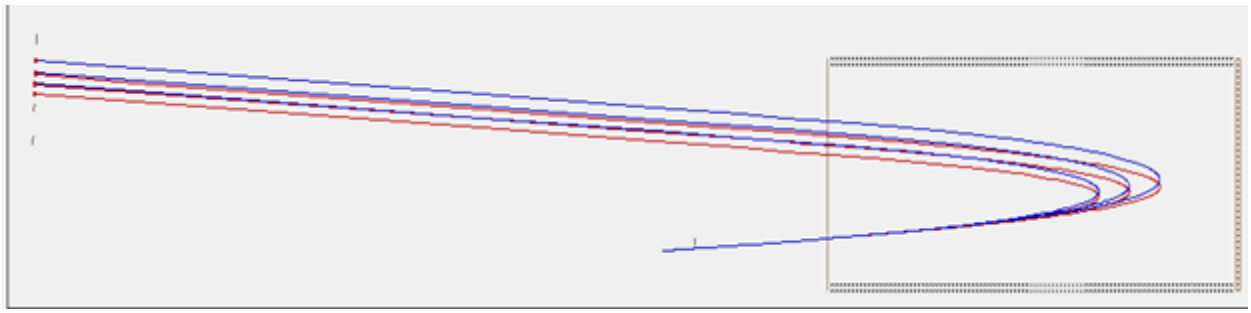

Figure 20: Simulation of ions with different mass and kinetic energies entering a single gradient TOF-MS, done with SIMION 7.0. The lighter ions travel along the blue path, while the heavier ions travel along the red path.

Initial Ion Energy (eV)	***TOF, 10^{-6} amu (μs)***	***TOF, 100 amu (μs)***
1	0.00172179	12.6966
91	0.00175317	12.6652
181	0.00179287	12.722

Table 2: Time of arrival of different ion masses with various initial energy, from our SIMION 7.0 simulation, to demonstrate the use of the reflectron in our system.

Figure 20 above demonstrates a basic single gradient TOF setup with ions of different masses and kinetic energies. One of the set of ions has a mass of 1E-06 amu, which is very small. However, the figure is to show visually how those ions have different paths from heavier ions, and that mass was chosen because of its visual clarity, compared to higher ion masses.

With this example, the ions with higher energy penetrate further into the TOF-MS, but they still arrive at roughly the same time onto the detector, within 60 nanoseconds for the heavier ions (100 amu, red) and 70 picoseconds for the very light ions (1E-06 amu, blue). The heavier ions don't travel as far transversally as the lighter ions (because they have similar energy and higher mass, so their velocity is lower), so we must know if the ions are indeed contacting the detector. That can be adjusted with the X and Y deflector plates (3.4.3).

3.5 Detection and Acquisition of Data

Creating ions and making them travel a specific path that separates them by mass per charge is all well and good, but it serves nothing to a mass spectrometer if we do not have a detector or a data acquisition system. For a detector, we use a dual microchannel plate (MCP) inside the TOF system. It came pre-installed in the TOF system.

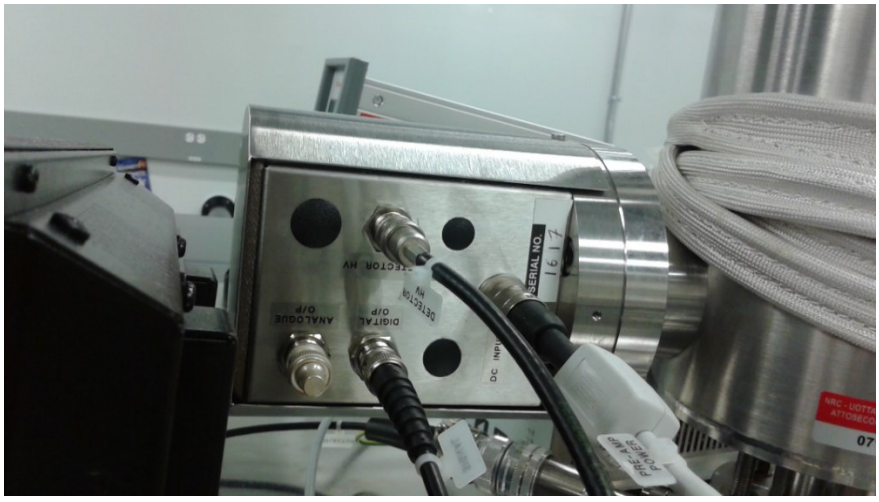

Figure 21: MCP pre-amplifier system, with the TOF flight tube to its right.

As the ion collides with the detector, it sends a signal which is amplified by a pre-amplifier towards a Time-to-Digital Converter (TDC). Typically, a TDC recognizes the interval of time of a particular signal (in our case, the signal of ions detected on our MCP) after an initial event/signal (the extraction of our ions into the TOF cylinder), and outputs a digital signal that corresponds to the interval of time between these two signals. In our system, there is a signal sent to the TDC

for every signal detected by the MCP made by each ion that is extracted from the sample. Comparing these signals to the initial signal of extraction, the TDC calculates the flight time of each ion and, based on that time, previous calibration tests and the parameters calculated from those tests (which will be discussed in further detail in Chapter 4 and Appendix B), the mass per charge ratio is calculated for each particle that was ionized in that particular cycle. This process is then repeated until the user is satisfied or the sample spot has been completely ablated.

Since we have two modes of operation, we need two distinct signals applied to the TDC to correspond as the beginning of the ions' flight time. For the constant DC voltage mode, we use the signal from the laser pulse as it focuses on the substrate. For pulsed operation, we use the signal from the extraction pulse which sends the ions up into the mass analyzer. These signals are a value of 5 Volts, as they are simply needed to indicate the start of the cycle. No stronger power is required for the TDC. The MCP detector indicates the end of their flight.

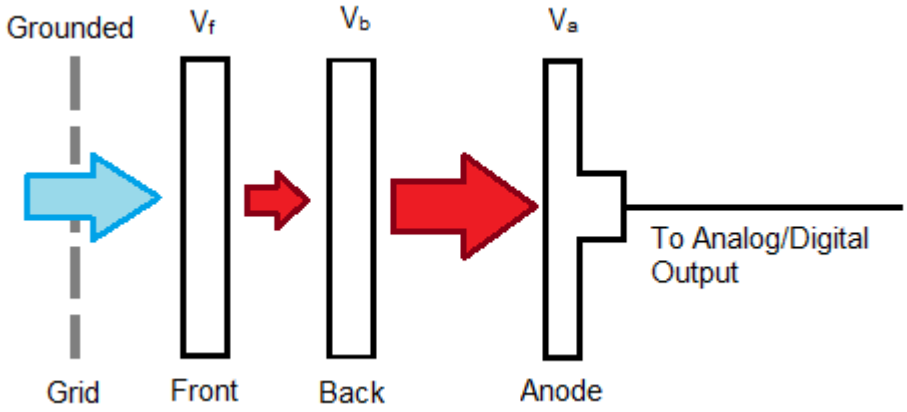

Figure 22: Sketch of the MCP detector, with V_f, V_b and V_a all representing negative voltage, and $|V_f| > |V_b| > |V_a|$. The ions (blue arrow) pass through a grid, grounded in our setup before colliding with the front plate, resulting in secondary electrons (red arrow) from the collision. These electrons collide with another plate, causing even more electrons, which will then be picked up by the anode. This signal is then sent to our Analog/Digital output for analysis.

The MCP detector has a diameter of 25 millimeters to compensate for the fact that the path and point of arrival of ions of different mass per charge ratios are different from one another. The front plate of the MCP can be biased with a voltage between 0 and - 4900 volts, but we set it at -2700 volts to prevent any high voltage damage. The voltage also determines the bias on the back plate and the anode of the detector. This bias leads to the ions producing secondary electrons that avalanche through the plates, amplifying the signal. This bias also prevents ions that weren't created by the ablation process from being detected, since they do not follow the

proper path to the MCP. This way, we are certain that whatever we detect comes from the sample and not from a secondary ion source created in the intervening time.

Considering the signals created by ions colliding with a detector can be quite weak, they are amplified by the MCP. This is to distinguish the signals that we obtain from the detector from any noise, be it electrical or from an outside source. These amplified digital signals are then sent to the TDC. To eliminate any noise from being detected on our system, the digital output has a threshold of 30 mV, cutting off any signals below that. An analog output can also be viewed if desired.

The TDC functions as a series of cycles, combined together to run as a single experiment. For each of these cycles, there are three different times that can be adjusted in the mass spectrometer's acquisition software; the cycle time, and the start and end of the data range. The data range represents during what time in the current cycle the data that is collected will be stored into the software, and calculated. If there is a signal that arrives at a time that is not within the data range interval, the signal is rejected by the TDC.

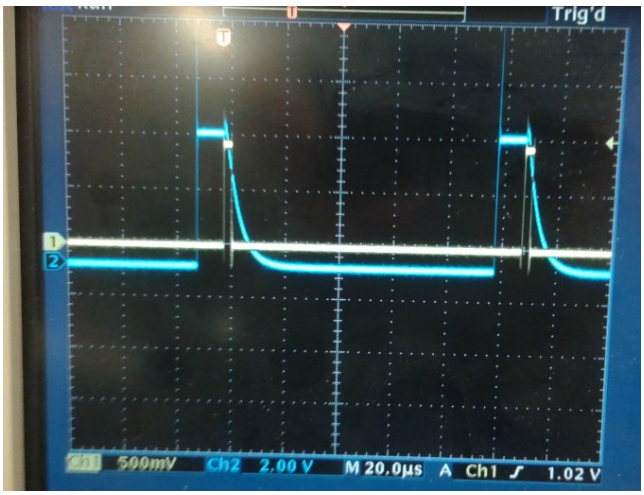

Figure 23: Input (yellow) and output (blue) signal from the TDC. The input represents the extraction pulse that is synched with the ionizing laser pulse inside the system. The output signal represents the cycle time. When it is on the rising edge, the TDC is ready for detection. The falling edge represents the end of the measurement interval, while data is only kept for a certain range of this measurement time, as inputted on the measurement software.

For each of our two modes of operation (DC voltage and pulsed extraction), we need to define the start of their respective cycle time. For pulsed voltage, the cycle time represents the delay between the extraction pulses on the substrate that sends the ions up into the TOF tube. It

is set in a way that an extraction pulse coincides with a single laser pulse ablating and ionizing the sample, and the second extraction pulse coincides with the second laser pulse, and so on. For DC voltages, the cycle time starts from the signal received from the Master Clock of the laser system being used.

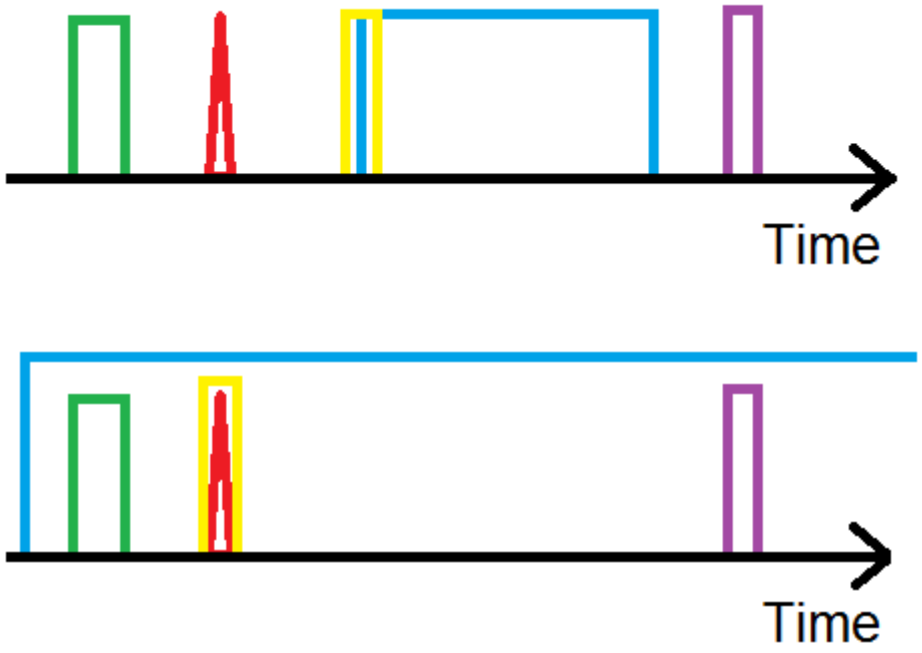

Figure 24: Visualization of the timing of the measurement cycles, for pulsed (above) and constant (below) extraction. The green signal corresponds to the Master Clock and the red corresponds to the laser pulse. The time interval between these two can't be altered. The blue signal corresponds to the extraction field on the stage. The yellow signal corresponds to the start of the measurement cycle, related to the start of the flight time of the ions, and the purple signal corresponds to their measurement on the MCP.

In order to sync the start of the cycle time to the extraction field on the stage, a digital delay generator was placed to delay the Master Clock signal to the TDC, so that this pulse can coincide in time with the extraction of the ions with picosecond precision within the system. We also utilize the previously described leak valve to leak noble gases into the system to calibrate the software to sync the proper mass per charge ratio to the signal's arrival time compared to the extraction pulse. The process to obtain the calibration parameters of the software and the optimal ion yield based on the delay between the extraction and laser pulses can be found in the following chapter.

For constant extraction, the delay doesn't matter as much as for pulsed extraction, since the ions won't have time to spread; they will be sent directly. Since the Master Clock signal and the laser pulse don't arrive respectively to the TDC and at the substrate simultaneously, the delay between two will affect the calibration parameters. However, this will only shift the peaks in time linearly with the delay placed on the digital delay generator. To find the proper delay, we placed a photodiode (Thorlabs PDA10A) to detect the laser pulse in our optical setup before it reaches the main chamber, and adjust the delay so that the two pulses overlap.

Figure 25: The digital delay generator (DDG) for the Legend laser system (Stanford Research Systems, Model DG645), used when in pulsed operation. This delay is between the master clock of the laser system and the extraction pulse, not between the later and the arrival of the laser pulse. Considering that the delay between the master clock and the laser pulse is fixed, changing the delay between either of them to the extraction pulse will delay the other as well. It has a resolution of a picosecond.

4 Calibration and Results

Considering it was finished being built slightly before my arrival in Ottawa, the mass spectrometer that we are using was tested and shown to be operational. However, these tests were only on lighter gases such as nitrogen and water particles, and a few noble gases such as argon and krypton. Not only was it not used for any papers, articles or publications, it was never tested for solids. This is crucial because we can't efficiently test the spatial imaging prospects of this mass spectrometer, let alone the idea of using ultrashort laser pulses as the ionization and ablation method, on gases. I'm the first student to test this mass spectrometer for solids, calibrating the mass spectrometer and laser for this purpose, and to test the spatial imaging properties and limits of this machine.

4.1 Noble Gases

I performed tests on noble gases with both the Legend and RegA laser systems. Noble gases were used because they won't react nor recombine with any molecule or ion in the chamber during their flight. Because of their well-defined m/q values, noble gases are ideal for calibrating the time-of-flight to a specific mass value. Additionally, noble gases have well defined isotope values and ratios between them, which will be useful to calibrate quantitatively our results for not only gases, but for solids later on.

4.1.1 Pulsed Extraction

For pulsed operation, we tested mainly Argon and Krypton. We also used Xenon to calibrate for heavier ions. To properly detect and calibrate the system for Argon, first we looked at other gases that would naturally be inside our system. Considering that the vacuum in our chamber will never be perfect, we will always note a peak for O_2 and N_2 from ambient air in our system, as well as H_2O.

We were able to calibrate, somewhat, the conversion settings of the TDC by looking for these peaks in our spectrum, corresponding to 32, 28 and 18 atomic mass units (amu) respectively. With that, finding argon at roughly 40 after leaking it into the chamber was simple. Thus, we calibrated further down the m/q axis with this peak. It also helped that the second ionization of argon appeared as a small peak at 20, to add precision to our calibration. However, this does indicate that our pulse energy is too high.

After this, Krypton gas was leaked into the system. With the calibration done with Argon previously, finding the right values for this gas was easy. However, the ratios between isotopes of krypton was not correct. The three rare stable isotopes of krypton at 82, 83 and 86 all appear, but they should be at 11.5%, 11.6% and 17.3% compared to the main isotope's 57.0%. This is due to the gain on the MCP being too weak to amplify these small peaks past the 30mV threshold of the pre-amplifier. To fix this, we increased the gain value on the MCP detector. This is further explained in Chapter 4.1.3.

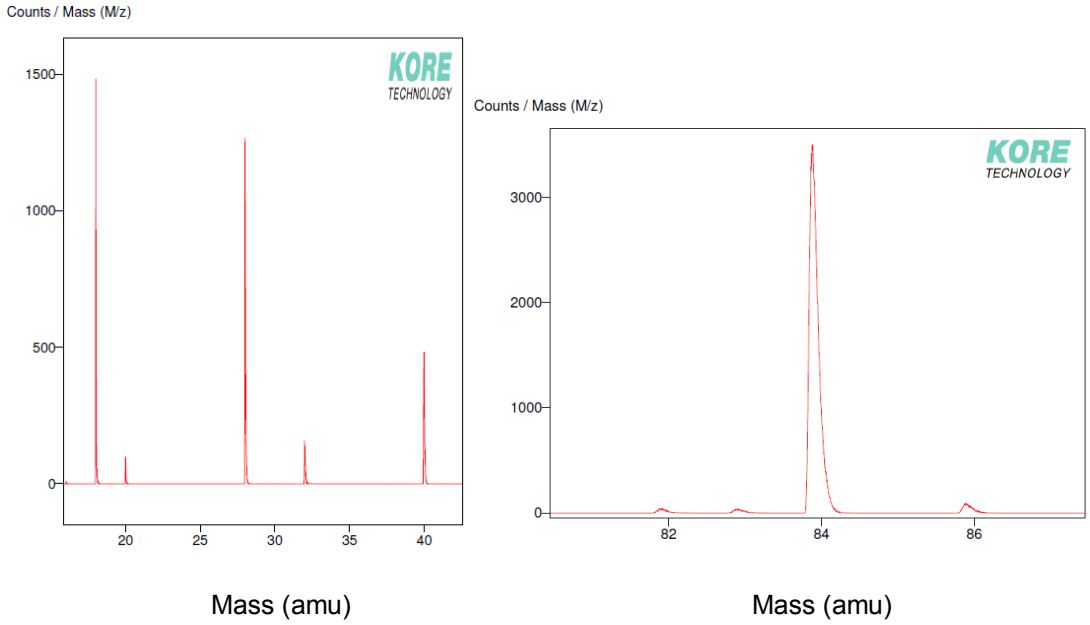

Figure 26: Counts per mass of gases inside the mass spectrometer after calibration. Tested for leftover air in the chamber and argon (left), and krypton and its isotopes (right).

Lowering the focal spot closer to the substrate does cause some problems. When the extraction pulse is set to its lowest value of 2065 Volts during pulsed operation, we note that there is a blind spot where no gases were detected, anything closer to the substrate than 700 microns (Figure 28). This is because the extraction pulse is too strong for the reflectron to properly send the ions towards the MCP.

4.1.2 Constant Extraction

For our continuous voltage operation, we tested noble gases with the RegA laser system (Chapter 2.4). We tried Krypton and Xenon, noting the similarities from our tests with gases during the pulsed voltage configuration. When the focal spot of the pulse is located above the substrate, the results of both configurations are quite similar. Their location on the mass spectrum

was constant, maintaining their atomic mass unit value for each isotope. There is a small change in isotope ratios between pulsed and constant extraction, but the ratios still do not correspond to their theoretical values. However, when we approach the focal spot much closer to the grounded funnel entrance to the TOF cylinder, we note another blind spot, compared to none for pulsed extraction. This is because the ions receive much less energy because of the lower extraction field, not receiving enough energy to pass through the ion optics in a way to be detected by the MCP.

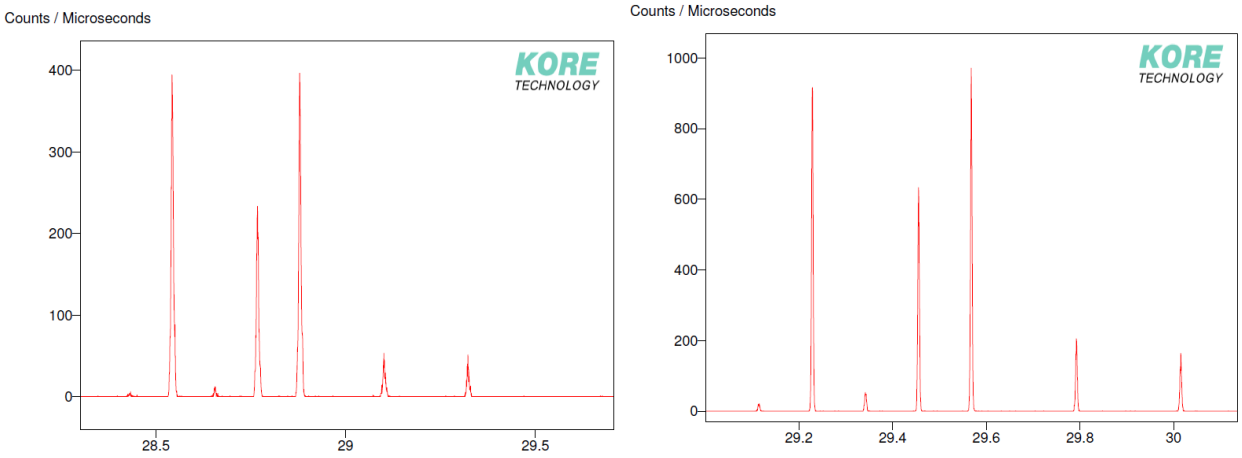

Figure 27: Count per flight time of Xenon with pulsed extraction (left) and constant extraction (right). The flight time difference corresponds to the different starting point of the cycle time of the two configurations.

When not in this blind spot located close to the entrance of the mass analyzer, switching from pulsed operation to constant voltage as our extraction field has made no significant difference for noble gases. The only change is that the calibration parameters have slightly changed to account for the new start time for our measurement cycles, from the extraction pulse to the master clock signal.

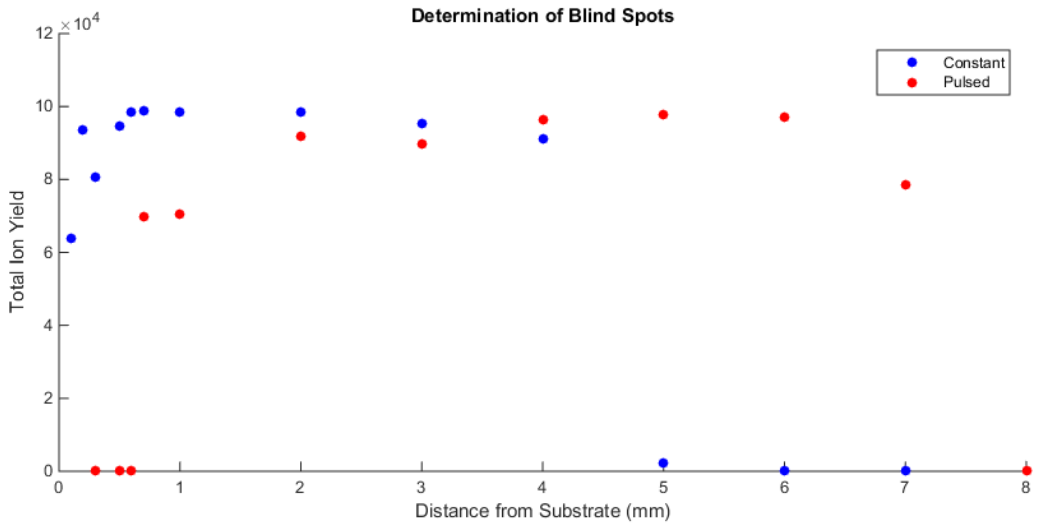

Figure 28: Finding the blind spots for both extraction configurations by observing the total ion yield from Krypton when approaching or distancing from the ITO substrate. For pulsed extraction, the blind spot can be seen below a millimeter in distance from the substance on the left.

The most significant change in our tests of noble gases between pulsed and constant extraction is the elimination of the blind spot when in the pulsed configuration. If we recall, any location of the focal spot of the laser below 700 microns above the substrate yielded no ions whatsoever. This was because when the ions were too close to the extraction pulse and obtaining copious amounts of energy, the reflectron couldn't correct them and they would simply collide onto the edge of the cylinder. Considering that the constant extraction configuration has a weaker amplitude than pulsed extraction, switching the configuration to a constant output voltage allowed for a smaller extraction field, reducing the energy of these ions to a point where they can be reflected towards the detector.

With this, we can say that for noble gases, both configurations can function for mass spectrometry. However, with our current configurations, only the DC voltage configuration can be lowered towards the substrate while still being able to process data. Further work will be done to find a lower voltage power unit that can be used for our pulsed field configuration, to see how the results of noble gases are affected when the focal spot is closer to the source of the electric field.

4.1.3 Gain Change for Improved Isotope Ratios

The proper ratios of the gases can be achieved by altering the gain on the MCP. The main problem with the detector, its digital output and its transfer of data to the GRAMS software

is the 30 mV threshold that eliminates noise from the signal. While this is needed, if the signal isn't strong enough, the resulting peak caused by the ion and its corresponding signal will be truncated. This is harmful for weak peaks, like the smaller isotopes from krypton, the 133 peak from indium, etc. Furthermore, the MCP degrades over time, and thus so will the resulting signal.

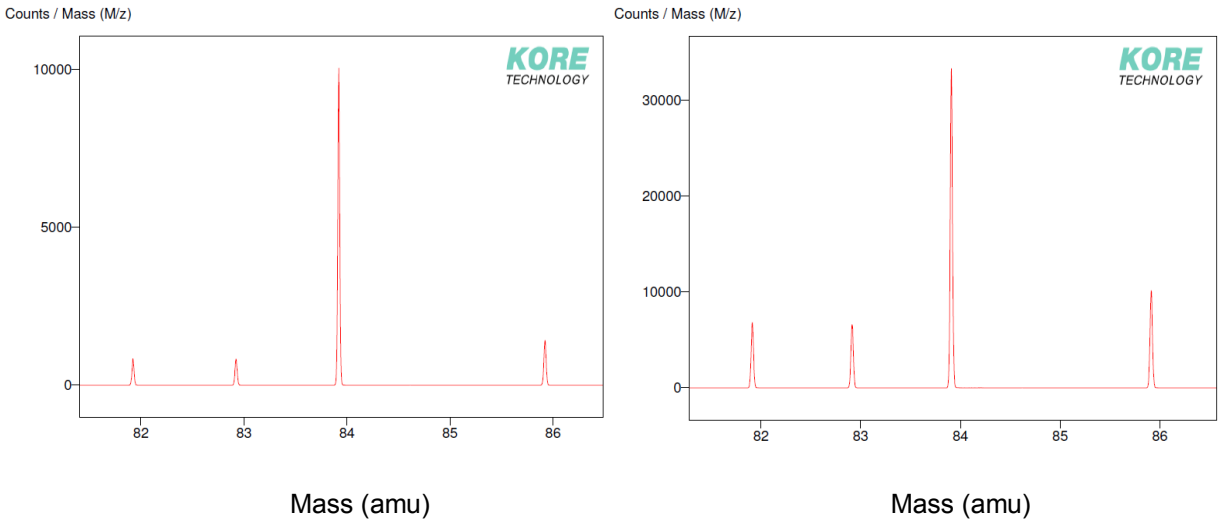

Figure 29: Signal of Krypton isotopes before (left) and after (right) (from -2738 to -2849 Volts) change of gain on the front plate of the MCP.

By altering the gain, the resulting electron avalanche from the MCP will be stronger, increasing the amplification of these signals, passing the voltage threshold for the digital output, which is useful for the smaller isotopes peaks that we find in our scans. As the signal made by the electron avalanche won't be perfectly constant, this will result in some data from a peak not crossing over the threshold, for lower intensity peaks. Thus, increasing the gain will verify that every peak will cross over the threshold. We cannot set the gain on the MCP too high however, as this could lead to saturation of the signal, leading to the wrong isotope ratios. With this increase in gain, the isotope ratios between the peaks match with the theoretical results required. Thus, we calibrated these noble gases quantitatively as well as their position on the mass spectrum.

4.2 Solids and Substrate

Most of our preliminary tests on solids were done on ITO substrates. This is useful, as future samples that are to be tested will either be placed or deposited on the substrate. The stability of this substrate because of its deposition on glass is also advantageous over other conductive substrates, such as a metallic mesh. Before testing other samples, analyzing ITO will

also allow us to know which peaks comes from this substrate and which peaks come from the tested sample.

To find the proper height of the focal spot to ablate our sample, we reduced the height of the laser spot by lowering the reflective lens, and scanning the substrate at this height. We would then note the ion yield from the sample at this height, and then lower the focal spot again, scanning through the ITO substrate. Further tests are done at the height where the ion yield is maximized. For this, we used the pulsed extraction configuration.

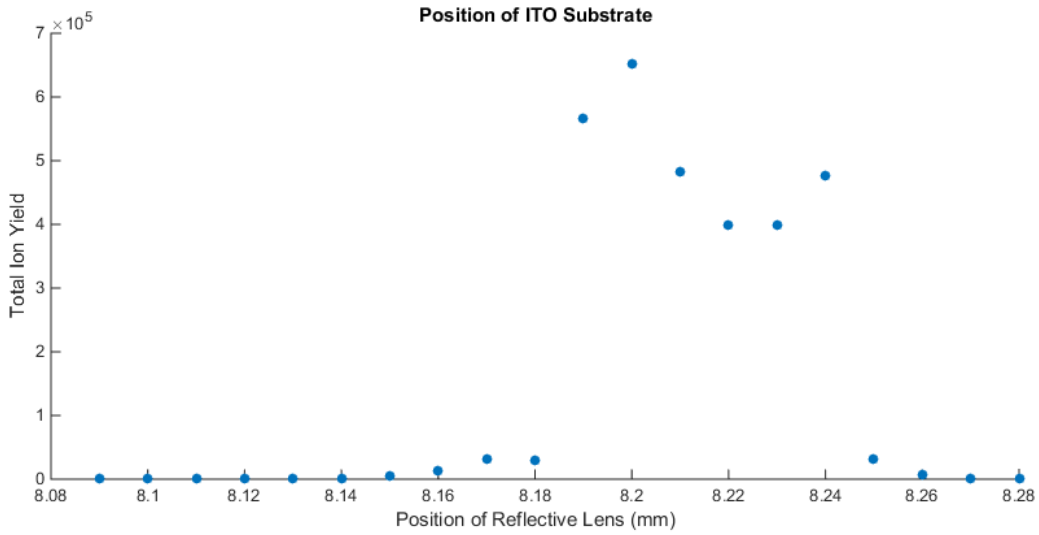

Figure 30: Determination of the position of the ITO substrate in relation to the position of the reflective lens. The second peak in total ion yield, located at 8.24 mm, is likely from a second focal spot caused by the nonlinearity of the ITO slide [13]. The pulse energy used in this test was 2 μJ.

Note that we are able to detect ions at this height, compared to the blind spot of noble gas detection we saw just above it. This can be explained by the expansion of the ion cloud of the solid passing through this blind spot, before being pulsed upwards by the extraction field. The ions that we detect are those that are above the blind spot, while the ions below won't be detected. This is a significant problem as we are trying to maintain quantitative data from our sample. Without detecting all of these ions, this is an impossibility. Unless stated, most of our tests on solids were done with the RegA system, as higher repetition rates will lead to a higher ion yield and better resolution during imaging scans (See Chapter 4.3 for further information).

4.2.1 Pulsed Extraction

We tested solids with the Legend and the RegA laser systems. Our preliminary tests at the ARC building with the Legend system at 100 µJ yielded some questionable results. The main peaks on our spectrum are located at values of 25, 37, 57 and 145 amu, which doesn't correspond to any mass value in glass or ITO. Moreover, the main peak of Indium at 115 amu is dwarfed by these other peaks, and its signal is very noisy. There also appears to a shoulder that appears next to these peaks, some of which stretch over an atomic mass unit. This noise might be coming from the strong intensity of the laser pulse, but the shoulder width and the source of these unknown peaks remains unclear.

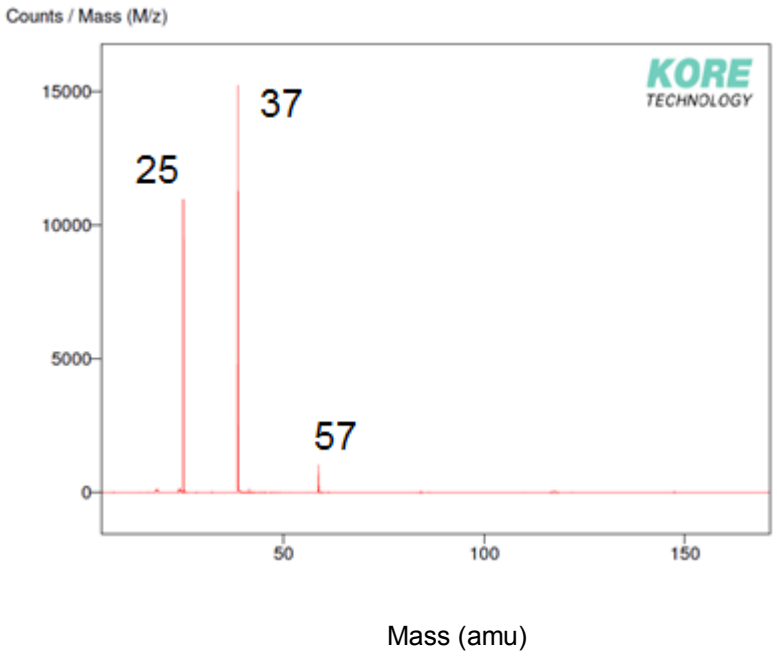

Figure 31: Count per mass spectrum of ITO substrate with pulsed extraction. In this particular test, the 145 amu peak was quite weak. It can be seen in figure 32 on the right. For more tests with a stronger 145 amu peak, consult Chapter 5.

Investigating further into the nature of the 37, 57, 145 and 25 amu peaks yielded inconclusive results. For this, the RegA pulse energy was set at 2 µJ. On the time spectrum, these peaks never shifted while constantly varying the delay between extraction and ionization. The arrival time remained constant even when the delay was set so that the ionization would appear during the extraction pulse at various times. Instead of shifting the peaks either forward or backwards during the spectrum, not only did they remain constant, but other peaks would either appear or disappear. Other tests showed a significant peak at 145 amu, while the 25 amu peak

would disappear, not appearing for any other tests. A scan with a significant peak located at 145 amu can be seen in Chapter 5.1.

To test if it was a calibration error, I also tried increasing both the pulse energy to 4 µJ and the delay significantly to ionize Krypton on the substrate, while giving the ion cloud enough time to expand past the blind spot. The resulting peaks was centered on 84 amu, the typical value for the main Krypton isotope. Thus, it is not a calibration error. The Krypton peak was susceptible to shifts in the time spectrum when the delay was altered, but the unknown peaks remained in place. Not only this, but the Krypton peak was split into two, meaning that the ITO slide is contributing to a second focal spot slightly higher than our substrate, due to its high nonlinearity (100 times that of glass, [13]). Considering this, the unknown peaks don't appear to be real.

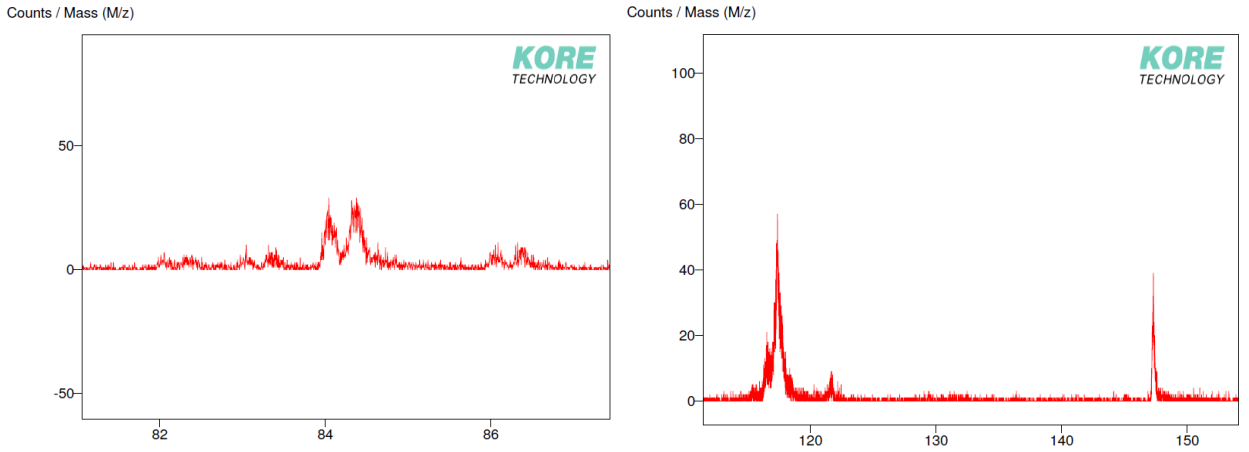

Figure 32: Count per mass spectrum of ITO with pulsed extraction zoomed in for the masses of Krypton (left) and Indium (right). These are taken from the same scan as that of figure 31.

4.2.2 Constant Extraction

For constant extraction on solids, we used exclusively the RegA laser system. This configuration generated ten times the amount of ions compared to pulsed extraction. This indicates that the ions that were too close to the substrate are now detected, compared to those at the edge of the ion cloud when the extraction pulse is activated. The pulse energy of these tests is set at 1 µJ.

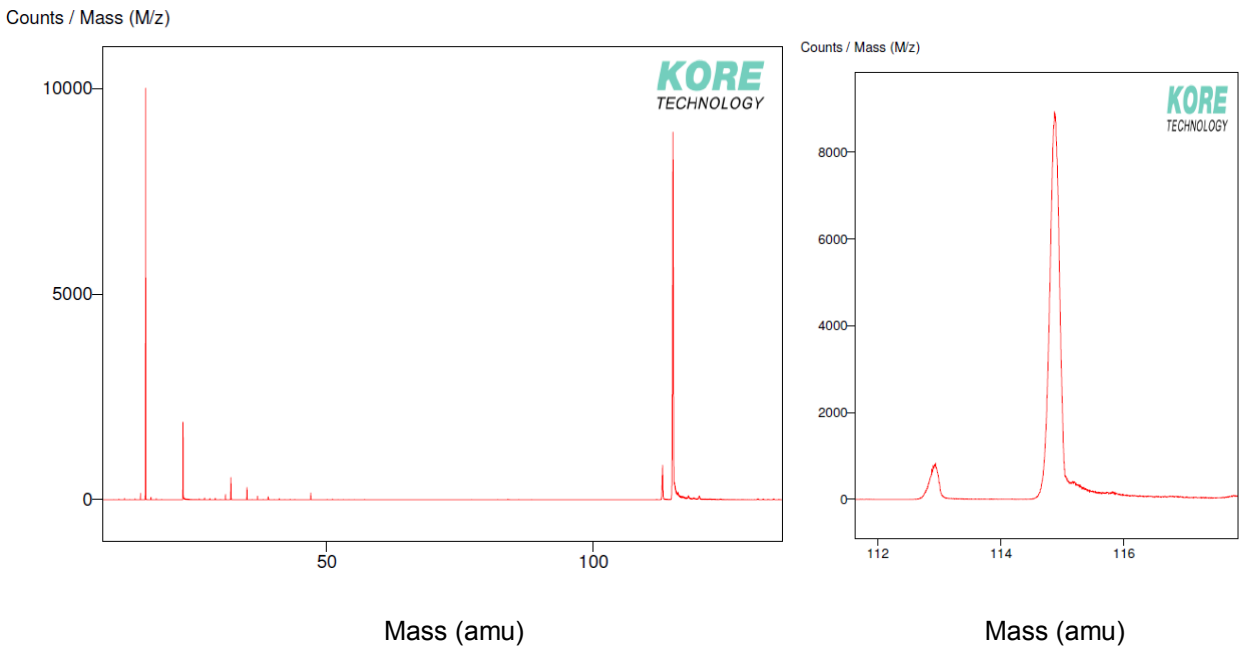

Figure 33: Counts per mass per charge ratio with constant extraction of ITO slide, with the entire spectrum (left) and a close up of indium from the slide (right).

Immediately, we noticed that our peaks are much easier to identify, as the 37, 57 and 145 amu peaks have disappeared, with peaks at 16, 23, 32, 39 and 115 amu taking their place. These peaks correspond to a single oxygen ion (likely the oxygen from the ITO mixture), sodium, dioxygen (likely from recombination of the previously mentioned oxygen ions), sodium monoxide (NaO, easier to ionize than silicon in glass, thus its signal is stronger), and indium. Even though silicon oxide is more abundant in glass composition than sodium oxide, silicon isn't as dominant of a peak as sodium because it requires more energy to ionize. There is also the appearance of peaks in the high 110's amu, corresponding to tin isotopes. They are much weaker than what the components of ITO suggests because tin needs 3 eV more than indium to be ionized.

The indium peak indicates that we are indeed ablating the ITO on top of the glass substrate, as it is not a component of glass. The validity of this indium peak is confirmed with the presence of its 113 m/q isotope. Theoretically, the ratio between the 113 and 115 peaks for Indium is 5% to 95%. Although they don't correspond exactly to these numbers, it suffers the same fate as Krypton, where the bottom of the peaks are cut off on the software program. This allows the dominant peak to appear much stronger than what it is in reality. The gain change fixes this issue. By increasing the gain, we notice a miniscule shoulder beginning to appear at the base of the 115 amu peak, meaning that the reflectron settings aren't perfected.

I also tried increasing the constant extraction field to a voltage that matches that of our pulsed configuration, to see if the extraction strength was to blame for the blind spot that we saw for gases. Instantly, we noted that the signal decreased dramatically when the constant extraction amplitude is increased. Because of this, we can say that the reason pulsed extraction doesn't work for our system in previous tests is that the field strength is too strong, even at its lowest setting.

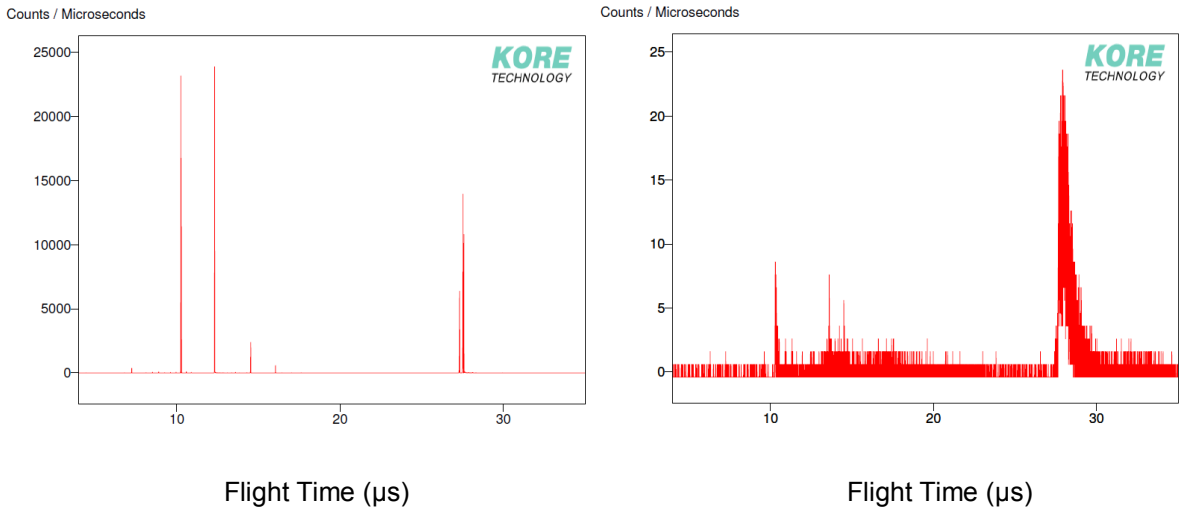

Figure 34: Signal over flight time of ions of two different constant extraction field strengths; one at 1687 Volts (left) and the other at 2065 Volts (right).

However, we've noted in previous tests (Figure 31, along with Chapter 5) that we were able to detect a signal from pulsed extraction with a similar extraction strength to that of the increased constant extraction amplitude (2065 Volts, Figure 34). This is because in pulsed extraction, there is a delay between ionization and extraction. This gives time for the ion cloud to expand past the blind spot before being sent into the mass analyzer. With constant extraction, they don't have time to expand, and the ions will collide at the end of the TOF cylinder without being reflected by the reflectron. We will work in the future to find a power source compatible with the pulser unit, to test the pulsed configuration with a weaker field strength.

With the higher signal count, the disappearance of the unknown peaks from pulsed extraction, and the fact we don't need to worry about the ion cloud and its expansion as there is no delay between ionization and extraction, the constant extraction configuration seems to be ideal for ionizing and measuring solids. However, there are some shortcomings. This configuration can only handle a single pulse at a time. If we were to do a pump-probe setup, this configuration would not work, as both pulses would be sent directly into the mass analyzer at

different times, with only one signal from the master clock starting the cycle time. Thus, the beam needs to have a high enough intensity in a single pulse. Pulsed operation would work in the case of multiple pulses before extraction, because it would collect all of these ions before sending them up into the TOF cylinder.

With all of this considered, we will use constant extraction to image our samples. Simply put, the configurations' stronger ion yield and the lack of variables that are present in the pulsed extraction configuration makes it ideal for our current setup.

4.3 Creating an Image

For our images, we shall use a method called oversampling [14, 15]. This technique consists of moving our stage in a direction while the laser continuously ablates. If the stage moves slowly enough, the two holes that two adjacent laser pulses will create will overlap each other, ionizing any particle that weren't ionize with the first pulse, while accumulating a small part of the sample that wasn't touched by the first pulse. The translation velocity will determine the amount of oversampling. The slower we go, our pixels will have more data and will be more precise, compared to a single shot and cycle per pixel. This is why the higher repetition rate of the RegA laser system is ideal compared to the Legend system, since there will more data per pixel.

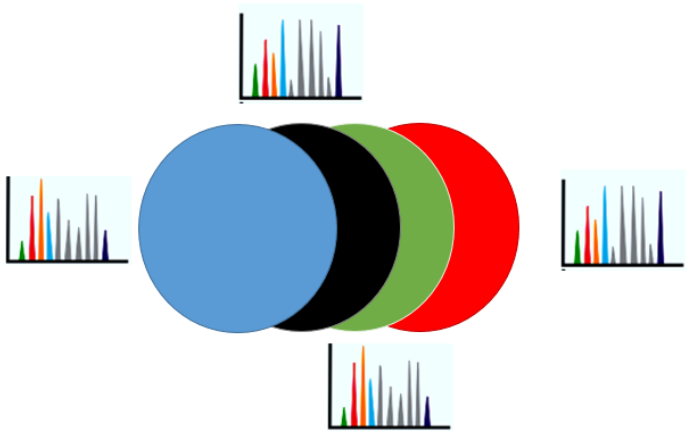

Figure 35: Visualization of oversampling. Every pulse will ablate the sample, get sent up into the TOF and will register a mass spectrum for that particular hole that the pulse creates. Moving the hole slightly (blue to black) will ablate a new area, smaller than that of the pulse crater by itself. With this, we could theoretically have a resolution for our images smaller than that of the focal spot.

The Atomic Force Microscopy (AFM) figure below demonstrates the ablation when the stage is moving at a velocity of 30 microns per second. The image also details the size of the laser's focal spot, which is 2.88 microns in diameter. With some calculations and approximating our beam as Gaussian, our theoretical spot size should be 1.274 microns in diameter. Our spot size is larger because I focused the beam at a spot slightly higher than the sample. This is because we don't want to attain a much higher intensity needed to ionize the sample, to prevent oversaturating the detector. Another reason is that our nano-stage isn't perfectly leveled, as some repairs are needed. If we were to focus directly on the sample, the spot size would greatly fluctuate in our scan because the distance between the focal spot and the sample would change. Focusing a couple of Rayleigh ranges above the sample will allow the spot size to fluctuate at a much smaller rate in our scans. Further work will be done on decreasing the spot size while maintaining the same order of power of intensity by decreasing the overall intensity and pulse energy of the beam, while also repairing the nano-stage.

Our laser's repetition rate is 8930 Hz, which means that the amount of shots while the sample has moved the distance equivalent to the focal spot is 1155. This many shots would ablate completely the sample, leaving no trace behind (This is ideal because the entire sample will be detected, and thus increasing our quantitative accuracy).

The spot size also indicates the intensity at our focal point. With a spot of 2.88 microns in diameter, our pulse length of 45 femtoseconds and a pulse energy of a microjoule, while including a 30% loss in energy from transmission through the glass substrate and the obscuration of the reflective lens, we have an intensity of 2.35×10^{14} W/cm^2. This is above the intensity needed to ionize ITO (in the order of 10^{13} W/cm^2), maybe slightly too high, but indium is one of elements with the lowest ionization energies. Considering that we need to ionize whatever is placed into the chamber, the intensity is enough for our scans without being too strong.

We also note that the ITO adjacent to the ablation scan is quite smooth. This follows what we see with ultrashort laser pulse machining, where the laser pulse doesn't have time to spread through the sample, leading to smaller, well defined holes [8, 9, 16]. This leads to little lost information.

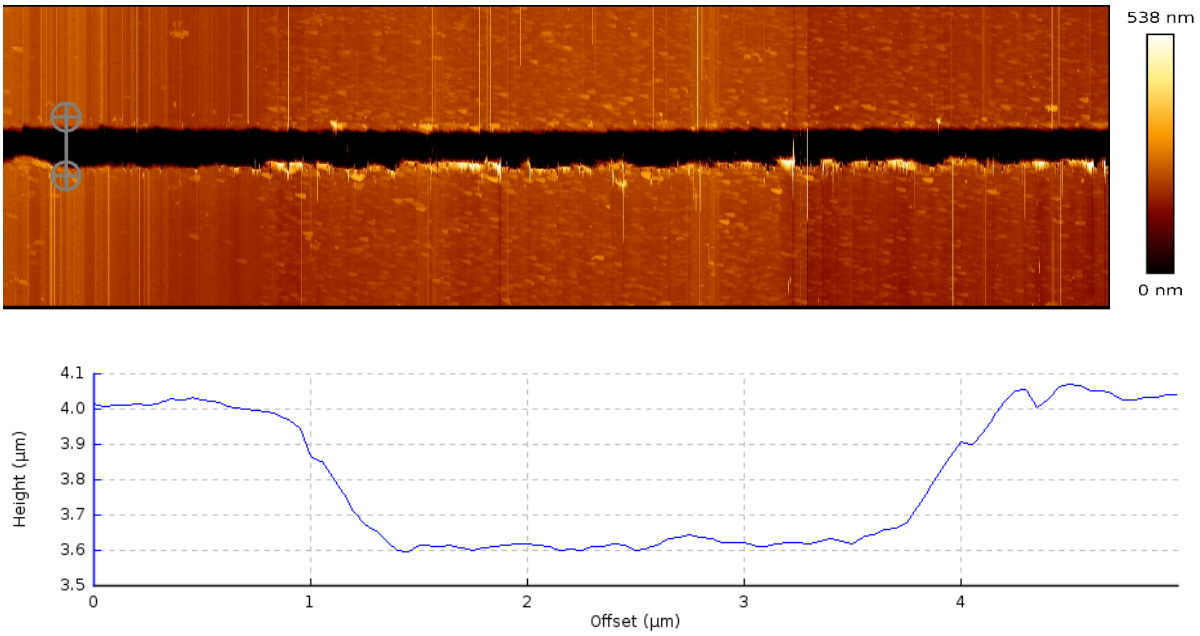

Figure 36: AFM image of an oversampling scan, and the cross section of the ablation section. With this, we can say that the laser diameter at the ablation spot is 3.88 µm.

Considering that a constant extraction field has yielded us better results for our mass spectrometer design, we proceeded to obtain an image of a sample using this configuration. I went to l'Université de Moncton and deposited a simple WO_3 structure onto a slide of ITO [17]. I chose the smallest mask that was available, and did a thermal deposition onto the ITO slide. This method was chosen because of my previous experience with it during my undergraduate studies. WO_3 was chosen for its availability for thermal deposition in the laboratories at l'Université de Moncton, the fact that tungsten will be easy to identify in our mass spectrum, and my previous work with MoO_3, which has similar properties and structure.

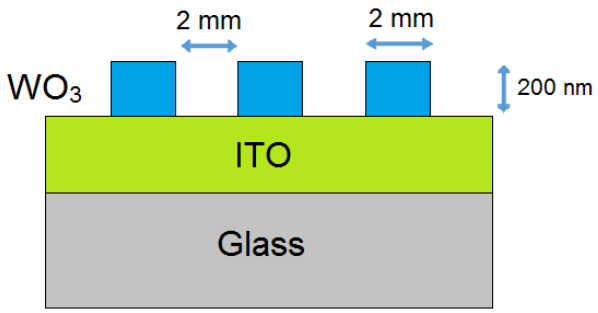

Figure 37: Sketch of the structure of tungsten trioxide on our ITO film, not to scale.

With this sample placed into the chamber, we performed a scan through the length of it with the RegA laser system, with an energy of 1 μJ, at a motor velocity of 30 microns per second. By doing this, we found peaks located at 198, 199, 200, 202, 214, 215, 216 and 218 amu, corresponding to the isotopes of WO and WO_2. Further evidence of these peaks being representative of tungsten oxides is that the ratios compare to those of tungsten, with ratios of each peak of 26.5%, 14.3%, 30.6% and 28.4% being respected for both groups of tungsten oxides (oxygen only has one abundant stable isotope at 15.9949 amu). WO_3 doesn't appear because the laser intensity is too high for soft ablation, and the appearance of WO and WO_2 results from the smaller enthalpy energy of reaction for these compounds resulting from the hard ionization [18].

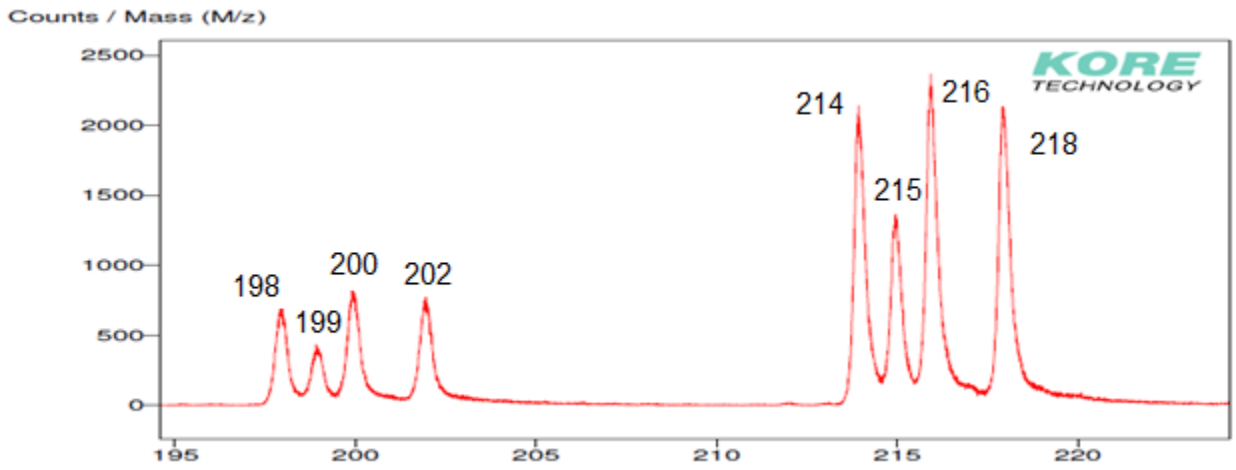

Figure 38: Mass spectrum of WO_3 sample, with peaks resulting from WO and WO_2 recombination.

Now that we found traces of tungsten that are coming from our sample, we performed multiple sets of 30 micron scans from our sample, determining the ion yield within the interval of time representative of these tungsten oxide compounds (between 35.8 and 38 microseconds). These scans on our sample surface were only in one dimension, as the structure only varies in one dimension. The pulse energy and the motor velocity remained constant from the previous scan.

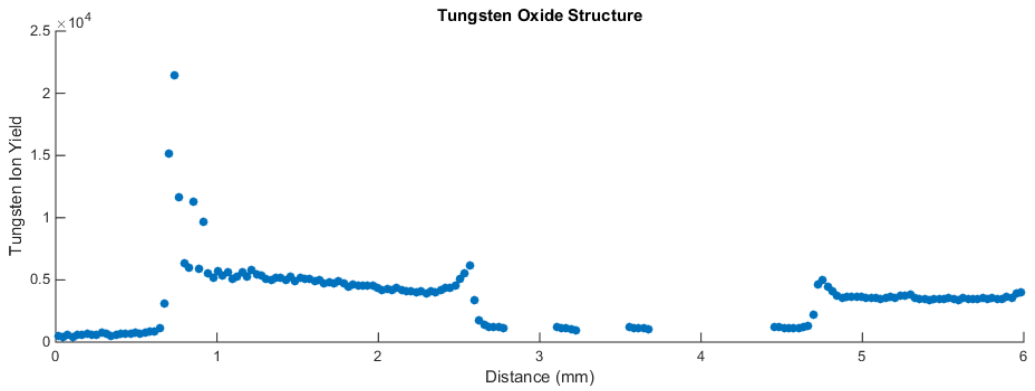

Figure 39: Determination of the Tungsten Oxide structure by examining the ion yield of WO and WO_2 at various locations on the sample.

Observing the figure above, we can state that we've imaged our sample qualitatively. There is the allusion of a step function, with each step width and the distance between them being 2 millimeters, which matches our sample's structure. Between the tungsten oxide steps, we noticed also that the signal isn't zero. This is a combination of noise and some spread of the thermal deposition, as the mask used to construct the structure of the sample had a gap between it and the sample. We also see peaks appearing at each of the edges of the WO_3 peaks, with the first edge encountered in our figure the most prominent. This is likely due to a significant surface enhancement that augments the laser intensity, similar to surface-enhanced Raman scattering (SERS) in silver and gold [19].

With this, we've shown that our mass spectrometry system can indeed create images of our sample. However, creating quantitative images with our system might pose a challenge. We see that there is a descending slope in our step function, which can be explained by the nano-stage not being perfectly leveled. Also, the results can never be completely repeatable. Considering that our laser pulse ablates completely the sample, we cannot rescan the same area. However, rescanning the sample in an area adjacent to the first scan yields similar results to this scan, thus it is somewhat repeatable.

I also tried some preliminary tests on similar structures of Tungsten Oxide with different thickness, but the stage's angle has gradually increased. Preliminarily, we were able to say that the peaks on the edges of the step function arrive from surface enhancement due to a smooth transition to the step function when the signal is weak enough (see Figure 40). We were also able to say that the ionization rate relates more to the density of atoms in the focal area, rather than the deposition thickness of the sample. However, these are preliminary and will require more work once the stage has been fixed and levelled.

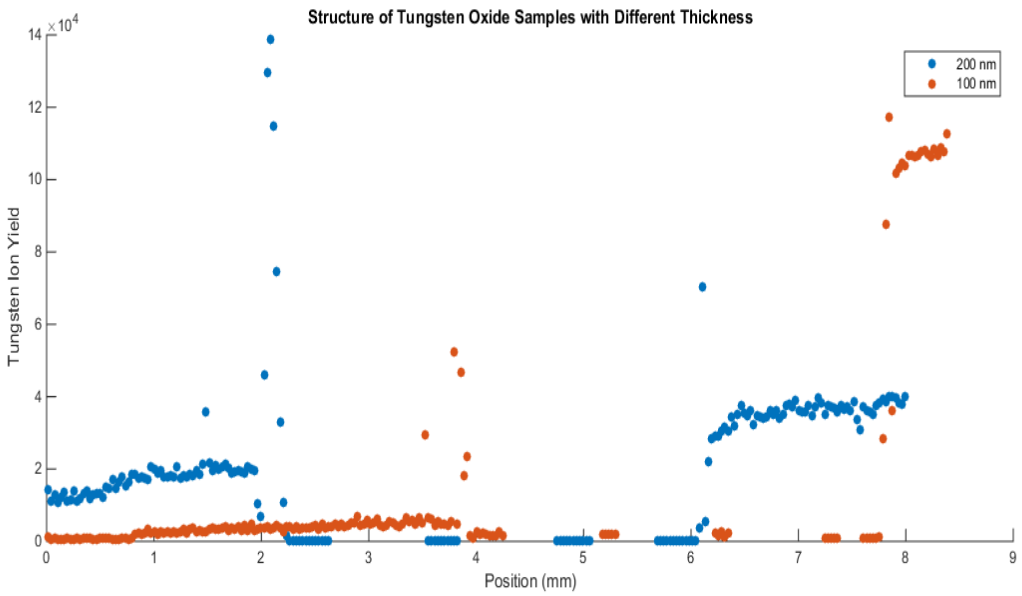

Figure 40: Tungsten Oxide Structure at different thickness, with 200 nm and 100 nm and a period of 7 mm. The lack of a peak for the 100 nm at 800 microns indicates a smooth transition in the Tungsten Oxide step function when the transition is small. This adds value to our argument that the peaks at the edges are caused by surface enhancement. One can also observe the 200 nm step function being above the 100 nm step function below 4 mm, but the reverse is true above 8 mm.

Since we have a focal spot of 2.88 microns and the spatial precision of techniques such as SIMS can reach the order nanometers, our precision isn't anywhere near that of other established imaging techniques. However, considering that the sample's structure was quite large compared to the focal spot (period of 4mm compared to a focal spot of ~3 microns), we are confident we can image more complicated samples and structures. We are trying to increase the repetition rate of the laser to achieve a higher rate of oversampling. We can also reduce the transition speed of the stage down to a micron per second. With this, the oversampling rate will increase, and so will our precision of our images. On top of this, research has shown that we can ablate holes in our samples much smaller than the focal spot of our laser, from a few hundred nanometers in radius [20] down to 38-43 nanometers in diameter [21]. This along with oversampling will further increase the precision of our images. Hopefully with these alterations, we can increase the precision down to that of SIMS (nanometers), and maybe even the order of hundreds of picometers.

With all this said, I've shown that, with ultrashort laser pulses, we can image our samples qualitatively, but there is still some work that needs to be done for quantitative images.

5 Issues Encountered

To be completely honest, we didn't achieve the results shown above straight away. There were some issues that I encountered that proved troublesome and needed to be addressed. For these problems, I altered the settings of the system so that they were resolved. Here are some of the issues that we addressed. I list these problems here just in case future students who will be working with the imaging mass spectrometer encountered similar issues, or at least raise awareness of these problems.

5.1 Appearance of Shoulder after Peaks (Pulsed Extraction)

Our preliminary tests at ARC with pulsed extraction on solids with 100 µJ per pulse yielded not only the unknown peaks mentioned earlier, but next to these peaks were the appearance of a shoulder that were as wide as an entire mass atomic unit. These shoulders need to be addressed, as they create not only a noisy mass spectrum, but it raises questions about the validity of the peaks that appeared. For this, we need to find the contributing source.

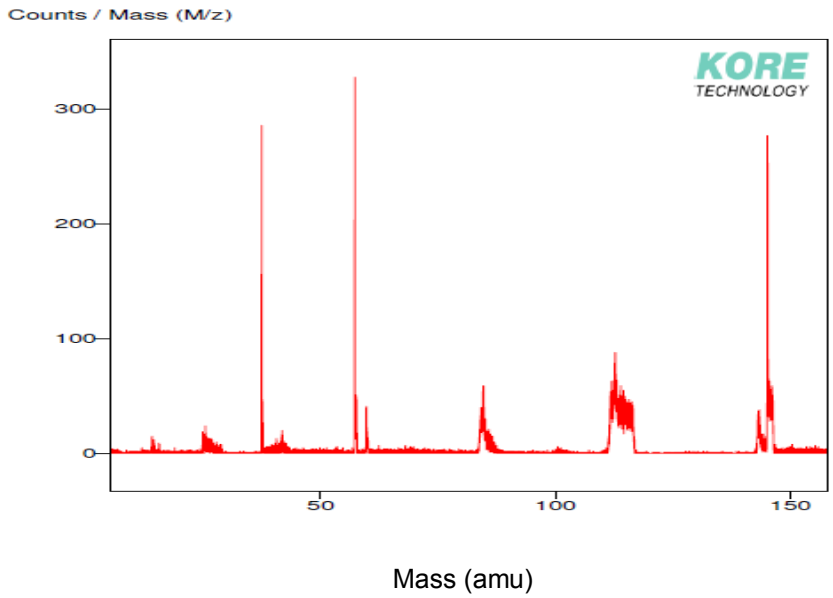

Figure 41: Preliminary count per mass result after move from NRC to ARC, with pulsed extraction.

5.1.1 Reflectron

Considering that the flight time of the ions with similar m/q values do not coincide, leading to a shoulder after peak, we decided to investigate how the reflectron affects the shoulder width at different voltage settings. We used the SIMION 7.0 software to see how the reflectron could contribute to the shoulder qualitatively, and compare it to our findings off the substrate.

Firstly, during testing at NRC before the move, we realized that the shoulder only appears for peaks corresponding to solids, the ions that are ablated from the substrate. However, when testing and calibrating for gases, no such shoulder ever appeared. This could be explained by the difference of kinetic energies between the ions from gases and those from solids, caused by their proximity from the extraction field. As explained before, the closer they are to the extraction field, the ions will be more energetic. This means that the reflectron might be able to correct for the low energy ions (such as from the gas), but cannot correct for the higher energies (from the solid).

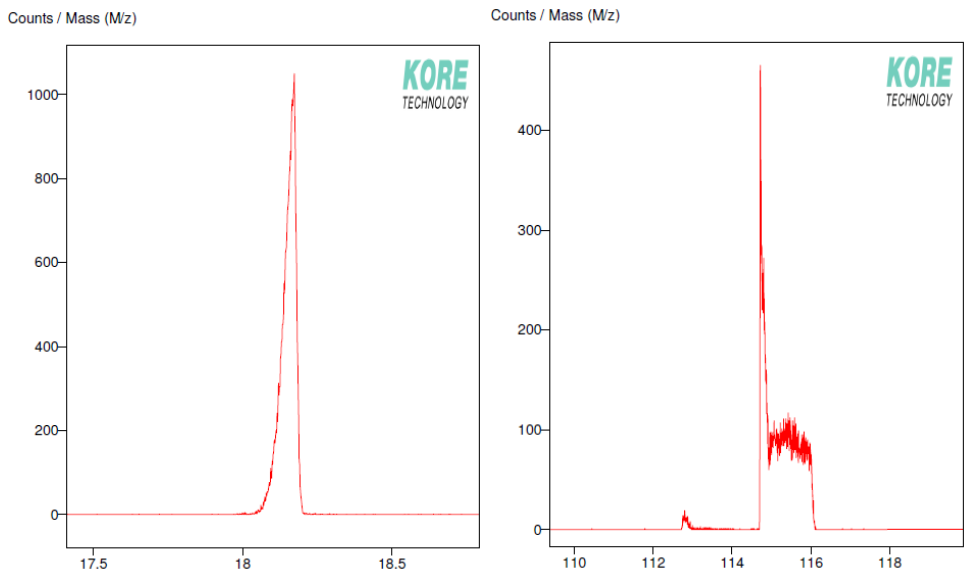

Figure 42: Comparison of the shape of the water particles peak (left) and the indium peak (right). It is clear that ionizing solids in our mass spectrometer provide problems that don't arise with gases.

Secondly, as previously stated, it seems that the shoulder increases in size as the m/q value becomes higher and higher. This is also seen in the time spectrum, as shown in Table 1. Thus, considering it has the largest tail out of the 3 strongest peaks in our spectrum (37, 57 and

145 amu), we will analyze the shoulder width of the 145 amu peak before and after reflectron adjustments.

Mass per charge ratio (m/q) (amu)	***Size of shoulder after peak on time spectrum (ns)***
37.484	55
57.286	73
145.093	114

Table 3: The size of the shoulder on the time spectrum for a corresponding m/q value. These were measured by converting the mass spectrum (Figure 38) back to its flight time axis (Figure 41) and determining the width of the shoulder after the flight time corresponding to the masses above.

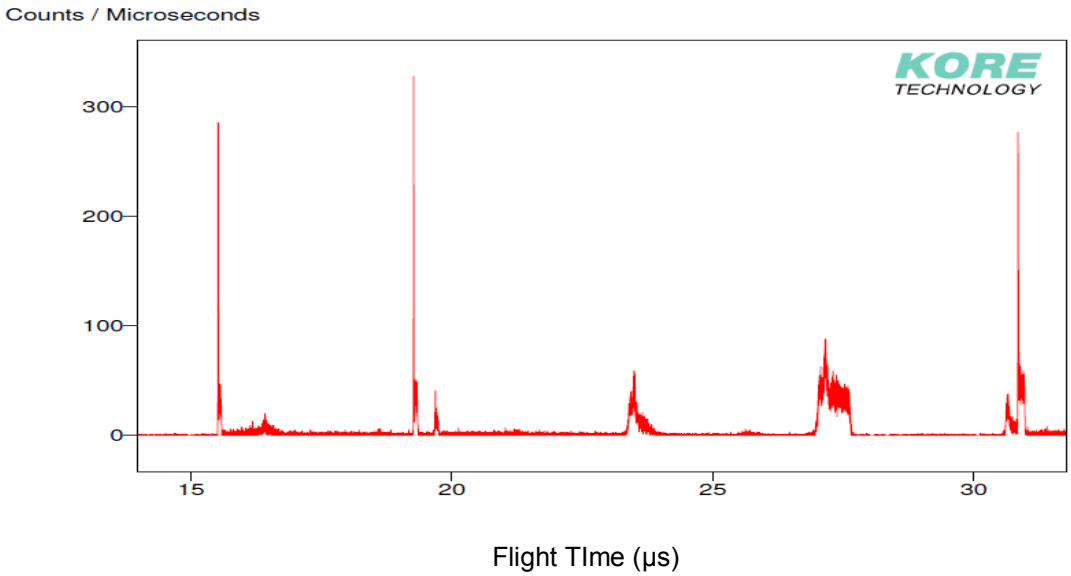

Figure 43: Intensity of ion signals per flight time in microseconds. The shoulder width increases further along the time axis.

The reflectron could possibly fix this problem because of the extra amount of time it takes for heavier ions to travel through the system compared to lighter ions. This amount of time could allow the ions with higher energies to spread out farther from the ions with the same m/q value, but lower energies. Thus, this could contribute to a shoulder to our peaks. By adjusting the reflectron, the spread of ions could be narrowed and allow them to arrive at the MCP at roughly the same time, thus eliminating the shoulder.

This is entirely speculative and theoretical, so went back to SIMION 7.0 to see if these ideas can be reproduced qualitatively. In our program, we have a simple setup of an ion source shooting ions of the same m/q value with different initial energies. These ions travel into a single gradient reflectron system. We could use a two gradient system, but since we only want to see if our data can be reproduced qualitatively, it isn't necessary. Once reflected, the ions collided with a detector, which indicates the time of flight for each ion. We did this for three different m/q value. These results can be found on Table 4.

Initial Ion Energy (eV)	***TOF, 50 amu (μs)***	***TOF, 100 amu (μs)***	***TOF, 150 amu (μs)***
1	9.91519	14.0222	17.1736
11	9.90384	14.0054	17.1540
21	9.90328	14.0061	17.1530
31	9.90575	14.0089	17.1573
41	9.90995	14.0148	17.1645
51	9.91531	14.0224	17.1738
61	9.92157	14.0312	17.1847
71	9.92855	14.0411	17.1968
81	9.93613	14.0518	17.2099
91	9.94422	14.0633	17.2239
101	9.95277	14.0753	17.2387
111	9.96172	14.0880	17.2542
121	9.97104	14.1012	17.2704
131	9.98070	14.1148	17.2871
141	9.99066	14.1289	17.3043

Table 4: Time of arrival of different ion masses with various initial energy, from our SIMION 7.0 simulation.

Looking at the ions with lower initial energy, those with similar m/q values arrive at the detector almost simultaneously. This would correspond to a peak in our spectrum because since they all arrive roughly at the same time, they would all be roughly correspond to the same m/q value. When observing the arrival time of the ions with higher initial energy however, not only do they move away from the somewhat simultaneous arrival time of the ions with lower energy, but

the interval of time between the ions with similar interval of energy increases with higher initial energy. This would correspond to a shoulder in our spectrum as these ions arrive later and would represent a slightly higher value of m/q than the peak (lower energies). Not only that, but the time interval between the ions close to the peak and that of the ion with the highest energy is drastic, which would correspond to a shoulder of noticeable and non-negligible size, similar to what we obtain with our mass spectrometer (such as Figure 42 on the right, 43 and 44).

In addition, the interval of time (and thus shoulder size) increases as the m/q value increases. Between the ions with an initial energy of 61 eV (the end of the peak and start of the shoulder) and those with 141 eV (the end of the shoulder), the m/q of 50 amu has an interval of time of 69.09 ns. For m/q values of 100 and 150 amu, the interval of time is 106.5 and 130.5 ns respectively. This increase corresponds to a wider shoulder for larger m/q values, similarly to what we obtain with our mass spectrometer.

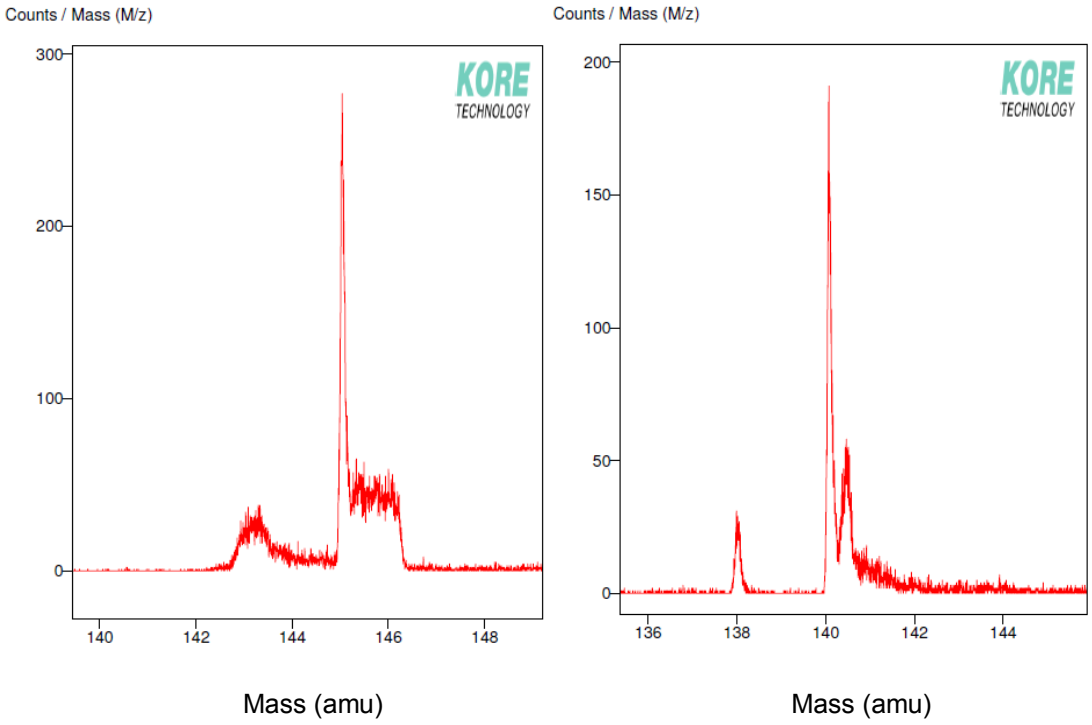

Figure 44: Counts per mass of the substrate with two different settings of the reflectron. One setting is at 959 V and 1893 V at the midpoint and end of the reflectron respectively (left), while the other is at 949 V and 1955 V (right). The shift in mass between the two different settings can be explained by the shorter flight time of the ion caused by the increase in reflectron voltage.

We have noted many similarities between our mass spectrometer results and our SIMION simulation, namely the increase in time intervals for larger m/q values, the peak that arises for low

initial energies, and the spread and consequent shoulder that arises for higher energies. Because of this, we can say that the reflectron is a big contributing factor to the shoulder in our results. Thus, we have to adjust the voltages on the reflectron so that it can compensate the higher energy ions in our experiments.

Adjusting the voltages inside the reflectron leads to a huge improvement in terms of the shoulder width (0.3117 amu compared to 1.0127 amu). This shoulder shape, where it creates a second peak, seems to be a result of saturation of the peak at 140 m/q, instead of an isotope. Saturation is explained in further detail in Chapter 5.2. Even looking at the peak at 138 amu on the right in the figure above, it corresponds to a suitable peak compared to its counterpart on the left at 143 amu. Increasing the voltages inside the reflectron reduces the travel time of the ions inside the TOF cylinder, which explains the shift towards lower m/q values. Even with saturation, the peak has shown a dramatic improvement. It is fair to say that the reflectron seems to be the main contributor of the shoulder.

5.1.2 Intensity

Now that we know the contributing factor of the shoulder width next to the peaks corresponding to solids, we will lower the intensity on the substrate by lowering the pulse energy with a combination of a half wave plate and polarizer. Not only will that eliminate much of the noise in our spectrum that we believe is caused by Coulomb explosion [22] and similar effects when the intensity is too high, but it will also cut off many of the peaks that aren't from the substrate itself, as the intensity will be reduced below the ionization threshold of glass.

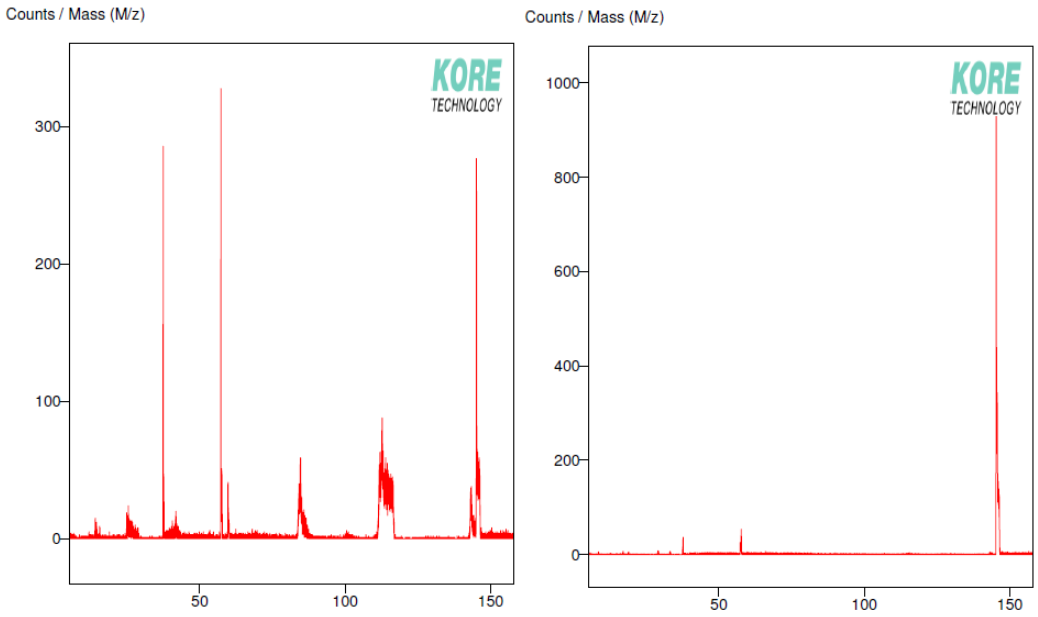

Figure 45: Counts per mass of the substrate with two different laser pulse energies, one at 100 µJ (left) and 15 µJ (right).

As we can see from the figure above, not only is the spectrum improved in terms of noise and shoulder width, but most of the peaks have been eliminated. Only peaks at a value of 37, 57 and 145 amu remain, indicating that these values were actually from the substrate. The peaks that were eliminated came from the glass underneath our ITO substrate. Since the intensity just below the focal spot isn't enough to ablate and ionize the glass, decreasing it allowed us to focus onto the substrate with better accuracy. Since the ratio of the remaining peaks have been greatly altered from lowering the intensity, it is possible that much of the 37 and 57 amu peaks were part of the glass substrate. It is also possible that there was saturation for these peaks at these levels of energy per pulse, which would have been corrected by lowering the energy. After all adjustments are made, we have a mass resolution in the order of 3×10^{-3}.

5.1.3 Other Possible Sources

Other possible sources of the shoulder were also tested independently of the intensity and reflectron settings, such as the delay time between ionization and extraction, the voltage strength on the einzel lens, and the strength of the extraction pulse itself. When modifying the first two, there was no significant alteration in size of the shoulder width; negligible compared to the alterations done to the laser intensity and the reflectron settings. However, increasing the

strength of the extraction pulse seemed to decrease the size of the shoulder width. One could argue that the increase in extraction pulse strength would eliminate the ions at the transversal edge of the ion cloud, which would have a longer path to the MCP, increasing their flight time and thus contributing to the shoulder width. This is misleading, as the strength increases the blind spot where we can't detect any ions (see Chapter 4.2.2, Figure 34). As this blind spot increases, the amount of ions that are detected decreases, since the reflectron cannot handle the increased kinetic energy. Thus, the shoulder decreases in size because we have a lower ion efficiency.

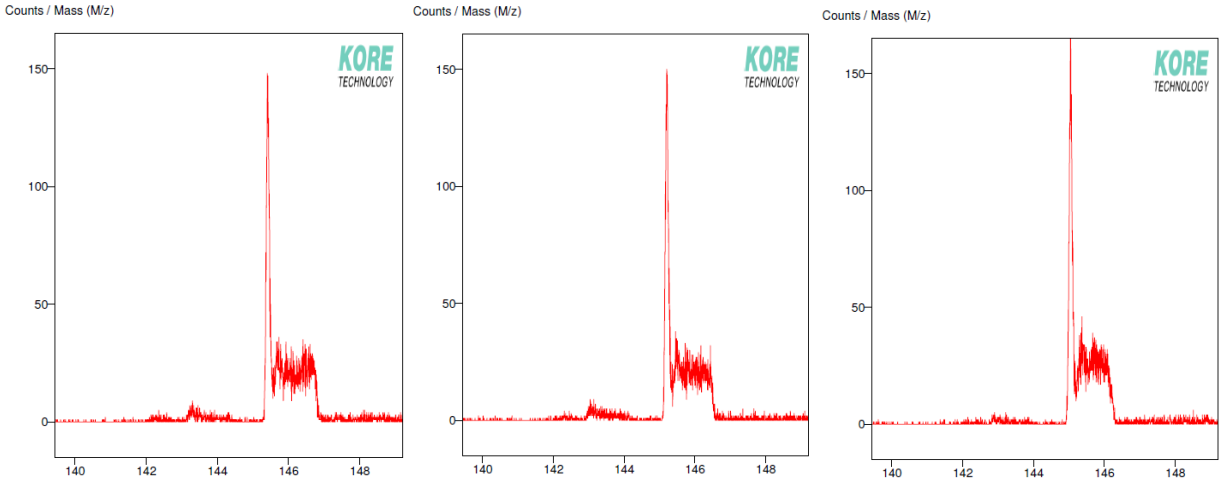

Figure 46: Counts per mass of the substrate with the extraction pulse strength at various voltages. These voltages are 2151 V (left), 2258 V (centre) and 2407 V (right), with shoulder widths of 1.1858, 1.0908 and 0.9807 amu, respectively.

5.2 Saturation

Since the MCP can only handle a certain amount of ions in an interval of time before its signal begins to fade, saturation can be present in our results. To show and discuss the effects of saturation in our mass spectrometer, after eliminating the shoulder from our results, we focus the laser spot onto the substrate at two different depths; one where detection of the ions from the substrate commences, and the other 40 microns deeper. As we see in the figure below, ionizing deeper into the substrate causes a second peak to appear. These were done with a pulse energy of 15 μJ.

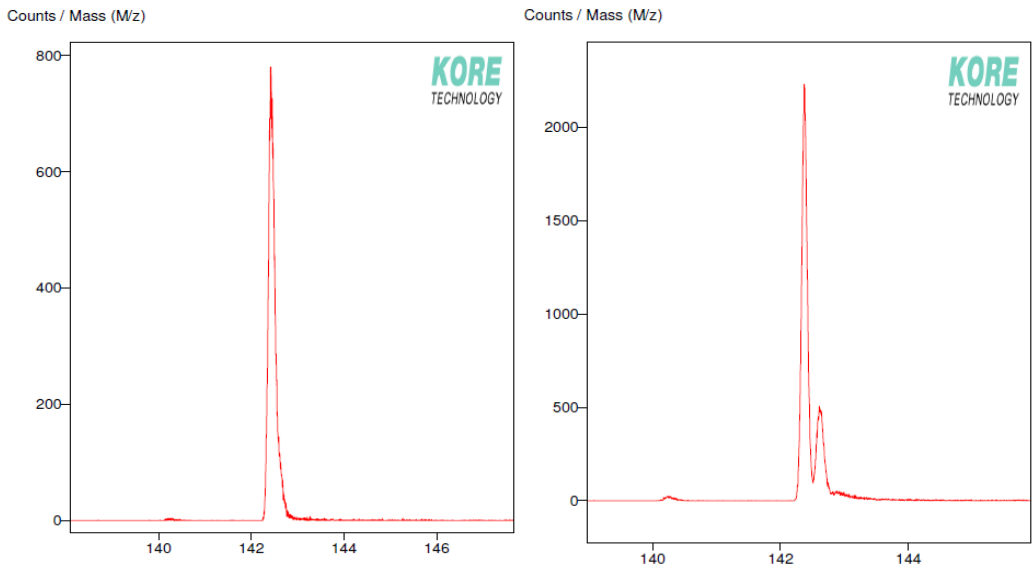

Figure 47: Counts per mass of the substrate at two different positions of the laser focal spot (A-iv-c), one at 7.90 mm (left) and 7.94 mm (right).

This second peak comes from the MCP trying to read too many ions in a short amount of time. The detector has a "dead time" of 4-8 ns, where its capacity for detection trails off before being ready to fully register another ion. If two distinct ion signals arrive within this "dead time", the MCP can't distinguish one signal from the other. The MCP will instead register them as a single ion, which leads to the software incorrectly stating that there was only one signal. Since the time spectrum peaks are wider than this "dead time", if there are too many ions of a particular peak, many of them won't be registered and their information is lost. This can be seen in the above figure on the right. Because we focus too much into the ITO substrate, many more ions are created compared to its counterpart on the left. Because of this, too many ions collide with the detector per cycle. The first ion is detected normally, which is why the second peak of saturation always appear at heavier masses. After this, the MCP has its "dead-time" when a second ion would arrive. This signal will not be properly registered and will be much weaker compared to the first ion's signal, leading to a dip in the peak. For ions that arrive after the "dead time", they will be registered normally, creating this second peak. . If the saturation is too severe, the dip between the peaks can drop to zero counts, effectively separating the peaks altogether.

Even without this second peak, saturation can still be identified by the isotope ratios of a specific element. Since the software counts multiple ions as a single signal if they arrive too close together on the MCP, this will lead to false data for the higher peaks on the spectrum, considering

they will have more ions to detect compared to smaller peaks. Thus, these signals will be much lower than their theoretical reality. This is why the peaks should be optimized to have an ion rate slightly lower than one ion per cycle, to register properly all the ions of the peak of that particular m/q value. The isotope ratios can be used as a baseline test to see if any of the peaks are saturated. If the ratio between the peaks doesn't correspond to their theoretical values, then there is saturation in the system, and the ion rate needs to be lowered.

In the figure above, saturation was demonstrated by focussing too much into the ITO substrate, creating too many ions per cycle. However, it can also be caused by having too much energy per laser pulse, which would contribute to too many ions per cycle as well.

5.3 Mapping the MCP

According to simple energy laws and our simulations, ions with lower mass will attain higher velocities and will be pushed farther laterally inside the TOF cylinder. This might cause lighter ions to miss the detector completely. To see how much heavier ions shift laterally compared to lighter ions, we changed the voltage on the X and Y plates to map the detection of ions in relation to these two voltages. This will also create a map of the location of our detector. If this map shifts, then we can confirm that the ions are indeed laterally shifting.

We tried two different masses, water particles and krypton isotopes. We chose these because they are very easy to detect, and they are considerably different in mass (18.0153 amu compared to 83.912 (peak of main krypton isotope)).

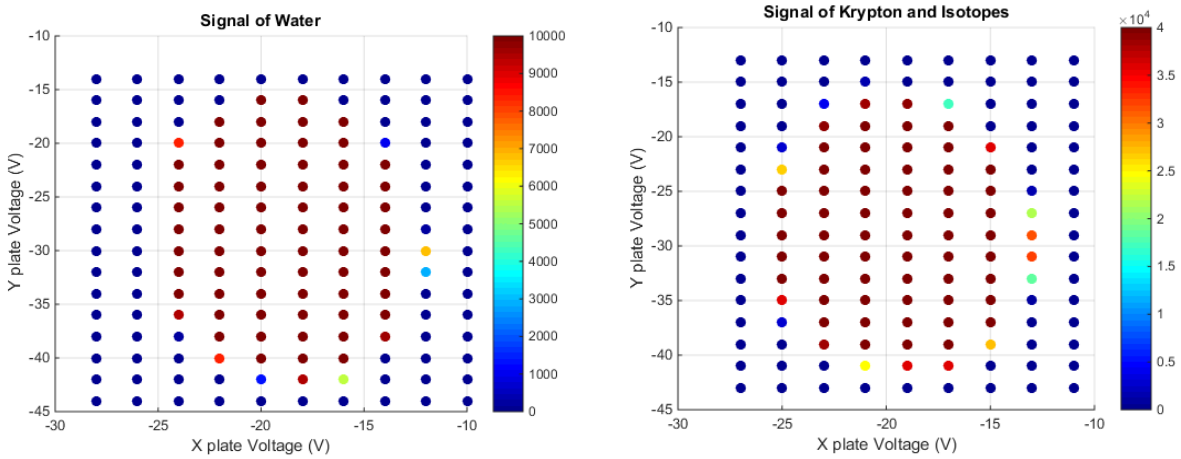

Figure 48: Intensity of the signal from various gases in the system at different voltages of the X and Y deflector plates.

Comparing these two maps, we can see that there seems to be a small shift of a volt in both the X and Y direction, meaning that there is a lateral shift. However, the detector map is so big compared to this shift that it really seems negligible. Simply setting the X and Y plate voltages to correspond for roughly the center of this map (-19 for X, -27 for Y) will be enough to properly detect masses of all sizes, regardless of small lateral shifts.

6 Outlook

We've successfully shown that our imaging mass spectrometer indeed functions as intended. Considering that our sample only had a structure in one dimension instead of two and its periodicity was 4 millimeters wide, we can move to smaller, more complicated structured samples. Our scans were done at a motor velocity of 30 microns per second. This can be slowed down to a single micron, leading not only to a higher precision spatially, but the oversampling technique will ablate completely the spot, so that the entire scan will be ionized and sent into the TOF cylinder to be detected. While we aren't at a precision that rivals that of MALDI and SIMS yet, the results shown in the thesis indicates that there is potential for this system to one day rival these methods.

We are also acquiring software from Kore to acquire multiple chromatograms, which measures the signal of a specific mass (or time-of-flight) range as it evolves through time. By scanning the sample in a single direction, we can attribute the evolution in time to the distance travelled by the scan. With this, we can acquire with a single scan multiple one dimensional images of the sample structure for various molecules and elements on our sample. Afterwards, these chromatograms can be superimposed to form a single one dimensional image containing all of these elements and molecules. We can then move to two dimensional structures. Since we've shown that a one dimensional image can be acquired, this is simply a question of moving the laser focus adjacent to the previous scan and repeating the process. Then, all of these one dimensional images can be placed adjacent to one another to form a single two dimensional image of the sample.

However, this doesn't mean our imaging mass spectrometer isn't without fault. While we have shown that the constant extraction configuration does work for our current settings, it is limited to a single pulse per cycle. The pulsed extraction can theoretically work for multiple laser pulses, be it as a pump-probe setup or increasing the repetition rate of the laser. If done correctly, we can increase the repetition rate of the laser above 10 kHz and only trigger the extraction pulse at or below 10 kHz. This would allow the collection of data from these multiple laser pulses in a single cycle, bypassing the frequency limit of the software and the pulsed extraction unit. In order to test this properly, we need to find a weaker power source compatible for pulsed extraction operation. This will help fix the issue of the blind spot and the collection of ions on solids. Further investigation will then be done on the origin of the unknown peaks previously mentioned.

Moreover, we have had some difficulties with our nano-translation stage for its tip and tilt settings. This will be looked into and repaired. To improve not only oversampling but also the size of our pixels in our images, we also want to look into how we can decrease the size of our laser focal spot. We are also going to decrease the intensity slightly, hopefully achieving soft ionization to maintain the molecule's structure during ablation and ionization, instead of detecting its fragments.

Once these issues have been fixed, we can then move forward towards imaging biological cell tissues that have been tagged with rare earth elements. We can acquire flash frozen cell tissues that can be placed under vacuum and create images of these cells. With the rare earth element tags, we can detect these with our mass spectrometer and create detailed images of these cells, especially through oversampling to hopefully achieve a spatial resolution that rivals that of SIMS. Creating a detailed image of cells can have multiple applications in the medicinal fields, such as analyzing and studying cancerous cells and how they infect neighbouring cells, or analyzing cells that have been treated with a vaccine to treat a disease. The imaging mass spectrometer can also be used to analyze other components that are thin enough to be focussed through, ablated and ionized, such as samples from asteroids and meteorites.

In conclusion, the imaging mass spectrometer has come a long way since my arrival. I deconstructed the system and moved it from the NRC to ARC, and calibrated its measurements for noble gases. Afterwards, I was able to successfully detect ions from solids and was able to show that this mass spectrometer can image samples with ultrashort laser pulses. I also wrote this thesis in a way so that new students can read it as a training/user manual, to serve as a jumping point for further research with this new mass spectrometer. While the system isn't perfected yet (there is still much to do), it has shown to be a useful machine and tool in our labs.

7 References

[1] Donna Strickland, Gerard Mourou, “Compression of Amplified Chirped Optical Pulses”, 1985

[2] Sterling Backus, “High Power Ultrafast Lasers”, 1997

[3] Thomas Brabec, Ferenc Krausz, “Intense Few-Cycle Laser Fields: Frontiers of Nonlinear Optics”, 2000

[4] Thomas Brabec, “Kerr Lens Mode Locking”, 1992

[5] Michel Piché, “Self-Mode Locking of Solid-State Lasers without Apertures”, 1993

[6] Jackson O. Lay, Jr., Rohana Liyanage, “An Introduction to MALDI-TOF MS”, 2006, pg. 48 onwards from the book “Identification of Microorganisms by Mass Spectrometry”

[7] Alfred Benninghoven, “Secondary ion mass spectrometry, basic concepts, instrumental aspects, applications and trends”, 1987

[8] CY Chien, MC Gupta, “Pulse width effect in ultrafast laser processing of materials”, 2004

[9] P. Simon, “Machining of submicron structures on metals and semiconductors by ultrashort UV-laser pulses”, 1996

[10] Kurt Brunée, “The Ideal Mass Analyzer: Fact or Fiction?”, 1987

[11] Igor V. Chernushevich, “An introduction to quadrupole-time-of-flight mass spectrometry”, 2001

[12] B.A. Mamyrin, “Time-of-flight mass spectrometry (concepts, achievements, and prospects)”, 2001

[13] Hendry Elim et al., “Carrier concentration dependence of optical Kerr nonlinearity in indium tin oxide films”, 2006

[14] John C. Jurchen et al.,"MALDI-MS Imaging of Features Smaller than the Size of the Laser Beam", 2005

[15] Shizhou Ziao et al., "Incubation effect and its influence on laser patterning of ITO thin film", 2012

[16] A. de Bonis et al., "Pulsed laser ablation of indium tin oxide in the nano and femtosecond regime: Characterization of transient species", 2005

[17] P.V. Ashrit et al., "Electrochromic properties of nanocrystalline tungsten oxide thin films", 1998

[18] G. de Maria et al., "Mass Spectrometric Study of Gaseous Molybdenum, Tungsten, and Uranium Oxides", 1960

[19] Esther Rebollar et al., "Laser-induced surface structures on gold-coated polymers: Influence of morphology on surface-enhanced Raman scattering enhancement", 2015

[20] L. Mercadier et al., "Femtosecond laser desorption of ultrathin polymer films from a dielectric surface", 2013

[21] A. P. Joglekar et al., "Optics at critical intensity: Applications to nanomorphing", 2004

[22] Z. Vager et al., "Coulomb Explosion Imaging of Small Molecules", 1989

Appendix A: Standard Operating Procedure (SOP) of the Mass Spectrometry System

I wrote the following Standard Operation Procedure for the imaging mass spectrometer. Considering that the system had been modified after the move from NRC to ARC and the lack of a SOP at the Advanced Research Center, this manual will prove useful for new students who will operate this system. This manual can also serve as a surplus to Chapter 3 of this thesis, as it explains further in detail the operation of the stages and the vacuum pumps for example.

i. Vacuum Operation and Maintenance

The entire chamber is pumped down to a pressure below 50 milliTorr by a roughing pump located in the adjacent room (the same roughing pump that pumps the load-lock system (Chapter 3.3) and the TOF-MS (Chapter 3.4), not to be confused with the Edwards nor the Pfeiffer turbo pumps). Once it has reached a pressure below 5E-02 Torr, as indicated on the pressure gauge (as seen in Figure 50), it is pumped by a turbo pump (Pfeiffer HiPace 700) on the back of the chamber.

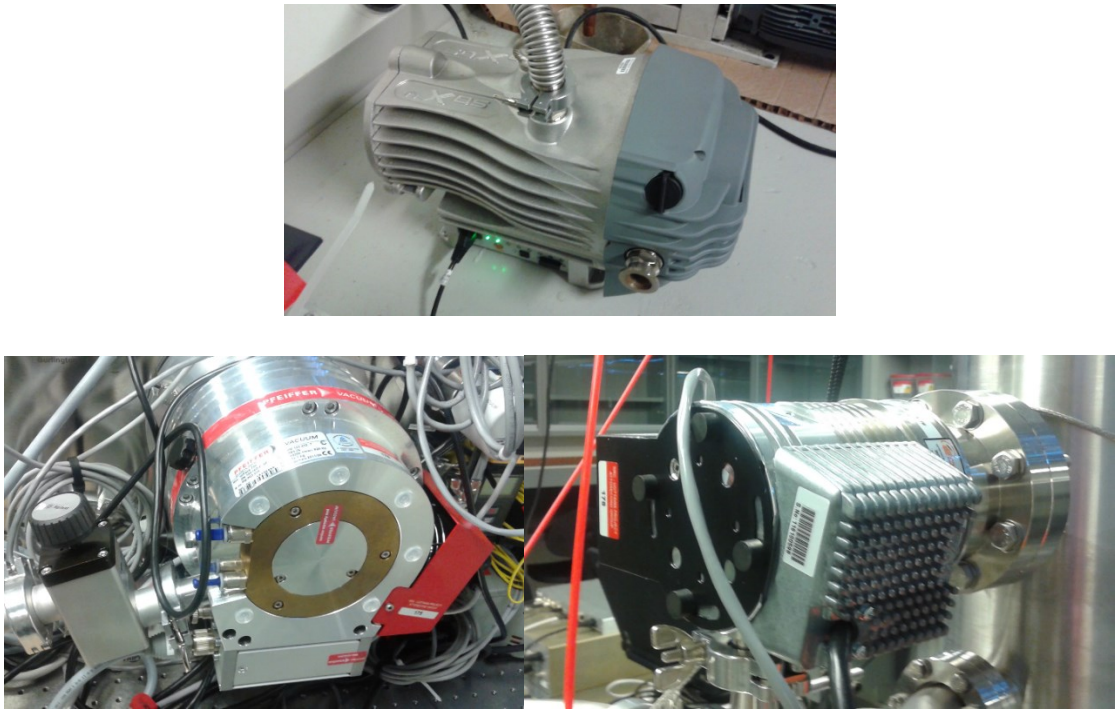

Figure 49: The roughing pump (top), the Pfeiffer turbo pump for the main chamber (bottom right) and the Edwards turbo pump for the TOF system (bottom left).

a. Removing and placing the front panel

If the chamber ever needs to be open for any reason, turn off both the turbo pump for the chamber and the TOF-MS (Chapter 3.4), and close the vacuum valves connecting both these sections of the system to the roughing pump. Pump clean nitrogen gas into both the chamber and the TOF-MS (to avoid dust and water particles entering the system as the microchannel plate inside the TOF-MS is sensitive to it) through the nitrogen line. The chamber gauge will read a pressure slightly higher than atmospheric pressure (760 Torr). This is normal as the gauge is calibrated for sub-atmospheric pressure. Unscrew the window at the front of the chamber to know when the pressure in the chamber is at or above atmospheric. Once this has been achieved, the front panel can be unscrewed and removed. Place Styrofoam underneath the panel when removing it as to not damage it nor the optical table.

Figure 50: Pressure gauge of the mass spectrometer (Edwards, left) and main chamber (Pfeiffer, right)

To close the system, simply place and screw the front panel back in place. Place Styrofoam underneath the panel next to the chamber when placing it as to not damage it nor the optical table. Don't screw the bolts too tightly to cause damage to the panel or the base of the chamber. Stop the flow of nitrogen entering the system and shut the window in the front panel. Afterwards, open slowly the vacuum valve leading to the TOF-MS, so that it can be pumped first. The TOF-MS needs to be pumped before the main chamber in order to minimize humidity and damage inside it (the vacuum inside the time of flight system takes first priority over any other vacuum in the system). Once it starts pumping, both valves leading to the TOF-MS and the chamber can be open slowly until fully opened. At this point, the bolts on the front panel can be screwed tightly, since the vacuum pressure shall help create the necessary seal.

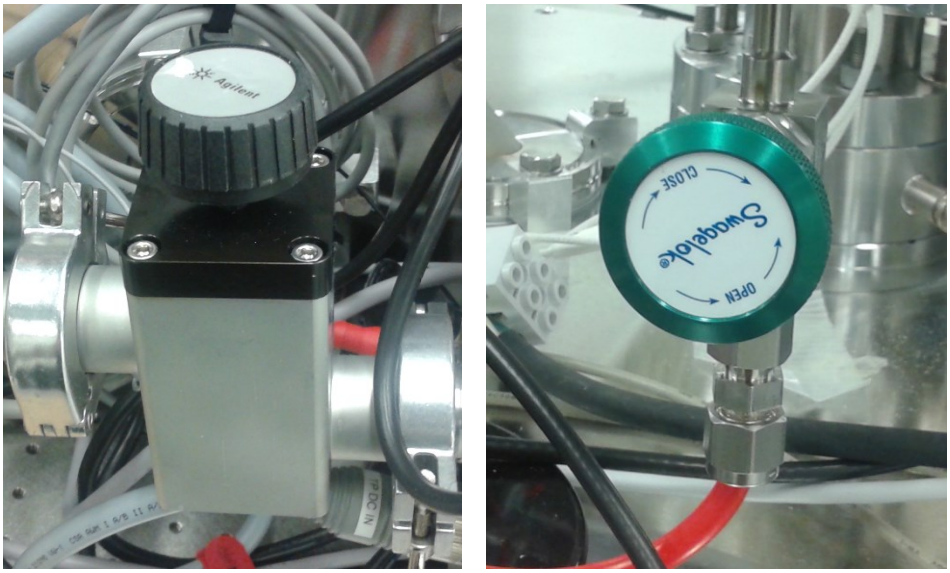

Figure 51: The two different types of valves of the system; the vacuum valve (left) and the nitrogen valve (right). There is one of each for the TOF cylinder, the main chamber and the load-lock system.

b. Pumping the system to vacuum

To pump the chamber from atmosphere to vacuum once the chamber panel is sealed, consult the following instructions (please note that if the chamber is already at a pressure of around 50 mTorr, the user can directly jump to powering the turbo pumps):

- Close the nitrogen valves on the main nitrogen manifold (Figure 52).
- Close the small nitrogen valves to the main chamber and the mass spectrometer, in that order.
- Verify that the roughing pump is functioning, and that the pressure at the roughing line behind the chamber's turbo pump (RLBT on the Pfeiffer pressure gauge) is being monitored.
- Slightly open the mass spectrometer's vacuum valve, slowing pumping the gas out of the system. After a minute, slightly keep opening the valve little by little.

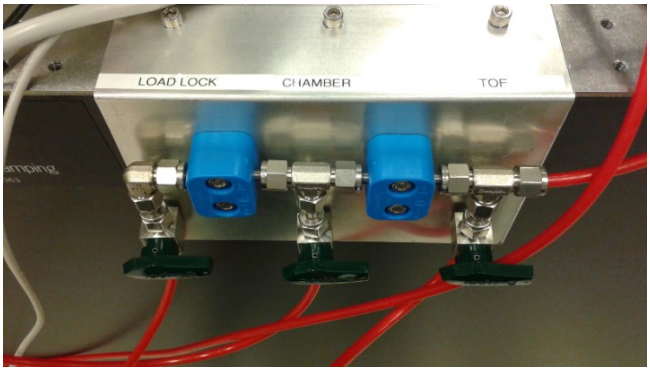

Figure 52: Main nitrogen manifold to allow gas flow to the load lock, main chamber and TOF tube. In the picture, all three valves are closed.

- Once the pressure decreases in the mass spectrometer as indicated by the Edwards pressure gauge, repeat the preceding step, but with the chamber's vacuum valve. Alternate between the two valves until they are both completely open.
    - The valves need to be open slowly in order to prevent damage to the roughing pump, and said damage to be transferred to the main system.
    - If the chamber has recently been opened, tighten the bolts of the chamber's panel with an allen key to create a better vacuum seal.

Note: Usually, the chamber is pumped down to a moderate vacuum, a pressure in the order of mTorr. If this is the case and the user simply wishes to turn on the turbo pumps, he can simply skip the steps above and continue from here.

- Once the pressure of the mass spectrometer is below 5E-2 Torr, turn on the Edwards turbo pump. Turn on the full range pressure gauge.
    - Highlight the first column on the display screen of the Edwards Pressure gauge. Press the cycle button (bottom right button).
    - Highlight TURBO OFF on the display screen, and press the cycle button. The turbo pump should be running and be displayed as on. The bar on the top of the display screen should gradually fill up as the turbo pump spins up to speed.
    - Press the menu button (bottom left button) to return to the main display screen, to check on the pressure of the system.
- Once the pressure inside the chamber is below 5E-2 Torr, run the Labview "Master Program" to turn on the Pfeiffer turbo pump. Turn on the full range pressure gauge.
    - Consult the Labview "Master Program" operations in section A – iv - d.

c. Bringing the system to atmosphere

To break vacuum and bring the chamber pressure back up to atmospheric, follow these directions (if both turbo pumps are already off and the pressure inside the system is around 50 mTorr, skip to the step leading to leaking nitrogen into the system) :

- Verify that the valves on the nitrogen manifold (figure 52) and the nitrogen lines leading to respective parts of the system are closed.
- Turn off the Pfeiffer turbo pump on the Labview "Master Program" program. Turn off the full range pressure gauge.
- Turn off the Edwards turbo pump on the pressure gauge. Turn off the full range pressure gauge.
- Once both turbo pumps have stopped spinning, close the vacuum valve leading to the main chamber. Following that, close the vacuum valve leading to the TOF cylinder.

Note: If the turbo pumps were already off and the pressure inside the system is around 50 mTorr, follow the instructions from this point on:

- Open the valves on the nitrogen manifold leading to the TOF cylinder and the main chamber.
- Open the green valves on the nitrogen lines leading to the TOF cylinder and the main chamber. Open the valve leading to the TOF cylinder slightly more than that of the main chamber.
- Unscrew the window port on the front panel of the main chamber and leave it open. This will indicate when the system is at atmospheric pressure.
    - One might note that the Pfeiffer pressure gauge might read 1320 Torr when the chamber is brought to atmospheric pressure, instead of the normal 760 Torr. This is normal, as the pressure gauges attributed to the system are calibrated for vacuum pressures, and will be inaccurate for atmospheric pressure.
- Once the window port can be opened without any force, unscrew the screws on the panel with an allen key. The panel can then be removed and placed on the counter, with the handles pointing downwards.
    - Continuously flow nitrogen through the system when the panel is removed. This will prevent outside dust and particles from entering the system.

    - Lifting the panel will likely require two people. Ask for assistance from someone in the lab.
- Occasionally lube the O-ring that seals the panel and the chamber's base.
- Once all adjustments inside the chamber are made, simply place the panel back onto the chamber and screw it back into place.

Do not leave the TOF system under atmosphere for more than it is absolutely necessary, as water particles from the air can damage the electronics inside the system, particularly the MCP detector. If the system needs to be opened, leak nitrogen gas into the system to create a pressure gradient from the flight tube to air, and let the gas exit the system, so that the damage by water particles is limited if not completely avoided.

ii. Load Lock System

For proper operation of the load lock system on how to remove and replace a sample that is already on the sample manipulation stage in the main chamber, consult the following instructions:

- Before operation, check to see if both turbo pumps are turned off and completely spun down, the vacuum valve leading to the load lock is closed, and the vacuum valves leading to the TOF-MS and the main chamber are open.
- Close the main chamber's vacuum valve, then the TOF-MS's valve.
    - The order needs to be respected to minimize any possible damage inside the mass spectrometer.
- Once the pressure inside the main chamber and the TOF-MS is around 50 mTorr, slowly open the gate valve.
- With the help of the camera screen on top of the main chamber, slide the metallic rod with the magnetic slider (Figure 53) into the chamber, and screw it into the sample holder.

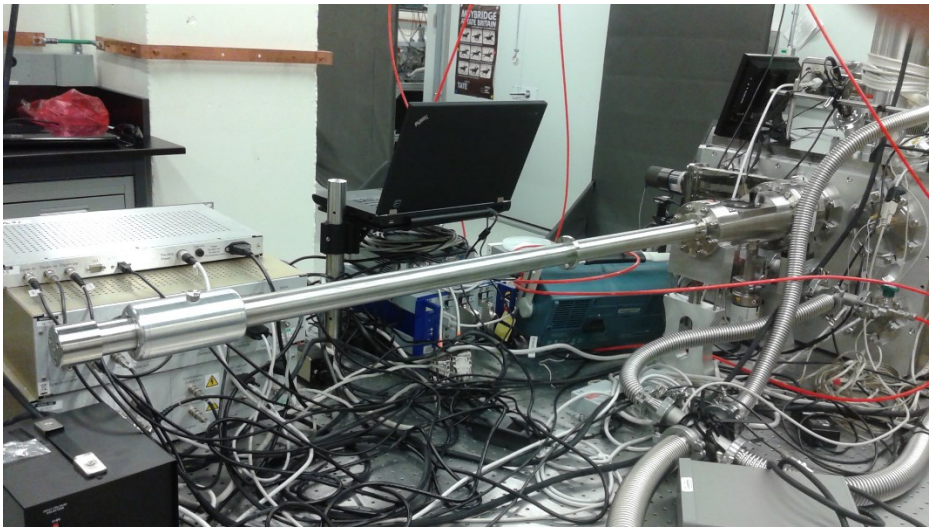

Figure 53: Metallic rod of the load-lock system. The cylinder at the edge of the rod is the magnetic slider, and can slide the length of the rod, moving another rod holding the sample inside. This is how samples are placed inside the chamber.

- Once it is firmly connected, slide the sample holder out of the chamber into the load lock system, and close the gate valve.
- Close the load lock's vacuum valve.
    - If desired, the valves leading to the TOF-MS and the main chamber can be opened.
- With nitrogen gas, pump the load lock up to atmospheric pressure and open the chamber. In order to minimize dust and other outside sources from entering the system, keep the nitrogen gas flowing in order to create a pressure gradient.
    - The sample holder can be unscrewed and taken out of the system if desired.
- After manipulating/replacing the sample, verify that an electric current can pass through the sample holder's clamps to the substrate with a multimeter.
- Screw the sample holder into the metallic rod, and close the load lock chamber.
    - Don't screw the sample holder too tightly into the rod, as it could be hard to remove from the rod when placing it into the chamber.
    - If the valves leading to the TOF-MS and the main chamber were opened, close them again.
- Stop the flow of nitrogen to the load lock system and open its vacuum valve, keeping the chamber shut.

- Once the pressure inside the load lock is roughly the same as the one in the chamber, slowly open the gate valve.
- With the help of the camera screen, place the sample holder onto the manipulation stage inside the main chamber, and unscrew the rod from the sample holder.
- Slide the rod out of the chamber back into the load lock system, and close the gate valve.
- Close the load lock's vacuum valve and then open the TOF-MS and the main chamber's vacuum valve, in that order.

iii. Leak Valve

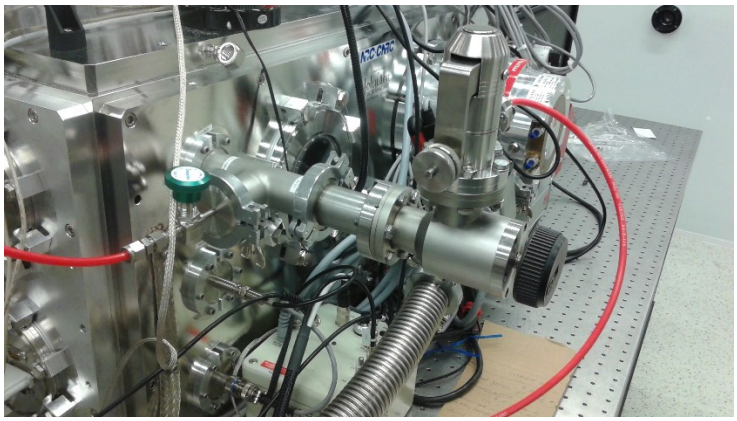

Figure 54: Leak valve to the main chamber. The green valve allows the nitrogen flow to fill the chamber to atmosphere, while the rest of the aperture allows minimal flow of another gas of our choosing into the chamber. The leak valve itself has two valves, one for macro-adjustments and exposure to the main chamber (black valve) and the micro-adjustment valve (silver valve connected above the black valve).

The leak valve is located on the back of the main chamber, next to the Pfeiffer turbo pump and above the pulsed extraction unit. It leaks a gas of the user's choosing into the system. It is commonly used to leak noble gases into the main chamber to calibrate the mass spectrometer.

Use the leak valve only when both turbo pumps are up and running.

To operate the leak valve, follow these instructions:

- Verify that the main nitrogen flow valve (the green valve in the figure above) is shut. Verify that the black valve for macro-adjustments is also shut.

- Connect the other end of the red line that is connected to the leak valve to the gas cylinders in which the user wants to leak into the chamber. These cylinders are in the service area.
- Allow the gas to flow out of the cylinder into the red tube connecting to the leak valve. Keep the pressure under 20 PSI out of the cylinder.
- Slightly open the black valve to allow the gas to enter the main chamber.
    - At this point, the pressure inside the chamber can be set to any value that the user would desire, by opening and closing both the silver valve for small adjustments and the black valve for larger adjustments. Constantly monitor the pressure during these adjustments using the Pfeiffer pressure gauge.
        - The pressure inside the TOF cylinder, however, cannot pass 1E-06 Torr, as the interlock to the high voltage supplier and controller will activate and disable any high voltages from entering the system. Constantly monitor the pressure during leak valve adjustments with the Edwards pressure gauge.

To cease operation, simply close the black valve completely, as it shuts all connection between the main chamber and the gas cylinder. Afterwards, close the gas cylinder to prevent overflow into the red gas line.

iv. Labview Programs for Sample and Laser Pulse Manipulation, and Pfeiffer Turbo Pump Operation

Multiple programs are required in order to properly manipulate both the laser pulse and the sample. This section is an introduction on how to use and operate the Labview programs made to control the motors inside the main chamber of the system to properly manipulate the location of the laser pulse and the sample. The Pfeiffer turbo pump that drains the main chamber is also controlled by a Labview program as well.

a. Micos micro-precision translation stage

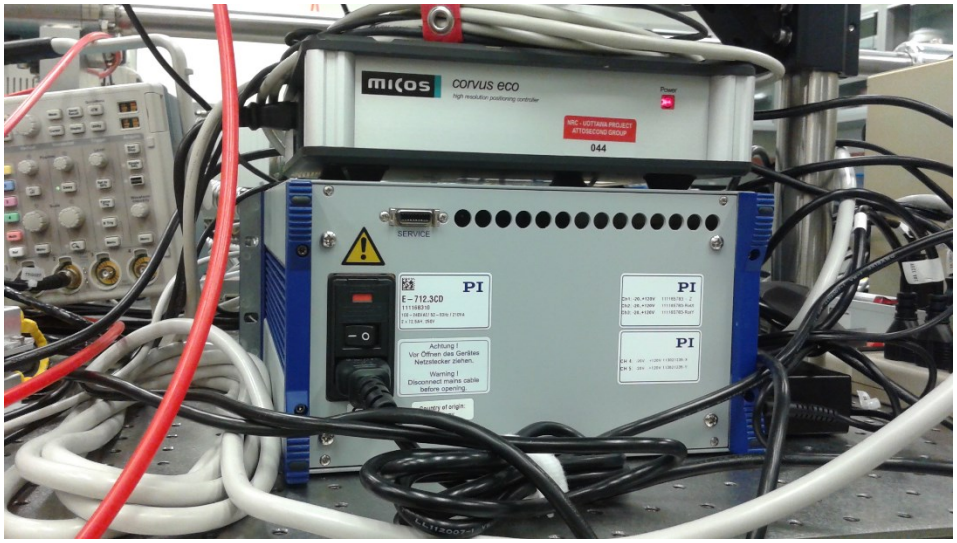

Figure 55: The Micos micro-precision translation stage motor (top) and the PI nano-precision translation stage motor (bottom).

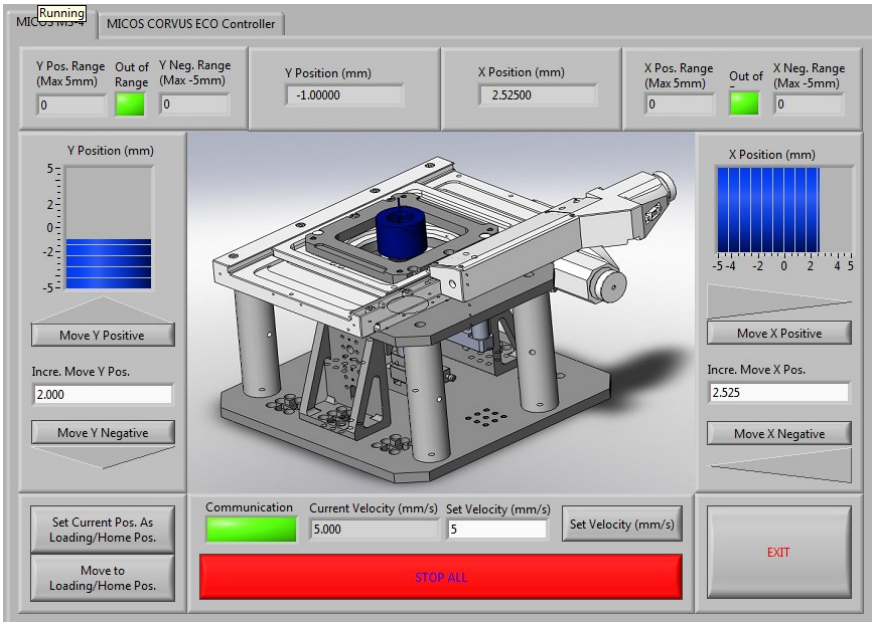

Figure 56: Labview program of the micro-precision translation stage.

To operate the micro-precision translation stage with the Labview program:

- Verify that the Micos stage driver is on.

- Run the “MicosMS-4” program found in the Labview folder. The program will remember the stage’s current position and displays it in the “Y Position (mm)” and “X Position (mm)” textboxes.
- To set the velocity of the stage’s movement, change the value in the “Set Velocity (mm/s)” textbox and press the button next to it.
- Enter the desired increment of translation in the Y axis in the “Incre. Move Y Pos.” textbox and press either the “Move Y Positive” or “Move Y Negative” button to move the stage by that certain increment in that direction. Do the same for the X axis on the other side of the program’s window.
    - On the camera, the stage’s movement can clearly be seen.
    - The translation is limited to a range between -5 and 5 millimeters for both axis.

To stop any motion in progress, press the “Stop All” button. To exit the program, press the “Exit” button.

b. PI Nano-Precision Translation Stage

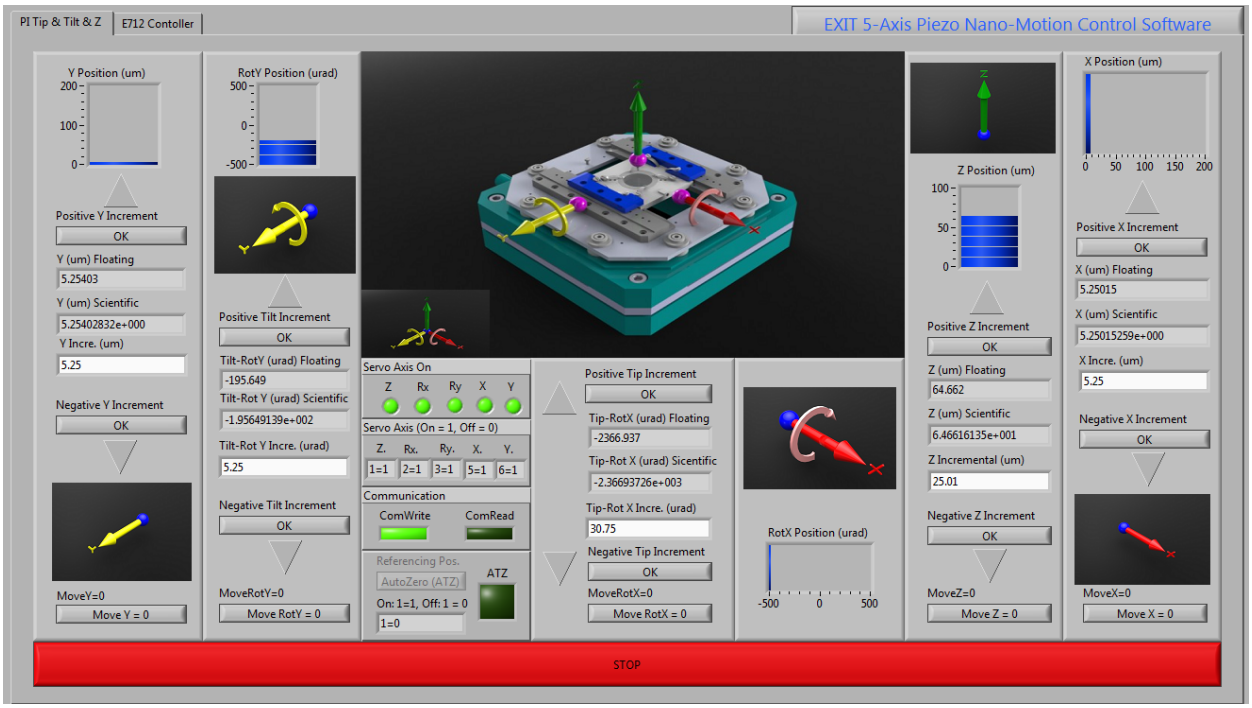

Figure 57: Labview program of the nano-precision translation and rotation stage.

To operate the nano-precision translation and rotation stage with the Labview program:

- Verify that the Piezo stage driver is on.
- Run the “PI-Tip-Tilt XY clean” program found in the Labview folder. The program will remember the stage’s current position and orientation and displays it in their appropriate textboxes (either Floating or Scientific).
- Enter the desired increment of translation in the Y axis in the “Y Incre. (µm)” textbox and press either the “Positive Y Increment” or “Negative Y Increment” button to move the stage by that certain increment in that direction. Do the same for the X and Z axes, and the rotation around the X (Tip) and Y (Tilt) axes.
    - The translation for the X and Y axes is limited to a range between 0 and 200 micrometers for both axis. The translation for the Z axis is limited to a range between 0 and 100 micrometers. The tip and tilt rotations are limited to a range between -500 and 500 microradians.
    - If at any point, the desired value of a certain axis or orientation is 0, simply press the “Move (desired Axis or Rotation) = 0” button.

To stop any motion in progress, press the “Stop” button. To exit the program, simply close it.

c. PI Translation Stages for Focussing Objective

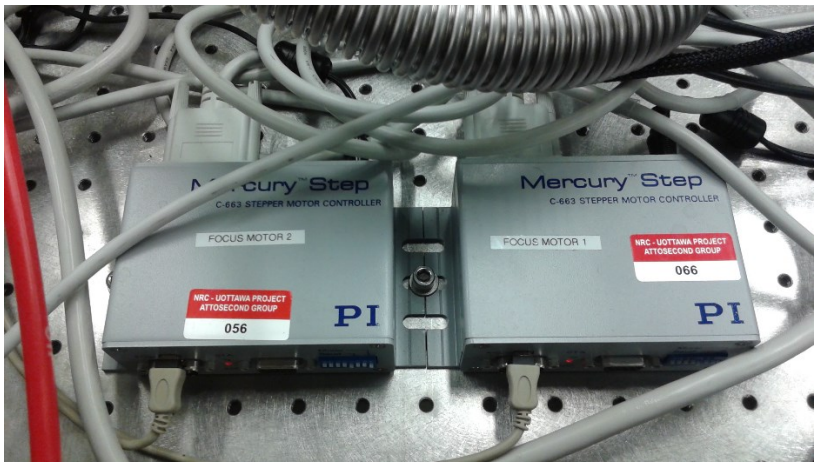

Figure 58: Both PI Stepper motors for the translation of the focussing objective beneath the sample and substrate inside the chamber.

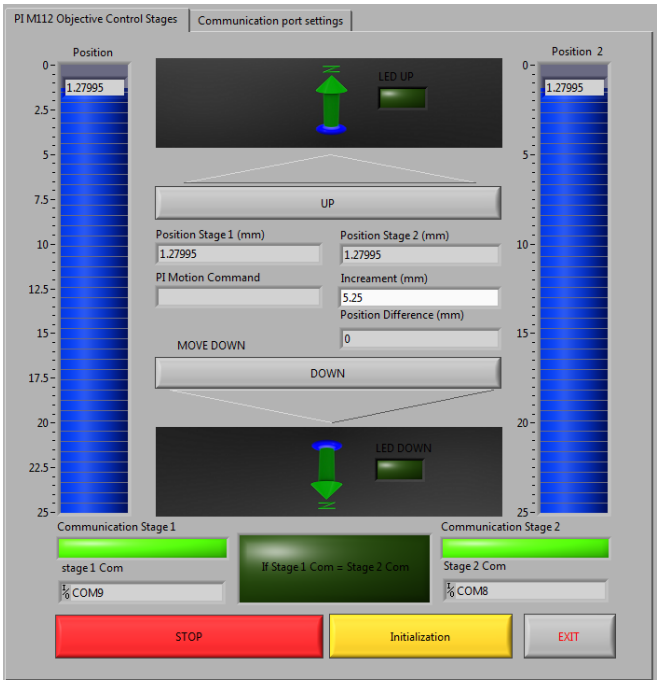

Figure 59: Labview program of the reflective lens' translation stage.

To operate the nano-precision translation and rotation stage with the Labview program:

- Verify that both PI translations motors are functional.
- Run the "PI Vertical –B" program found in the Labview folder. The program will remember the motors current positions and displays them in their appropriate textboxes.
- Verify that both stage ports (stage 1 (or 2) Com) are properly connected to the proper communication ports for the PI stepper motors.
- If any difficulties arises with the motors, or it is the first time in a long time that the program has operated, pressing the initialization button will set both stages to a level of 22.9998mm, insuring that both motors are synchronized.
- Enter the desired increment of translation in the Y axis in the "Y Incre. (μm)" textbox and press either the "Positive Y Increment" or "Negative Y Increment" button to move the stage by that certain increment in that direction. Do the same for the X and Z axes, and the rotation around the X (Tip) and Y (Tilt) axes.
    - The translation for the X and Y axes is limited to a range between 0 and 200 micrometers for both axis. The translation for the Z axis is limited to a range between 0 and 100 micrometers. The tip and tilt rotations are limited to a range between -500 and 500 microradians.

- If at any point, the desired value of a certain axis or orientation is 0, simply press the “Move (desired Axis or Rotation) = 0” button.

To stop any motion in progress, press the “Stop” button. To exit the program, press the “Exit” button.

d. Pfeiffer Turbo Pump Operation

Figure 60: Labview program of the Pfeiffer turbo pump system.

To operate the Pfeiffer turbo pump with the Labview program:

- Run the Master Program found in the Labview folder.
- Verify that both stage ports (Maxigauge COM and Turbo COM) are properly connected to the proper communication ports for the pressure gauge and the Pfeiffer turbo pump, respectively.
- Press the “Open Pressure Port” button.
- Once the chamber and backing pressure is below 5E-2 Torr, press the “Open Turbo Port” button.
- Verify that the Edwards turbo pump is already running.
- Press the “Turbo On or Off” button to turn on the Pfeiffer turbo pump.

The program can be closed and lead to no error to the turbo pump itself. To shut down the Pfeiffer turbo pump, simply run the program again, and turn off the buttons in reverse order.

v. Kore High Voltage Supplier, Controller and Time-to-Digital Converter (TDC)

In order for the ions to follow the proper path from their point of creation to the detector inside the mass spectrometer, the system needs a series of high voltage pulses and plates in order to properly direct the ions along this path. The high voltage supply and voltage control units sets all the high voltages inside the system.

Figure 61: The three crucial units for the mass spectrometer and the pulsed extraction unit. The top unit is the Time to Digital Converter (TDC), the middle unit is the Voltage Controller and the bottom unit is the High Voltage Supply Unit.

The high voltage supply unit supplies the voltages to both the active element in the lens system, in order to focus the ions in flight, and the voltage sent to the pulsed extraction unit, which then is pulsed through the stage and substrate, sending the ions up into the TOF-MS and commencing their path to the detector. Both these voltages can be controlled within a certain range with their own distinct control knobs. The lens system has a range between -4090 and -4910 volts, while the stage has a range of 2065 and 2493 volts. Both of these scales are linearly proportional to their gauges. It also supplies the high voltage to the voltage controller, where the high voltages of various electrodes in the mass spectrometer can be set.

The voltage control unit provides the gain voltage to the microchannel plate (MCP) detector inside the TOF-MS, while also setting the high voltages of the reflectron and the X and Y directional plates. The gain voltage switch needs to be flicked to operate in order to function. The detector has a control knob to control its gain in a linear range from 0 to -4890 volts. The

higher the voltage, the more ions it can detect. However, the detector can saturate so it is best not to adjust it too high. Naturally, the detector degrades over time and as such, slightly increasing the gain compensates for it.

The other five control knobs control the high voltages inside the TOF-MS. Both the Retard and Reflect gauges change the voltage at the midpoint and the end of the reflectron. The first electrode in the reflectron is always grounded. This creates two distinct linear gradients for second-order correction of the ions' different initial kinetic energies. The Retard's voltage linear range is between 937 and 1139 volts, while the one for the Reflect gauge is between 1891 and 2092 volts. The X and Y gauges alter the voltages being applied to the directional plates inside the mass spectrometer, after the lens system. Their output is located in the Deflector Supply section of the back panel. The 9 pin socket controls both the positive voltage and negative voltages of each pair. Each gauge has a range of -50 to 50 volts. There is also a Stage control knob, but since its output is for a non-pulsed sample stage, we use it for the constant extraction configuration. Its range is between 1687 and 1891 volts.

Additionally, each unit also has an interlock light that, when tripped, cuts all voltages supplied from the unit to prevent damage either inside the system or the units themselves. This interlock is triggered through the pressure gauge of the TOF-MS. If the full range gauge is over a set pressure (1E-6 Torr at time of writing), the interlock is tripped and will only be restored once the pressure is pumped below the set pressure on the gauge.

For more information on the specific values of each gauges at various points, please consult the Kore Power Supply test notes, as they have been accurately tested at the University.

To operate the High Voltage Supply Unit, Voltage Control Unit and Time to Digital Converter;

- Verify that the pressure in the TOF-MS is underneath the set pressure of the interlock (1E-6 Torr at time of writing)
- Turn on the 110V to 240V power converter. This provides power to the other three units.
- Turn on the High Voltage Supply Unit
- Turn on the Voltage Control Unit
    - The interlock light of the High Voltage Supply Unit will turn on before the Voltage Control Unit has power. This is normal because the interlock of the

gauge goes through the Voltage Control Unit before reaching the High Voltage Supply Unit.

- Flick the Gain switch to Operate.
- Turn on the Time to Digital Converter.

In order to cease operation, power down the units in the reverse order above.

vi. Kore Pulsed Extraction Unit

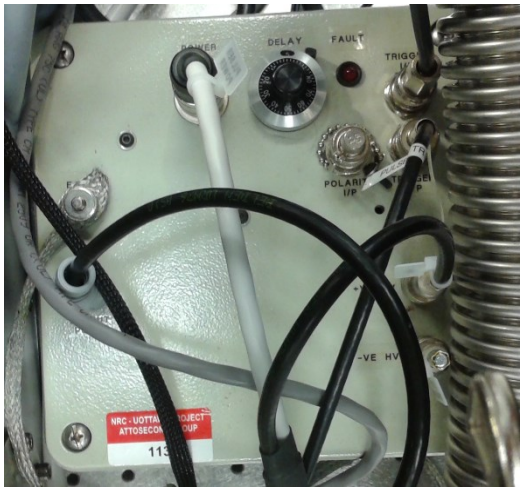

Figure 62: The pulsed extraction unit. Connections to this unit are all towards either the substrate or the high voltage supply unit.

The pulsed extraction unit obtains the high voltage given by the HV supplier, and delivers a short electrical pulse of that magnitude through the substrate on the manipulation stage in the main chamber. It is also connected to the input trigger of the TDC, where it reads the output trigger of unit and serves as the start of a cycle (Chapter 3.5, relates to Figure 23). On the unit itself, there is a control knob controlling the delay between the trigger input and output of the system. Since there is already a digital delay generator in place, the value on the control knob can be left as it is (on 5.0 at time of writing) and the delay can be controlled entirely by the generator.

If constantly switching between the RegA and the Legend system, make sure that the proper digital delay generator (DDG) that corresponds to the laser system used in the experiments is attached to the pulsed extraction unit. The DDG for the RegA system is located next to the chamber, while the DDG for the Legend system is located near the XUVM system.

Considering that there are two configurations of extraction, the proper connections need to be made.

If in the pulsed extraction configuration, make sure that the voltage output from the unit is connected directly to the main chamber's stage, its input located underneath the leak valve. Verify also that the digital delay generator is connected to the trigger input of the unit, while the trigger output is connected to the T-slot that is connected to the trigger input of the TDC.

If in the constant extraction unit, verify that the digital delay generator is connected directly to the T-slot connected to the trigger input of the TDC. Disconnect any wires connected to the trigger input and output of the pulsed extraction unit. Connect the main chamber's stage to the Stage output on the Kore High Voltage Controller.

vii. Baking the Chamber

In order to eliminate any humidity and other outside contamination inside the main chamber, it can be baked with a lightbulb. To bake the chamber, simply turn on the gray variable autotransformer that is beside the Pfeiffer turbo pump (Figure 60, left). The voltage can be varied, but to prevent the lightbulb from burning out too quickly, it is best left at its current setting of 28 on the autotransformer. The temperature can be checked with the thermocouple beside the autotransformer (Figure 60, right). The bake-out is done in vacuum. When baking, the chamber should be at a temperature of 44.7 ^{o}C. It is best to bake the chamber for a few days, in order to reduce water particles and other gases inside the chamber, to achieve a better vacuum once the bake-out is complete. The pressure will rise as the chamber heats, but once the temperature inside the chamber returns to normal (22.8 ^{o}C), the pressure should be lower compared to before the bake-out.

Figure 63: The variable autotransformer for the lightbulb inside the main chamber (left), and the thermocouple indicating the temperature inside the chamber (right). At the time when the picture was taken, the lightbulb was turned off.

viii. Motorized Mirrors for Laser Alignment

Before trying to align the laser inside the main chamber of the system, verify that the laser is aligned with the two irises located on the black breadboard just before the window port on the side panel of the chamber.

Inside the chamber are two motorized mirrors that direct the laser pulse towards the sample on the manipulation stage. These motors are controlled by a picometer joystick located outside the chamber (Figure 61). Since the joystick can only control one motorized mirror at a time, two separate ports are located on the side panel of the chamber (Figure 62). Connecting the joystick to one of these ports controls one of the mirrors inside the chamber. To switch mirrors, simply connect the joystick to the adjacent port.

Figure 64: Joystick controlling one of the motorized mirrors in the main chamber. It can easily be connected to the other motorized mirror through the ports on the side of the chamber (Figure 65).

To use the joystick to align the laser, follow these instructions:

- Block the beam path
- Descend the focussing apparatus to a height of 22.0 mm with the “PI Vertical –B” Labview Program (Chapter A-iv-c).
- Press the Set Axis/Enable button on the joystick until both the Set X and Set Y lights are turned on.
- Press the Driver button until the Driver 1 light is turned on.
- Press the Motor button until the Motor B button is turned on.
- Attach the 9-pin port on the side panel of the main chamber to the one on the top right (refer to Figure 64). This controls the second motorized mirror in the beam path.
- Unblock the beam
- While holding down the X+Y/Enable button (the button on top of the joystick), move the laser spot with the help of the camera and monitor on top of the chamber until it is centered with the reflective lens (Figure 66).

Figure 65: The ports connecting the joystick controller to the motorized mirrors inside the chamber. In the figure, it is connected to the first motorized mirror in the beam path.

If the joystick proves problematic or the beam is quite misaligned, the chamber can be brought up to atmospheric pressure, the chamber panel can be removed and the mirrors can aligned by hand. Before alignment, block the beam and descend the focussing objective to a height of 22.0 mm with the "PI Vertical –B" program (Chapter A-iv-c), then unblock the beam. Align the first mirror with the first iris inside the chamber, before the beam splitter. Align the second mirror with the focussing objective, with the help of the camera and monitor on top of the chamber. The spot should look similarly to that of figure 66.

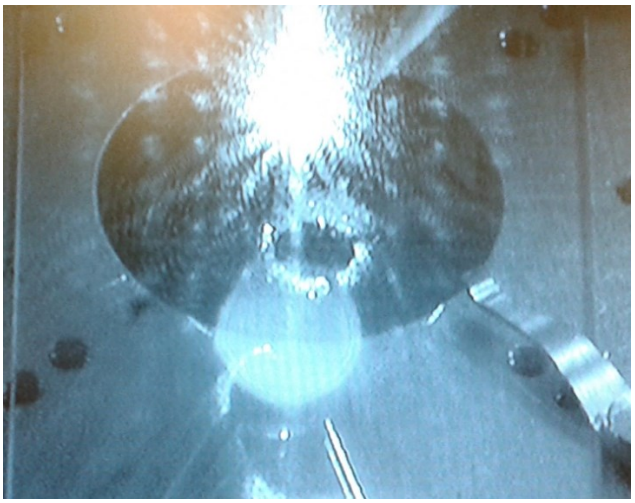

Figure 66: View of the monitor projecting the light from the expanding laser pulse reflected off the substrate. The spot comes from the primary mirror of the focussing objective. Refer to Figure 11 for more information on this spot. The spot should be aligned so that it is situated in the middle of the beam spot.

After this, the mass spectrometer is ready to use.

Appendix B: Using the GRAMS/AI Kore Software

This is a truncated version of the Kore Software User guide. If one would want more details about this program, please consult said manual. What follows are basic instructions for operation. I included this into this thesis for easy access for future students learning the software.

i. Acquisition of Mass Spectrum and Trace

Before being able to use the Kore software to measure our spectrums, the TOF cylinder needs to be at a pressure under 1E-6 Torr, which means both turbo pumps need to be on. Once this is done, the Kore high voltage supplier, controller and TDC can be turned on, and the software is ready to measure spectrums.

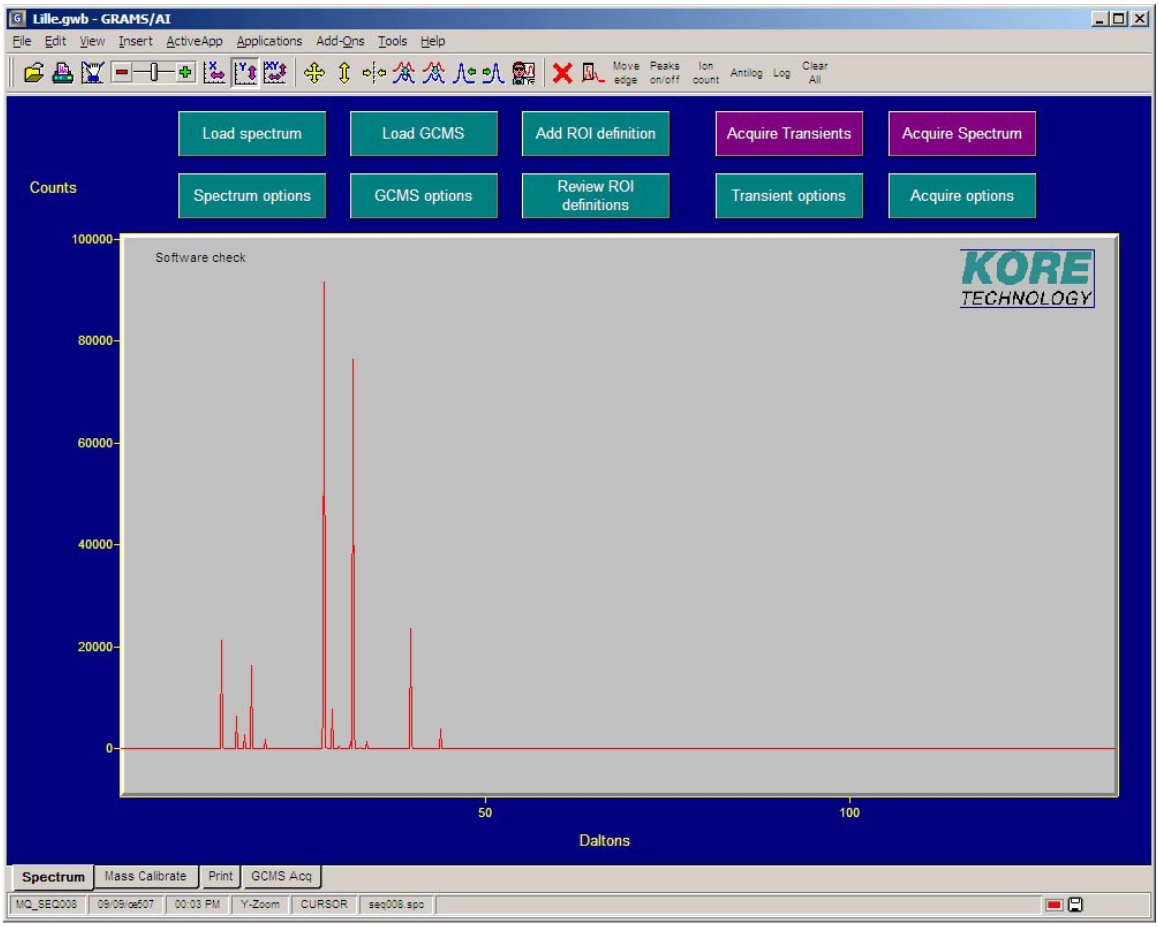

Figure 67: The GRAMS/AI software program, as it appears in the Software User Manual.

To measure spectrums with the Kore software, read the following:

- On the laptop next to the Kore HV supply boxes, open the SpectraK(Spectrum).wpg program

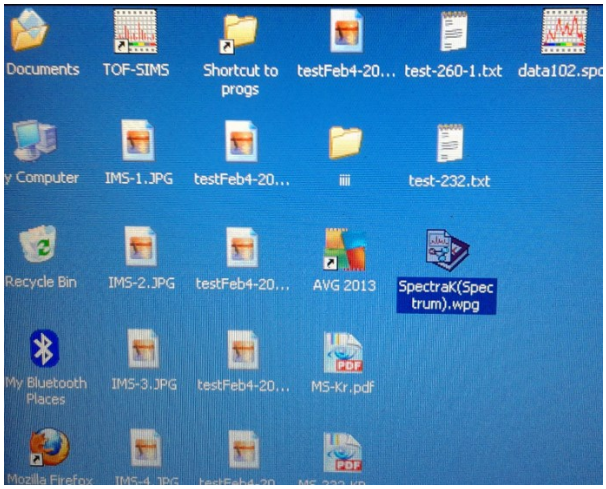

Figure 68: View of the desktop, and location of the programs needed for acquisition (SpectraK(Spectrum).wpg) and calibration (TOF-SIMS).

- Unplug and plug the USB connecting the TDC to the laptop. The software cannot properly detect the TDC if it has recently been turned on.

The view of the graph can be changed either directly to scale or to a view suitable to the user. The yellow arrows on the toolbar scales directly on the trace in either the Y axis or both the X and Y axis simultaneously. The buttons for the variable settings of the X and Y axis are the ones with purple arrows directly to the left of the yellow arrow buttons on the toolbar. When one of these buttons is pressed, the slider to the left of these buttons scales accordingly to the axis designated by the pressed button. These buttons can be seen in Figure 67.

The program has four buttons on top of the spectrum. The “Spectrum Options” allows the spectrum to measure the intensity of counts by the ion’s time of flight, or the m/q value after calibration. Using “Mass (High res.)” is a must for traces that are to be used for calibration purposes. The “Load Spectrum” loads a previous spectrum saved on the laptop. The “Acquire” button commences the collection of ions and displays them on the graph. The parameters of acquiring said data is set in the “Acquire Options” button.

There are four sections in the window that appears. In the “Spectrum Acquisition” section, we can note the length of a cycle (time between extraction pulses), the data range within this cycle that will be registered and displayed on the graph, and the amount of cycles we implement by setting the total experiment time. The amount of cycles that will run is the experiment time

divided by the cycle time. The minimum cycle time is 100 microseconds, which is why the laser frequency is limited to 10 kHz at absolute most. The "Ion counting parameters" section determines how fast the graph updates, but also specific regions of interest (ROIs) that maximises detection within these regions. The "Mass conversion parameters" determines the calibration values between the ions time of flight inside the TOF cylinder, and their m/q value. They can be calculated in the mass calibration section. The equation that these parameters follow is:

$$m/q = \left([t - t_0]/C_b\right)^2$$

This equation is similar to that shown in Chapter 3.4.1. Finally, the "Storage" section determines the file name of our traces. It is recommended to leave the box "Delete old traces" unchecked, to always have said trace, whatever it may be, available later for use.

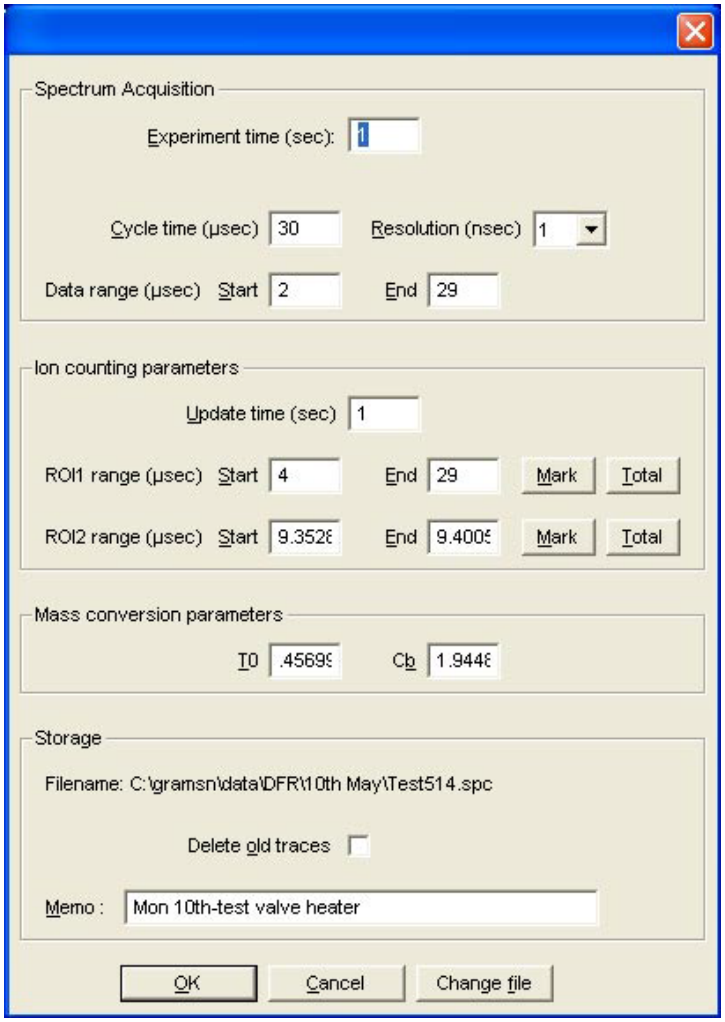

Figure 69: Pop-up window of the "Acquire Options" button, taken from the Software User Manual.

Once the “Acquire” button has been pressed, a pop-up window will appear indicating the number of cycles in the experiment, the current cycle number and the number of counts registered. The experiment can be stop at any time by pressing the “Terminate Run” button that appears once the experiment is running. Once the experiment has stopped running, the program will ask for a memo to attach onto the file. Once this is done, the file is saved for further analysis or calibration purposes.

If the “Acquire” button turns into a red “GetData” button, close the program immediately and open it again. The later can override the “Acquire” button, and a backup program, saved in multiple areas such as the software installation disc or the backup folder, will be needed.

When exiting, the program will ask if the user would like to save the Workbook modifications and the data files. While the data files can be saved, I recommend not saving the Workbook modifications, as they can lead to software errors if not done correctly. This is what happened to the TOF-SIMS program, with the “GetData” button remaining as a permanent fixture as described above

ii. Mass Calibration

To calibrate the mass conversion parameters, a trace of a known substance, be it a noble gas or ablated solids, is required. Follow these instructions:

- Open the TOF-SIMS program (see figure 67).
- At the bottom of the page, click on the Mass Calibrate tab. This will open a window with previously saved traces. Select the file you want to use for calibration.
- Once the trace has been loaded, zoom in on the first known peak.
    - Simply highlight over the peak and click on the box left over from the highlight.
- Click on the very top of the peak at its center, and click the “Set Point #1” button.
- Insert the exact value of this mass into the appropriate dialog box, then press OK.
- Repeat these past 3 steps for however many peaks the user desires.
    - The “Set Point #1” button will change to display “Set Point #2”, and so on.
    - Generally with more points, the calibration parameters will be more precise.
    - Try having both lighter and heavier masses to add precision to the calibration parameters throughout the spectrum, instead of a small region.

- When satisfied with the number of points, click the “Solve” button. The trace that displays should be the same trace, but with the newly calculated calibration parameters.

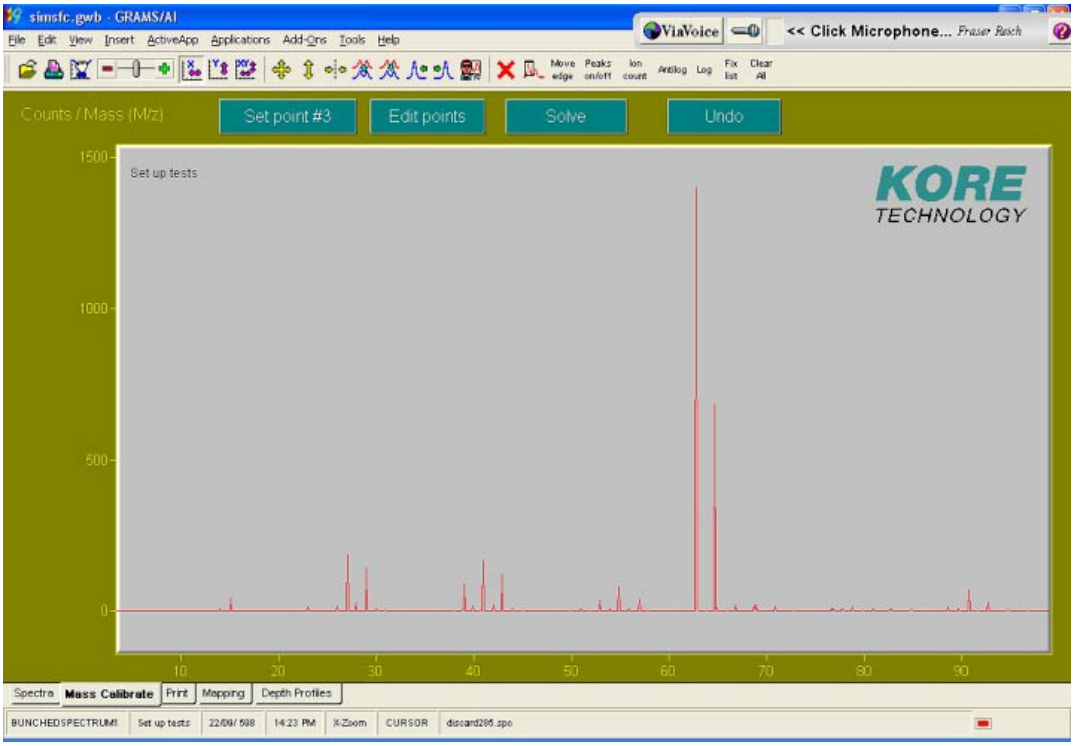

Figure 70: The Mass Calibration page on the GRAMS/AI software program, as taken from the Software User Manual.

- Click the “Save as auto-cal” button to remember these parameters, and then press the Spectrum tab to exit.
    - Exiting by closing the window immediately will not save the calibration parameters for further tests.
- When exiting, a pop-up window will appear asking to save the calibration. Press the “Update file and collect model” to not only save the newly calibrated trace, but to save the calibration parameters for future tests.

Acknowledgments

I would like to acknowledge the people at Kore, particularly Steve Mullock for their help with the inner workings of the Time-of-Flight Mass Spectrometer, Time to Digital Controller and the High Voltage Controller and Supplier. I also would like to thank Matthew Shiu for his help with the mass spectrometer.

From the National Research Council (NRC), I would like to thank Dr. David Rayner for showing me the ropes when it came to the Time-of-Flight mass analyzer, and for recommending SIMION to earn a better understanding of the ion optics in the system. I would also like to thank Andrei Naumov for helping me learn the laser system that I used at NRC, a homemade chirped pulse amplification system, and for his help with the mechanics of the mass spectrometer. On the subject, I would like to thank everyone from both NRC and the Advanced Research Complex (ARC) who helped to move the imaging mass spectrometer from the former building to the latter.

I also would like to thank for Dominik Geissler for his help with the system and generally being there to answer any question I would have with the system or some of the results that I would obtain. I will also thank Ladan Arissian for her help with the laser systems at ARC.

From l'Université de Moncton, I would like to thank Dr. Pandurang Ashrit, Dr. Normand Beaudoin and Gisia Beydaghyan for allowing me to deposit the WO_3 samples used to test the imaging mass spectrometer.

I want to thank the entire Attosecond group at NRC and ARC for their help and support. I want to especially thank my friends, both in Ottawa and back home in Moncton, for their support and helping me maintain my sanity in check during some of the frustrating moments during my research. I also want to especially thank my sister for her support, and my parents, without whom I would not have the opportunity to be where I am today. Last but not least, I would like thank my supervisor, Dr. Paul Corkum, who gave me the opportunity and his time to work on this system and present to you this very thesis.